Increasing Permeability of the Intestinal Epithelium to Enable Oral Delivery of Protein Drugs

Submitted in partial fulfillment of the requirements for

the degree of

Doctor of Philosophy

in

Chemical Engineering

Nicholas G Lamson

B.S., Biological Engineering, Cornell University

Carnegie Mellon University
Pittsburgh, PA

May 2019

ACKNOWLEDGEMENTS

First and foremost, I would like to express my profound gratitude to my advisor and committee chair, Dr. Katie Whitehead, for all of her patience, advice, and mentoring. I have grown so much as a scientist and as a person over the past five years, and you have been source and the catalyst for so much of the learning and development. You taught me how to be a much better presenter, researcher, and writer, and I cannot thank you enough for the foundation that you've given me to go out and be my own, independent researcher.

I would also like to thank the past and present members of the Whitehead Lab. It has been an honor and a pleasure to work with all of you. In particular, I am indebted to Sisi Xian, Kanika Suri, Adrian Berger, Vishal Ahuja, Anna Zhang, Becca Ball, Kyle Cochran, and Kathy Fein for all of your help and enthusiasm. Each of you have directly contributed to the work presented in this thesis, and it could not have all come together without you. To that end, I would like to acknowledge Dr. Brigitte Schmidt from the chemistry department over at MCS. I sincerely believe that we would still be trying to find the active strawberry component were it not for your help.

Thank you to my committee, Dr. Anne Robinson, Dr. Gloria Silva, and Dr. Robert Tilton for all of your guidance during my tenure here at CMU. I could never have covered the full breadth of these projects without your insight and willingness to offer knowledge and advice. I am also grateful to Thomas and Adrienne Klopack, as well as the NSF Graduate Research Fellowship Program (under Grant No. DGE1252522) for collectively funding me through most of my time here.

Without this support, we could have never ventured into the more innovative, sometimes bizarre, but surprisingly productive corners of the field that we did.

I must also express my thankfulness to all of the wonderful friends that I've found along the way, in Pittsburgh and beyond. There are way too many of you to mention everyone here, but I appreciate each and every one of you for the light and support that you've brought into my life. I would especially like to call out Dana, Schwegger, Bridgette, Khal, Boss, Wallitsch, Buddy, Janet, Chelsea, Iona, the Big Red Trumpets (and affiliates), and the CMU ChemE PhD graduating classes of 2018 and 2019 (and affiliates). You all have been instrumental in keeping me sane over the past five years, and I appreciate it more than I could ever eloquently describe.

Finally, I am extraordinarily grateful to my parents, sister, grandparents, and the rest of my family for their undying encouragement and love. You have always believed in me, even when I haven't, and I would never have made it this far without your support. Thank you.

ABSTRACT

Oral delivery of macromolecular drugs, especially bioactive proteins, is one of the greatest unmet needs in modern biomedicine. Although engineering solutions have been developed to overcome low pH and enzymatic degradation in the stomach, poor absorption across the intestinal epithelial barrier and into the bloodstream continues to hinder clinical viability of oral protein formulations. One common solution is to employ chemical permeation enhancers of the epithelium. Unfortunately, most efficacious enhancers have been thwarted by toxicity, and the mechanisms that contribute to this behavior are poorly understood. Thus, there is an ongoing need to develop and characterize nontoxic permeation enhancers.

First, this work seeks to expedite cell culture screening for permeation enhancer candidates by reducing the cost- and time inputs required for Caco-2 cell monolayers, the most common model of the intestinal epithelium. A new, 3-day system deemed “thrifty, rapid intestinal monolayers” (TRIM) is developed, comparing favorably with two current monolayer systems.

Next, the work explores the mechanism by which piperazines, a family of known permeation enhancers, interact with cells. Interestingly, the pH of the piperazine solutions presents as the controlling parameter, even when accounting for effects from pH change alone. The piperazines nonetheless suffer from narrow therapeutic windows, underscoring the need for a new generation of enhancers that do not permanently damage the intestines.

The next portion of this work screens an extensive, food-based library for nontoxic but effective chemicals to improve intestinal protein absorption. Of 106

crude food extracts, the vast majority are not cytotoxic, and only a small fraction increase epithelial permeability. An iterative separation-activity screening method is used to isolate a single, active compound: the polyphenolic molecule pelargonidin from strawberries. Pelargonidin is demonstrated as a reversible, efficacious permeation enhancer, enabling uptake of model drugs and insulin through the intestinal lining.

Finally, this work presents the surprising ability of anionic nanoparticles to act as physicochemical permeation enhancers. Orally administered silica particles induce dose-dependent permeabilization of the intestinal epithelium, allowing for oral delivery of insulin and exenatide. Histology of treated mouse intestines shows no evidence of particle-induced necrosis, inflammation, or changes in tissue architecture. These conclusive results underscore the ability of silica nanoparticles to safely increase epithelial permeability, enabling the oral delivery of macromolecular drugs without encapsulation or conjugation.

TABLE OF CONTENTS

LIST OF TABLES

LIST OF FIGURES

Chapter 1:
Introduction

1.1 – Advantages and Challenges to Oral Delivery

Oral drug delivery is painless and convenient, offering superior patient compliance and improved disease outcomes compared to injections. However, delivery challenges have thwarted its successful implementation for macromolecular (larger than 1000 Da or 1 kDa) drugs, especially proteins[1,2]. As a result, millions of patients across the globe are subjected to injections of macromolecule drugs, such as insulin for diabetes or heparin as an anticoagulant, on a daily basis. Unfortunately, a fear of injections is pervasive across populations, sometimes surpassing 80% prevalence in both children and adults[3,4]. An estimated 20%-30% of patients further classify as suffering from severe needle phobia[4,5]. As a result, many patients simply do not take their critical medications. For example, up to 33% of adults being treated for diabetes report feelings of dread associated with their insulin injections, and 45%-60% report intentionally skipping one or more doses[6,7]. Missed doses lead to poor disease control, which in turn results in more patient suffering and inflated healthcare costs. By enabling simple and painless administration, converting insulin and other protein drugs to oral dosage forms would drastically improve patient experience, compliance, and disease outcomes for a wide variety of maladies.

Unfortunately, the physiology of the gastrointestinal tract prevents the clinical translation of most oral protein formulations[8–11]. First, the drug is swallowed and enters

the stomach, which contains harsh acid and enzymes from which the drug and delivery vehicle must be protected. Most often, this is accomplished by coating the capsule or tablet with pH sensitive enteric polymers. These polymers dissolve to expose the protein cargo only once it reaches the more neutral pH of the intestinal lumen[12–14]. Even in the intestines, there remain several barriers through which the drug must pass to enter systemic circulation (**Figure 1.1**). First, the lumen is separated from the intestinal walls by a 130-530 μm thick layer of mucus, which is a highly viscous, hydrated polymer matrix comprising both hydrophobic and hydrophilic segments[11,15]. The mucus is a diffusive barrier to certain sizes and charges of protein drugs, and also harbors a diverse population of microbes, which can degrade protein drugs[11,15,16]. Thus, any carrier for oral delivery must be examined for its ability to pass through the mucus, as

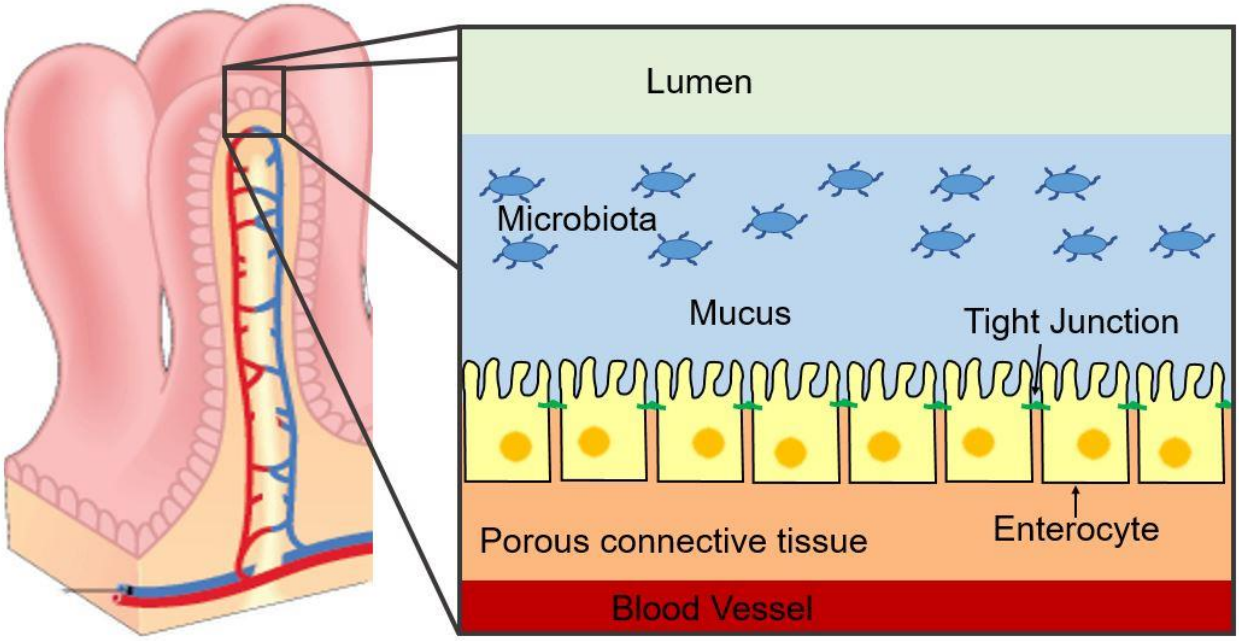

Figure 1.1 – The intestinal lining is the major mass transport barrier isolating orally delivered drugs from the blood stream. To reach circulation in the body, the drug must begin in the lumen, diffuse through the bacteria-rich mucus, and cross the epithelial barrier. The epithelium of the intestines is formed into finger-like shapes called villi, providing a large surface area for absorption. These villi are lined with a layer of enterocyte cells, which form tight junctions between one another to act as a barrier to mass transport of large solutes, particles, and bacteria.

well as protect its cargo from deterioration. More specifically, the intestines contain a wide variety of proteases, originating from both the human body and the microbiome, which must be inhibited or otherwise blocked to avoid degradation of the macromolecule drug[17]. This is usually accomplished by the inclusion of a protease inhibitor in the drug carrier formulation[17,18], deploying decoy proteins[1], or loading the protein into a protease-impermeable carrier[19].

Should a protein safely transit the mucus and reach the wall of the small intestine, it can then only be absorbed into the bloodstream by crossing the formidable intestinal epithelial barrier[20,21]. The epithelium consists of a monolayer of enterocytes that are tightly bound to one another by intercellular protein complexes called tight junctions[21–25]. Together, these cells and junctions exert specific control over what material can or cannot transit from the interior of the intestines to systemic circulation. To the chagrin of researchers and patients alike, they excel at preventing the migration of whole, active protein and peptide drugs into the bloodstream. As a result, escorting drugs across the epithelium is the focus of most ongoing oral protein delivery research.

1.2 – The Intestinal Epithelium Is Impermeable to Proteins

The primary purpose of the intestinal epithelium is to provide a high surface area for absorption of nutrients and other beneficial substances from food, while simultaneously acting as a barrier against the uptake of toxins, pathogens, and any other unwanted material[26]. The epithelium is primarily composed of enterocytes: absorptive cells that form a single layer, lining the walls of the intestines to govern both transcellular and paracellular permeability of the barrier. Transcellular, or through-the-

cell movement of material is restricted to small, hydrophobic molecules or important nutrients for which cells have evolved specific transporters (e.g. glucose, amino acids)[27]. By contrast, large or hydrophilic substances that pass through the epithelium must do so via the paracellular route, in the gaps between adjacent enterocytes. Transport through these gaps is regulated by the tight junctions, which exhibit highly specific size and charge specificity among material passing through the intercellular space[21,28]. As part of this size specificity, native tight junctions permit the passage only of molecules less than 1 nm in hydrodynamic radius[21]. As most proteins and peptides are much larger[9], they are unable to enter the bloodstream[29], and their systemic bioavailability following oral administration is negligible. Thus, to successfully deliver proteins or other large molecules across the epithelium, researchers must devise strategies to boost transport either through the enterocytes or through the tight junction space.

1.3 – Intestinal Permeation Enhancers: Rationale and Drawbacks

One possible strategy to improve transepithelial uptake of protein drugs is to introduce them with a delivery agent that induces transcellular transport. This typically takes one of two forms. First are transcellular permeation enhancers: molecules that permeabilize the cell membrane to allow diffusion of protein drugs directly through the enterocytes[30]. These often take the form of surfactants[30–32] or cell penetrating peptides[33,34], which open pores in the hydrophilic region of the membrane large enough to facilitate macromolecule transit. However, the possibility of cytosolic depletion and

permanent tissue damage due to this fenestration has led to concerns regarding the use of transcellular enhancers and their potential for toxic side effects[30].

The second common transcellular strategy is to load protein drugs into nanomaterials engineered for uptake by intestinal cells and subsequent release into the body. These can take the form of solid lipid particles[35] or nanoemulsions[36] as lipophilic carriers to improve permeability through cell membranes, or receptor targeted nanoparticles to stimulate endocytosis into epithelial cells[37–39]. Though some of these nanomaterials have produced promising preclinical results, they require careful engineering of their size and surface characteristics to avoid being trapped in the intestinal mucus or triggering an immune response[37,40–44], and none have yet advanced into late-stage clinical trials for oral protein delivery[12,45,46].

As a promising alternative to transcellular permeation strategies, there is a major opportunity in manipulation of the tight junctions by paracellular permeation enhancers[21,47,48] (**Figure 1.2**). The rationale behind this approach is not to modify the

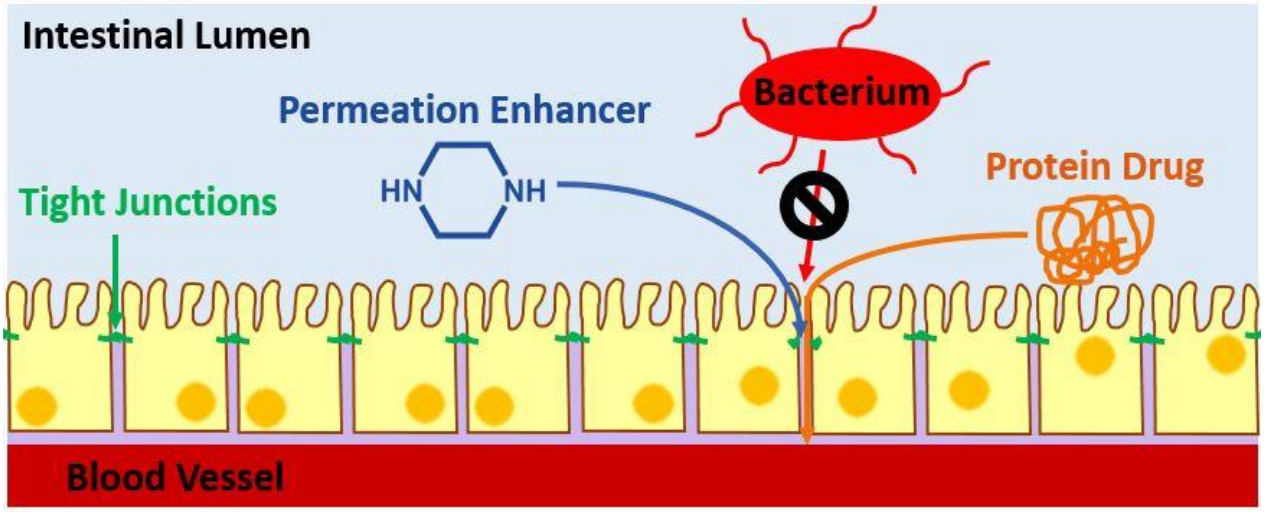

Figure 1.2: Paracellular permeation enhancers improve protein diffusion through the tight junctions. Here, a known permeation enhancer (piperazine) open the tight junctions to allow absorption of a protein therapeutic without opening the epithelial barrier to bacterial transit. Cells and molecules are not drawn to scale.

transport properties of the protein drug itself, but rather to eliminate the diffusive resistance of the paracellular space to protein transport. Given the high concentration of protein drug at the site of capsule dissolution, and effective sink conditions of the bloodstream, opening the tight junctions will allow a substantial flux of the protein drug through the epithelium and into circulation.

Several groups have previously studied intestinal permeation enhancers[49–54], with the most effective candidates being surfactants or amine-containing cyclic compounds. For delivery of insulin and other antidiabetic peptides specifically, some chemical permeation enhancers have even entered early stage clinical trials[12,55,56]. Unfortunately, no small molecule permeation enhancers have yet advanced through late-stage trials. Most often the roadblock stems from the mechanisms of permeabilization being unknown, leaving them prone to cytotoxicity or with narrow therapeutic windows[49,57,58]. Toxicity could be due to factors such as excessive permeabilization of the epithelium and bacterial uptake, induction of apoptosis, or permanent rearrangement of the epithelial architecture. This toxicity cannot be preempted without understanding how permeation enhancers interact with tight junctions to manipulate their barrier function. Thus there is a major need to identify molecules that alter tight junction transport regulation with known mechanisms and without inducing permanent epithelial damage.

1.4 – Experimental Design to Study Intestinal Permeation Enhancers

The first step for screening potential intestinal permeation enhancers is to examine their effects on cell culture models of the epithelium, most often employing the Caco-2 cell line. The unique ability of Caco-2 cells to differentiate into enterocytes was first reported in 1983[61], and it has since become the most popular model of the small intestinal epithelium[62,63]. Monolayers composed of differentiated Caco-2 cells are used by labs around the globe to aid research in oral drug delivery[2,30,64], gastrointestinal disease[65–68], safety testing[60,69,70], and more. To achieve differentiation, Caco-2 cells are cultured on porous membranes with separate media chambers feeding both the apical (top) and basal (bottom) surfaces of the cell monolayer (**Figure 1.3a**). These monolayers generally correlate well to human small intestines with regards to molecular permeability and gene expression[27], and they develop the same type of tight junction complexes as human intestinal enterocytes[21,71]. Paracellular permeability can be predicted by measuring the transepithelial electrical resistance (TEER), which quantifies the ease of ions flowing through the paracellular space, and confirmed by placing the paracellular diffusion marker[31] calcein in the apical well and measuring its accumulation in the basal well. A successful, reversible permeation enhancer treatment will reduce TEER and increase calcein permeability while it is in contact with the cells, but the monolayers will regain their barrier function (i.e. high TEER values) within 24 hours of treatment removal.

If a permeation enhancer is successful in Caco-2 monolayers, it can advance to testing in mice, which represent the first animal model for preclinical oral drug delivery research (**Figure 1.3b**). In some cases, materials can either be orally gavaged without

protection from stomach digestion, or orally administered in an enterically coated, mouse sized capsule. If neither of those administration strategies are possible, the mice are surgically opened and the material is injected directly into the duodenum. While this is not a clinically relevant method of delivery, it does allow for examination of protein drug uptake and permeation enhancer efficacy without the complicating factors of enteric coatings or digestion. In any case, after permeation enhancers and protein drugs are administered to the mice, blood is collected at pre-determined time points and examined for either model drug concentration, or activity of the delivered protein (e.g. reduced blood sugar resulting from insulin). It is primarily using these biological screening methods that we set forth to answer some major, lingering questions in the field of oral protein delivery.

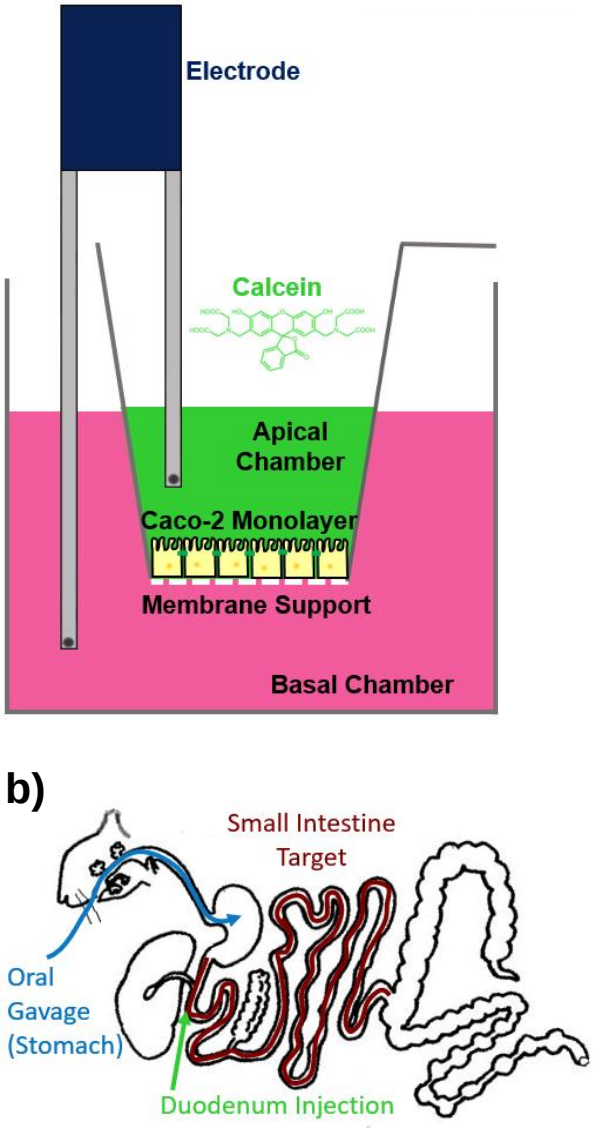

Figure 1.3: Biological models for permeation enhancer research. (a) Caco-2 cells are grown on a permeable support differentiate into enterocyte-like cells with physiologically relevant tight junctions. Materials introduced into the apical chamber represent orally administered species in the intestinal lumen, while appearance in the basal chamber indicates successful transport into the bloodstream. **(b)** Mice and their gastrointestinal tracts represent the simplest animal model for oral drug delivery research. Materials can either be orally gavaged, or injected directly into the intestines to avoid digestion in the stomach. Then, blood levels of model drug or measures of drug activity (e.g. lowered blood sugar resulting from insulin) are monitored to assess degree of uptake across the intestinal epithelium.

1.5 – Objectives of This Study

The purpose of this study is to address some of the critical challenges currently facing oral protein delivery research, specifically in paracellular permeabilization of the intestinal epithelium. First, we examine the current models employed for cell culture based oral delivery experiments. Available methods for Caco-2 monolayer formation are either costly, or required several weeks of development and careful maintenance by researchers. We sought an opportunity to expedite research progress by developing a faster and less expensive, but scientifically sound (i.e. expressing physiologically relevant tight junctions) model of the epithelium. The result, the TRIM system for Caco-2 differentiation, is discussed in **Chapter 2.**

Second, we sought to better understand the structure-function relationships and mechanisms by which successful permeation enhancers open tight junctions to reversibly improve paracellular permeability. To do this, we examined a family of known permeation enhancers, the piperazines[49,72], for both toxicity and permeabilization efficacy. As reported in **Chapter 3**, both some structural and chemical factors were able to predict which of these molecules are best suited to be permeation enhancers. However, even the most promising piperazines suffered from narrow windows between minimum effective and minimum toxic concentrations, highlighting a further need for nontoxic enhancers.

Third, we set out to examine two potentially safer strategies for permeation enhancement, each born out of materials that are known to be well tolerated by the intestines: food and nanosilica. We hypothesized that, by beginning with known non-

toxic materials then screening them for permeation enhancing efficacy (rather than vice versa), we may allow ourselves greater opportunity to discover and understand well-tolerated, clinically viable permeation enhancers. Indeed, both approaches yielded reversible permeation enhancers that successfully deliver oral protein drugs in mice. In **Chapter 4**, a diverse library narrows down to a single molecule from strawberries that enables transepithelial uptake of insulin. Then, **Chapter 5** describes how silica nanoparticles can induce a known cell signaling pathway to open tight junctions and allow oral delivery of antidiabetic peptides and proteins. These two studies encapsulate the most significant contributions of this work, and the best opportunity for future development and translation into the clinic.

1.6 – References

(1) Moroz, E.; Matoori, S.; Leroux, J. C. Oral Delivery of Macromolecular Drugs: Where We Are after Almost 100years of Attempts. *Adv. Drug Deliv. Rev.* **2015**, *101*, 108–121. https://doi.org/10.1016/j.addr.2016.01.010.

(2) Morishita, M.; Peppas, N. a. Is the Oral Route Possible for Peptide and Protein Drug Delivery? *Drug Discov. Today* **2006**, *11* (19–20), 905–910. https://doi.org/10.1016/j.drudis.2006.08.005.

(3) Mclenon, J.; Rogers, M. A. M. The Fear of Needles : A Systematic Review and Meta - Analysis. *J. Adv. Nurs.* **2018**, *00*, 1–13. https://doi.org/10.1111/jan.13818.

(4) Howe, C. J.; Ratcliffe, S. J.; Tuttle, A.; Dougherty, S.; Lipman, T. H. Needle Anxiety in Children With Type 1 Diabetes and Their Mothers. *MCN, Am. J. Matern. Nurs.* **2011**, *36* (1), 25–31.

(5) Sokolowski, C. J.; Giovannitti, J. A.; Boynes, S. G. Needle Phobia: Etiology, Adverse Consequences, and Patient Management. *Dent. Clin. North Am.* **2010**, *54* (4), 731–734.

(6) Peyrot, M.; Rubin, R. R.; Kruger, D. F.; Travis, L. B. Correlates of Insulin Injection Omission. *Diabetes Care* **2010**, *33* (2), 240–245. https://doi.org/10.2337/dc09-1348.

(7) Zambanini, A.; Newson, R. B.; Maisey, M.; Feher, M. D. Injection Related Anxiety

in Insulin-Treated Diabetes. *Diabetes Res. Clin. Pract.* **1999**, *46*, 239–246.

(8) McClements, D. J.; Li, Y. Review of in Vitro Digestion Models for Rapid Screening of Emulsion-Based Systems. *Food Funct.* **2010**, *1* (1), 32–59. https://doi.org/10.1039/c0fo00111b.

(9) McClements, D. J. Encapsulation, Protection, and Delivery of Bioactive Proteins and Peptides Using Nanoparticle and Microparticle Systems: A Review. *Adv. Colloid Interface Sci.* **2018**, *253*, 1–22. https://doi.org/10.1016/j.cis.2018.02.002.

(10) Salamat-Miller, N.; Johnston, T. P. Current Strategies Used to Enhance the Paracellular Transport of Therapeutic Polypeptides across the Intestinal Epithelium. *Int. J. Pharm.* **2005**, *294* (1–2), 201–216. https://doi.org/10.1016/j.ijpharm.2005.01.022.

(11) Atuma, C.; Strugala, V.; Allen, a; Holm, L. The Adherent Gastrointestinal Mucus Gel Layer: Thickness and Physical State in Vivo. *Am. J. Physiol. Gastrointest. Liver Physiol.* **2001**, *280* (5), G922–G929.

(12) Aguirre, T. A. S.; Teijeiro-Osorio, D.; Rosa, M.; Coulter, I. S.; Alonso, M. J.; Brayden, D. J. Current Status of Selected Oral Peptide Technologies in Advanced Preclinical Development and in Clinical Trials. *Adv. Drug Deliv. Rev.* **2016**, *106*, 223–241. https://doi.org/10.1016/j.addr.2016.02.004.

(13) Yu, F.; Li, Y.; Liu, C. S.; Chen, Q.; Wang, G. H.; Guo, W.; Wu, X. E.; Li, D. H.; Wu, W. D.; Chen, X. D. Enteric-Coated Capsules Filled with Mono-Disperse Micro-Particles Containing PLGA-Lipid-PEG Nanoparticles for Oral Delivery of Insulin. *Int. J. Pharm.* **2015**, *484* (1–2), 181–191. https://doi.org/10.1016/j.ijpharm.2015.02.055.

(14) Gupta, V.; Hwang, B. H.; Lee, J.; Anselmo, A. C.; Doshi, N.; Mitragotri, S. Mucoadhesive Intestinal Devices for Oral Delivery of Salmon Calcitonin. *J. Control. Release* **2013**, *172* (3), 753–762. https://doi.org/10.1016/j.jconrel.2013.09.004.

(15) Lichtenberger, L. M. The Hydrophobic Barrier Properties of Gastrointestinal Mucus. *Annu. Rev. Physiol.* **1995**, *57* (1), 7460–7479.

(16) Sinnecker, H.; Krause, T.; Koelling, S.; Lautenschläger, I.; Frey, A. The Gut Wall Provides an Effective Barrier against Nanoparticle Uptake. *Beilstein J. Nanotechnol.* **2014**, *5*, 2092–2101. https://doi.org/10.3762/bjnano.5.218.

(17) Pawar, V. K.; Meher, J. G.; Singh, Y.; Chaurasia, M.; Surendar Reddy, B.; Chourasia, M. K. Targeting of Gastrointestinal Tract for Amended Delivery of Protein/Peptide Therapeutics: Strategies and Industrial Perspectives. *J. Control. Release* **2014**, *196*, 168–183. https://doi.org/10.1016/j.jconrel.2014.09.031.

(18) Morishita, I.; Morishita, M.; Takayama, K.; Machida, Y.; Nagai, T. Hypoglycemic Effect of Novel Oral Microspheres of Insulin with Protease Inhibitor in Normal and Diabetic Rats. *Int. J. Pharm.* **1992**, *78* (1992), 9–16.

(19) Lautenschläger, C.; Schmidt, C.; Fischer, D.; Stallmach, A. Drug Delivery

Strategies in the Therapy of Inflammatory Bowel Disease. *Adv. Drug Deliv. Rev.* **2014**, *71*, 58–76. https://doi.org/10.1016/j.addr.2013.10.001.

(20) Al-Sadi, R.; Khatib, K.; Guo, S.; Ye, D.; Youssef, M.; Ma, T. Occludin Regulates Macromolecule Flux across the Intestinal Epithelial Tight Junction Barrier. *Am. J. Physiol. Gastrointest. Liver Physiol.* **2011**, *300* (6), G1054–G1064. https://doi.org/10.1152/ajpgi.00055.2011.

(21) Shen, L.; Weber, C. R.; Raleigh, D. R.; Yu, D.; Turner, J. R. Tight Junction Pore and Leak Pathways: A Dynamic Duo. *Annu. Rev. Physiol.* **2011**, *73*, 283–309. https://doi.org/10.1146/annurev-physiol-012110-142150.

(22) Van Itallie, C. M.; Anderson, J. M. Claudins and Epithelial Paracellular Transport. *Annu. Rev. Physiol.* **2006**, *68*, 403–429. https://doi.org/10.1146/annurev.physiol.68.040104.131404.

(23) Ikenouchi, J.; Furuse, M.; Furuse, K.; Sasaki, H.; Tsukita, S.; Tsukita, S. Tricellulin Constitutes a Novel Barrier at Tricellular Contacts of Epithelial Cells. *J. Cell Biol.* **2005**, *171* (6), 939–945. https://doi.org/10.1083/jcb.200510043.

(24) Furuse, M. Molecular Basis of the Core Structure of Tight Junctions. *Cold Spring Harb. Perspect. Biol.* **2010**, *2* (1). https://doi.org/10.1101/cshperspect.a002907.

(25) Anderson, J. M.; Van Itallie, C. M. Physiology and Function of the Tight Junction. *Cold Spring Harb. Perspect. Biol.* **2009**, *1* (2), 1–16. https://doi.org/10.1101/cshperspect.a002584.

(26) Yuen, K. H. The Transit of Dosage Forms through the Small Intestine. *Int. J. Pharm.* **2010**, *395* (1–2), 9–16. https://doi.org/10.1016/j.ijpharm.2010.04.045.

(27) Press, B.; Di Grandi, D. Permeability for Intestinal Absorption: Caco-2 Assay and Related Issues. *Curr. Drug Metab.* **2008**, *9* (9), 893–900. https://doi.org/10.2174/138920008786485119.

(28) Matter, K.; Balda, M. S. Functional Analysis of Tight Junctions. *Methods* **2003**, *30* (3), 228–234. https://doi.org/10.1016/S1046-2023(03)00029-X.

(29) Mrsny, R. J. Oral Drug Delivery Research in Europe. *J. Control. Release* **2012**, *161* (2), 247–253. https://doi.org/10.1016/j.jconrel.2012.01.017.

(30) Maher, S.; Mrsny, R. J.; Brayden, D. J. Intestinal Permeation Enhancers for Oral Peptide Delivery. *Adv. Drug Deliv. Rev.* **2016**, *106*, 277–319. https://doi.org/10.1016/j.addr.2016.06.005.

(31) Whitehead, K.; Mitragotri, S. Mechanistic Analysis of Chemical Permeation Enhancers for Oral Drug Delivery. *Pharm. Res.* **2008**, *25* (6), 1412–1419. https://doi.org/10.1007/s11095-008-9542-2.

(32) Krug, S. M.; Amasheh, M.; Dittmann, I.; Christoffel, I.; Fromm, M.; Amasheh, S. Sodium Caprate as an Enhancer of Macromolecule Permeation across Tricellular Tight Junctions of Intestinal Cells. *Biomaterials* **2013**, *34* (1), 275–282. https://doi.org/10.1016/j.biomaterials.2012.09.051.

(33) Zhu, X.; Shan, W.; Zhang, P.; Jin, Y.; Guan, S.; Fan, T.; Yang, Y.; Zhou, Z.; Huang, Y. Penetratin Derivative-Based Nanocomplexes for Enhanced Intestinal Insulin Delivery. *Mol. Pharm.* **2014**, *11* (1), 317–328. https://doi.org/10.1021/mp400493b.

(34) Kamei, N.; Khafagy, E. S.; Hirose, J.; Takeda-Morishita, M. Potential of Single Cationic Amino Acid Molecule “Arginine” for Stimulating Oral Absorption of Insulin. *Int. J. Pharm.* **2017**, *521* (1–2), 176–183. https://doi.org/10.1016/j.ijpharm.2017.01.066.

(35) Zhang, Z. H.; Zhang, Y. L.; Zhou, J. P.; Lv, H. X. Solid Lipid Nanoparticles Modified with Stearic Acid-Octaarginine for Oral Administration of Insulin. *Int. J. Nanomedicine* **2012**, *7*, 3333–3339. https://doi.org/10.2147/IJN.S31711.

(36) Karamanidou, T.; Karidi, K.; Bourganis, V.; Kontonikola, K.; Kammona, O.; Kiparissides, C. Effective Incorporation of Insulin in Mucus Permeating Self-Nanoemulsifying Drug Delivery Systems. *Eur. J. Pharm. Biopharm.* **2015**, *97*, 223–229. https://doi.org/10.1016/j.ejpb.2015.04.013.

(37) Lopes, M. A.; Abrahim, B. A.; Cabral, L. M.; Rodrigues, C. R.; Seiça, R. M. F.; de Baptista Veiga, F. J.; Ribeiro, A. J. Intestinal Absorption of Insulin Nanoparticles: Contribution of M Cells. *Nanomedicine Nanotechnology, Biol. Med.* **2014**, *10* (6), 1139–1151. https://doi.org/10.1016/j.nano.2014.02.014.

(38) Zhang, Z.; Cai, H.; Liu, Z.; Yao, P. Effective Enhancement of Hypoglycemic Effect of Insulin by Liver-Targeted Nanoparticles Containing Cholic Acid-Modified Chitosan Derivative. *Mol. Pharm.* **2016**, *13* (7), 2433–2442. https://doi.org/10.1021/acs.molpharmaceut.6b00188.

(39) Bakhru, S. H.; Furtado, S.; Morello, A. P.; Mathiowitz, E. Oral Delivery of Proteins by Biodegradable Nanoparticles. *Adv. Drug Deliv. Rev.* **2013**, *65* (6), 811–821. https://doi.org/10.1016/j.addr.2013.04.006.

(40) Jepson, M. a; Clark, M. a; Foster, N.; Mason, C. M.; Bennett, M. K.; Simmons, N. L.; Hirst, B. H. Targeting to Intestinal M Cells. *J. Anat.* **1996**, *189 (Pt 3*, 507–516.

(41) Liu, M.; Zhang, J.; Shan, W.; Huang, Y. Developments of Mucus Penetrating Nanoparticles. *Asian J. Pharm. Sci.* **2014**, *10* (4), 275–282. https://doi.org/10.1016/j.ajps.2014.12.007.

(42) Shan, W.; Zhu, X.; Tao, W.; Cui, Y.; Liu, M.; Wu, L.; Li, L.; Zheng, Y.; Huang, Y. Enhanced Oral Delivery of Protein Drugs Using Zwitterion-Functionalized Nanoparticles to Overcome Both the Diffusion and Absorption Barriers. *ACS Appl. Mater. Interfaces* **2016**, *8* (38), 25444–25453. https://doi.org/10.1021/acsami.6b08183.

(43) Pereira De Sousa, I.; Steiner, C.; Schmutzler, M.; Wilcox, M. D.; Veldhuis, G. J.; Pearson, J. P.; Huck, C. W.; Salvenmoser, W.; Bernkop-Schnürch, A. Mucus Permeating Carriers: Formulation and Characterization of Highly Densely Charged Nanoparticles. *Eur. J. Pharm. Biopharm.* **2015**, *97*, 273–279. https://doi.org/10.1016/j.ejpb.2014.12.024.

(44) Pereira De Sousa, I.; Moser, T.; Steiner, C.; Fichtl, B.; Bernkop-Schnürch, A. Insulin Loaded Mucus Permeating Nanoparticles: Addressing the Surface Characteristics as Feature to Improve Mucus Permeation. *Int. J. Pharm.* **2016**, *500* (1–2), 236–244. https://doi.org/10.1016/j.ijpharm.2016.01.022.

(45) Muheem, A.; Shakeel, F.; Jahangir, M. A.; Anwar, M.; Mallick, N.; Jain, G. K.; Warsi, M. H.; Ahmad, F. J. A Review on the Strategies for Oral Delivery of Proteins and Peptides and Their Clinical Perspectives. *Saudi Pharm. J.* **2014**, *24* (4), 413–428. https://doi.org/10.1016/j.jsps.2014.06.004.

(46) Agrawal, U.; Sharma, R.; Gupta, M.; Vyas, S. P. Is Nanotechnology a Boon for Oral Drug Delivery? *Drug Discov. Today* **2014**, *19* (10), 1530–1546. https://doi.org/10.1016/j.drudis.2014.04.011.

(47) Schmidt, E.; Kelly, S. M.; van der Walle, C. F. Tight Junction Modulation and Biochemical Characterisation of the Zonula Occludens Toxin C-and N-Termini. *FEBS Lett.* **2007**, *581* (16), 2974–2980. https://doi.org/10.1016/j.febslet.2007.05.051.

(48) Zhang, J.; Zhu, X.; Jin, Y.; Shan, W.; Huang, Y. Mechanism Study of Cellular Uptake and Tight Junction Opening Mediated by Goblet Cell-Specific Trimethyl Chitosan Nanoparticles. *Mol. Pharm.* **2014**, *11* (5), 1520–1532. https://doi.org/10.1021/mp400685v.

(49) Whitehead, K.; Karr, N.; Mitragotri, S. Safe and Effective Permeation Enhancers for Oral Drug Delivery. *Pharm. Res.* **2008**, *25* (8), 1782–1788. https://doi.org/10.1007/s11095-007-9488-9.

(50) Whitehead, K.; Karr, N.; Mitragotri, S. Discovery of Synergistic Permeation Enhancers for Oral Drug Delivery. *J. Control. Release* **2008**, *128* (2), 128–133. https://doi.org/10.1016/j.jconrel.2008.03.005.

(51) Amasheh, M.; Schlichter, S.; Amasheh, S.; Mankertz, J.; Zeitz, M.; Fromm, M.; Schulzke, J. D. Quercetin Enhances Epithelial Barrier Function and Increases Claudin-4 Expression in Caco-2 Cells. *J. Nutr.* **2008**, *138* (6), 1067–1073.

(52) Chen, W.; Lu, Z.; Viljoen, A.; Hamman, J. Intestinal Drug Transport Enhancement by Aloe Vera. *Planta Med.* **2009**, *75* (6), 587–595. https://doi.org/10.1055/s-0029-1185341.

(53) Lim, S.-L.; Lim, L.-Y. Effects of Citrus Fruit Juices on Cytotoxicity and Drug Transport Pathways of Caco-2 Cell Monolayers. *Int. J. Pharm.* **2006**, *307* (1), 42–50. https://doi.org/10.1016/j.ijpharm.2005.09.017.

(54) Lea, M. a.; Ibeh, C.; DesBordes, C.; Vizzotto, M.; Cisneros-Zevallos, L.; Byrne, D. H.; Okie, W. R.; Moyer, M. P. Inhibition of Growth and Induction of Differentiation of Colon Cancer Cells by Peach and Plum Phenolic Compounds. *Anticancer Res.* **2008**, *28* (4 B), 2067–2076.

(55) Zijlstra, E.; Heinemann, L.; Plum-Mörschel, L. Oral Insulin Reloaded: A Structured Approach. *J. Diabetes Sci. Technol.* **2014**, *8* (3), 458–465.

https://doi.org/10.1177/1932296814529988.

(56) Arbit, E.; Kidron, M. Oral Insulin Delivery in a Physiologic Context: Review. *J. Diabetes Sci. Technol.* **2017**, *11* (4), 825–832. https://doi.org/10.1177/1932296817691303.

(57) Fein, K. C.; Lamson, N. G.; Whitehead, K. A. Structure-Function Analysis of Phenylpiperazine Derivatives as Intestinal Permeation Enhancers. *Pharm. Res.* **2017**, *34* (6), 1320–1329. https://doi.org/10.1007/s11095-017-2149-8.

(58) McCartney, F.; Gleeson, J. P.; Brayden, D. J. Safety Concerns over the Use of Intestinal Permeation Enhancers: A Mini-Review. *Tissue Barriers* **2016**, *4* (April), 00–00. https://doi.org/10.1080/21688370.2016.1176822.

(59) Konsoula, R.; Barile, F. a. Correlation of in Vitro Cytotoxicity with Paracellular Permeability in Caco-2 Cells. *Toxicol. Vitr.* **2005**, *19* (5), 675–684. https://doi.org/10.1016/j.tiv.2005.03.006.

(60) Konsoula, R.; Barile, F. a. Correlation of in Vitro Cytotoxicity with Paracellular Permeability in Mortal Rat Intestinal Cells. *J. Pharmacol. Toxicol. Methods* **2007**, *55* (2), 176–183. https://doi.org/10.1016/j.vascn.2006.06.001.

(61) Pinto, M.; Robine-Leon, S.; Appay, M.-D.; Kedinger, M.; Triadou, N.; Dussaulx, E.; Lacroix, B.; Simon-Assmann, P.; Haffen, K.; Fogh, J.; et al. Enterocyte-like Differentiation and Polarization of the Human Colon Carcinoma Cell Line Caco-2 in Culture. *Biol. Cell* **1983**, *47* (323), 323–330.

(62) Sambuy, Y.; De Angelis, I.; Ranaldi, G.; Scarino, M. L.; Stammati, a.; Zucco, F. The Caco-2 Cell Line as a Model of the Intestinal Barrier: Influence of Cell and Culture-Related Factors on Caco-2 Cell Functional Characteristics. *Cell Biol. Toxicol.* **2005**, *21* (1), 1–26. https://doi.org/10.1007/s10565-005-0085-6.

(63) Sun, H.; Chow, E. C.; Liu, S.; Du, Y.; Pang, K. S. The Caco-2 Cell Monolayer: Usefulness and Limitations. *Expert Opin. Drug Metab. Toxicol.* **2008**, *4* (4), 395–411. https://doi.org/10.1517/17425255.4.4.395.

(64) Salama, N. N.; Eddington, N. D.; Fasano, A. Tight Junction Modulation and Its Relationship to Drug Delivery. *Adv. Drug Deliv. Rev.* **2006**, *58* (1), 15–28. https://doi.org/10.1016/j.addr.2006.01.003.

(65) Ball, R. L.; Knapp, C. M.; Whitehead, K. a. Lipidoid Nanoparticles for SiRNA Delivery to the Intestinal Epithelium: In Vitro Investigations in a Caco-2 Model. *PLoS One* **2015**, *10* (7), e0133154. https://doi.org/10.1371/journal.pone.0133154.

(66) Hua, S.; Marks, E.; Schneider, J. J.; Keely, S. Advances in Oral Nano-Delivery Systems for Colon Targeted Drug Delivery in Inflammatory Bowel Disease: Selective Targeting to Diseased versus Healthy Tissue. *Nanomedicine Nanotechnology, Biol. Med.* **2015**, *11* (5), 1117–1132. https://doi.org/10.1016/j.nano.2015.02.018.

(67) Zhang, M.; Viennois, E.; Prasad, M.; Zhang, Y.; Wang, L.; Zhang, Z.; Han, M. K.; Xiao, B.; Xu, C.; Srinivasan, S.; et al. Edible Ginger-Derived Nanoparticles: A

Novel Therapeutic Approach for the Prevention and Treatment of Inflammatory Bowel Disease and Colitis-Associated Cancer. *Biomaterials* **2016**, *101*, 321–340. https://doi.org/10.1016/j.biomaterials.2016.06.018.

(68) Schumann, M.; Kamel, S.; Pahlitzsch, M. L.; Lebenheim, L.; May, C.; Krauss, M.; Hummel, M.; Daum, S.; Fromm, M.; Schulzke, J. D. Defective Tight Junctions in Refractory Celiac Disease. *Ann. N. Y. Acad. Sci.* **2012**, *1258* (1), 43–51. https://doi.org/10.1111/j.1749-6632.2012.06565.x.

(69) Fisichella, M.; Bérenguer, F.; Steinmetz, G.; Auffan, M.; Rose, J.; Prat, O. "Intestinal Toxicity Evaluation of TiO2 Degraded Surface-Treated Nanoparticles: A Combined Physico-Chemical and Toxicogenomics Approach in Caco-2 Cells." *Part. Fibre Toxicol.* **2012**, *9* (1), 39. https://doi.org/10.1186/1743-8977-9-39.

(70) Yu, H.; Huang, Q. Investigation of the Cytotoxicity of Food-Grade Nanoemulsions in Caco-2 Cell Monolayers and HepG2 Cells. *Food Chem.* **2013**, *141* (1), 29–33. https://doi.org/10.1016/j.foodchem.2013.03.009.

(71) Volpe, D. A. Variability in Caco-2 and MDCK Cell-Based Intestinal Permeability Assays. *J. Pharm. Sci.* **2008**, *97* (2), 712–725. https://doi.org/10.1002/jps.21010.

(72) Bzik, V. A.; Brayden, D. J. An Assessment of the Permeation Enhancer, 1-Phenyl-Piperazine (PPZ), on Paracellular Flux Across Rat Intestinal Mucosae in Ussing Chambers. *Pharm. Res.* **2016**, *33* (10), 2506–2516. https://doi.org/10.1007/s11095-016-1975-4.

Chapter 2:

Thrifty, Rapid Intestinal Monolayers (TRIM) for Oral Drug Delivery Research on Caco-2 Epithelial Cells

2.1 – Introduction

Caco-2 monolayers are the most common cell culture model for intestinal research[1–6]. However, most currently available Caco-2 systems are expensive and/or labor intensive to develop. With hundreds of new publications relying on these cells every year[7] (**Figure 2.1**), there is a major need to streamline the monolayer assay for more efficient intestinal research.

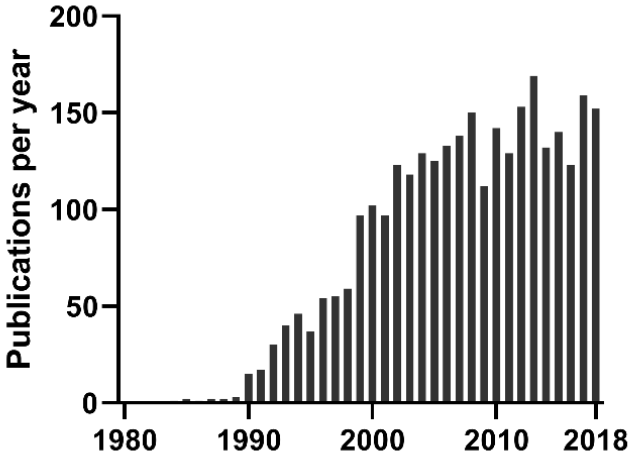

Figure 2.1: Medline Trends data for "Caco-2 Monolayers." Accessed March 2019

Traditionally, Caco-2 monolayers are seeded and maintained in antibiotic-free media for 21 days to allow full differentiation and tight junction formation[8,9]. These monolayers are well-established and highly characterized, but the tri-weekly media changes are tedious and often lead to bacterial or fungal infection in the cultures. To address this, Corning® introduced the Biocoat® Intestinal Epithelium Differentiation

Environment (BIEDE) in 1997, enabling Caco-2 monolayers to differentiate in only three days while maintaining strong correlation to the permeability of 21-day monolayers[10]. However, the BIEDE system and its current iteration, called Biocoat® HTS monolayers, carry much higher price tags than the traditional 21-day monolayers, potentially limiting the productivity of labs that depend on them for their experiments. As a result, in the approximately two decades since, many labs have developed and characterized their own monolayer systems[11–14]. However, it remains unclear how the systems compare to the traditional monolayers for different assay types (e.g. gene expression vs. permeability) and final costs.

Here, we investigated two possible strategies for reducing costs and time input for Caco-2 research and examine their effects on behavior of the resulting monolayers. First, we evaluate the fetal bovine serum (FBS) alternative FB Essence (FBE) for reduction of cell line maintenance expenses. 10% FBS has long been the standard serum addition to DMEM for Caco-2 cell culture media[15], but its use incurs skyrocketing costs, composition uncertainty, and ethical dilemmas regarding the fetal calf sourcing[16]. Unfortunately, the FB Essence cannot sustain dividing cells past approximately 10 passages and is not a viable long-term solution. Second, we describe a new variation of 3-day Caco-2 epithelia, which we have deemed thrifty, rapid intestinal monolayers (TRIM). TRIM represent a current minimum of time and money input to achieve fully-formed Caco-2 monolayers. Here, we will describe the process of their formation and assess how their gene expression and permeability behavior compare to two other common Caco-2 models: 21-day monolayers and the Corning HTS 3-day system.

2.2 – Methods

2.2.1 – Materials

Penicillin/streptomycin, trypsin-ethylenediaminetetraacetic acid (trypsin-EDTA), phosphate buffer saline (PBS), rat tail Collagen I, calcein, DAPI, Hoechst 33342, Alexa Fluor® 488 Phalloidin, Alexa Fluor® 488 anti-Claudin-1 antibodies, Alexa Fluor® 594 Anti-ZO-1 antibodies, and ClearMount™ solution were purchased from Life Technologies® (Thermo Fisher subsidiary, Carlsbad, CA, USA). The cDNA reverse transcriptase kit (Applied Biosystems) and primers for GAPDH (Hs02758991_g1), ZO-1 (Hs01551861_m1), and Claudin-1 (Hs00221623_m1) were also ordered from Life Technologies using the best coverage primer/probe set. Caco-2 cells were purchased from American Type Culture Collection® (ATCC, Manassas, VA, USA). Dulbecco's Modified Eagles Medium (DMEM), fetal bovine serum (FBS), Seradigm FB Essence (FBE), Falcon® 225 cm^2 tissue culture flasks, Corning® 1.0 µm porous support Transwell® plates and HTS plate kits, Falcon® 24-well plates, sodium butyrate, MITO+ serum extender, and Rhodamine 123 (Rhod123) were obtained from VWR® (Radnor, PA, USA). 4 kDa FITC-labelled dextran (FITC-DX4), p-Nitrophenyl phosphate (p-NPP), p-nitrophenol (p-NP), 1-phenylpiperazine (PPZ), low molecular weight chitosan, and sodium lauryl sulfate (SLS) were purchased from Sigma-Aldrich® (St. Louis, MO, USA).

2.2.2 – Caco-2 Cell Culture

Caco-2 lines were screened to ensure mycoplasma-free conditions by direct DNA staining with Hoechst 33342[17]. Cells were cultured in DMEM supplemented with 10% FBS, 100 IU/mL of penicillin, 0.1 mg/mL streptomycin, and 0.25 µg/mL

Amphotericin B (“Caco-2 media”). Cultures were incubated at 37°C in 5% CO_2 and 100% relative humidity. The cells were subcultured with 0.25% trypsin-EDTA and subsequent passaging every 3 to 4 days at ratios between 1:3 and 1:8. Cells at passage numbers 20–60 were utilized for experiments.

2.2.3 – Cell Proliferation Experiments

Caco-2 lines at p30 were transferred into media containing 10% FBS, 5% FBE, 10% FBE, 15% FBE, or 20% FBE in DMEM. All media also contained 100 IU/mL of penicillin, 0.1 mg/mL streptomycin, and 0.25 µg/mL Amphotericin B. Each group of cells was maintained for several more passages in its respective media composition. At passage numbers 32, 37, and 40, the cells were seeded into 24-well plates at 1.5×10^5 cells/well in their respective media compositions. Every day for four days, three wells of each cell population were trypsinized and counted using a hemacytometer.

2.2.4 – Collagen Coating for Transwell Plates

Transwell inserts were coated with collagen I from rat tails per the supplier-provided thin coating procedure. Briefly, collagen (5 µg per cm^2 of transwell membrane surface) was diluted into 20 mM acetic acid solution. The mixture was added to the apical compartments of the wells and incubated at room temperature for one hour. Plates were then rinsed three times with PBS and either used immediately or dried under sterile conditions and stored at 4°C for up to three months.

2.2.5 – HTS Monolayers

Cells were suspended in basal seeding medium (BSM) provided in the HTS kit, seeded at a density of 2×10^5 cells per well in the supplied HTS plate, and incubated for 24-48 hours. The media was then changed to the enterocyte differentiation medium (EDM) and incubated for 48 hours. The trans-epithelial electrical resistance (TEER) was monitored to confirm proper barrier formation, and only monolayers with initial TEER values of 150-750 $\Omega\cdot cm^2$ ("acceptable range"[18]) were utilized for further experiments.

2.2.6 – TRIM Monolayers

Cells were suspended in DMEM supplemented with MITO+ serum extender according to the manufacturer's instructions (basal seeding medium, BSM). They were seeded at a density of 2×10^5 cells per well on collagen-coated transwell supports, and incubated for 24-48 hours. The media was then changed to DMEM supplemented with MITO+ and 2 mM sodium butyrate (enterocyte differentiation medium, EDM) and incubated for 48 hours. The TEER was monitored and only monolayers with initial TEER values of 150-750 $\Omega\cdot cm^2$ were utilized for further experiments.

2.2.7 – 21-Day Monolayers

Cells were suspended in DMEM supplemented with 10% FBS ("21-day media") and seeded at a density of 2×10^5 cells per well on collagen-coated transwell supports. The media was then aspirated and replaced every 2-3 days for 21 days. The TEER was monitored to confirm proper barrier formation, and only monolayers with initial TEER values of 150-750 $\Omega\cdot cm^2$ were utilized for further experiments.

2.2.8 – Monolayer Permeability and Permeation Enhancer Experiments

Caco-2 monolayer trays were transferred to 24-well plates containing 1 mL DMEM per well and were allowed to equilibrate for 30 minutes before recording TEER values using a Millicell® voltohmmeter. Fluorescent paracellular diffusion markers were applied at 0.5 mM (calcein), 0.2 mM (FITC-DX4), or 0.1 mM (Rhod123) into the apical side of the monolayers. After one hour, media in the basal chambers was sampled and its fluorescence was measured at 495/515 nm (calcein), 485/515 nm (FITC-DX4), or 510/535 nm (Rhod123) using a Biotek Synergy2 plate reader. Application of calibration curves yielded the amount of mass transferred across each monolayer, which was used in the permeability equation $P_{app} = \frac{\Delta M}{C_a A \Delta t}$, where P_{app} is the apparent permeability through the monolayer, ΔM is the marker mass accumulated in the basal compartment, C_a is the apical marker concentration, A is the monolayer area, and Δt is the time between samples.

To characterize the effects of permeation enhancers, chitosan (1 mg/mL), SLS (0.1 mg/mL), or PPZ (1 mg/mL) was dissolved in EDM and applied to the apical chambers with the fluorescent markers. Negative control wells received fresh EDM. DMEM in the basal compartments was refreshed once per hour to maintain sink conditions for diffusion. TEER and permeability measurements are expressed as the ratio of each monolayer's permeability for the first hour after permeation enhancer addition to its permeability before treatment, normalized to any change in untreated control monolayers during that time.

2.2.9 – Alkaline Phosphatase Activity Assay

Alkaline phosphatase activity was measured as previously described[19]. Briefly, monolayers or mouse intestinal segments were washed with calcium- and magnesium-supplemented PBS. A reaction buffer containing p-nitrophenyl phosphate (p-NPP) was added, and the samples were incubated at room temperature. Ten minutes later, 100 µL buffer samples from each well were transferred to a 96-well plate, with 50 µL/well of 0.5 M NaOH, and the temperature was decreased to 4°C to halt the reaction. The plate reader was used to measure the absorbance of the samples at 405 nm, which was compared to a calibration curve of p-nitrophenol (p-NP) to determine the amount of p-NPP degraded by alkaline phosphatase. For monolayers, the amount of p-NP produced was normalized to the area of the porous membrane filter. For intestinal samples, the size of the section and a surface amplification factor for the villi [20] were used to determine epithelial area for normalization.

2.2.10 – Gene Expression by qPCR

RNA was isolated from Caco-2 cells, monolayers, and mouse intestinal segments using Qiagen RNeasy Kit according to the manufacturer's protocol. Reverse transcriptase PCR was carried out using the high capacity cDNA reverse transcription kit according to the manufacturer's protocol.

Quantitative PCR (qPCR) was performed using the ViiA 7 Real-Time PCR system and Taqman universal PCR master mix (Applied Biosystems). Each qPCR reaction contained a total reaction volume of 20 µL (100 ng cDNA + 10 µL Taqman mastermix + 1 µL Taqman endogenous control + 1 µL Taqman gene expression). All

runs were performed in comparative Ct mode with a temperature profile of 50°C for 2 minutes, 95°C for 10 minutes, and 40 cycles of [95°C for 15 seconds and 60°C for 1 minute]. All qPCR samples were tested with three biological replicates and three technical replicates each. The expression of each tight junction mRNA was normalized to expression of the housekeeping gene GAPDH and is displayed relative to expression levels for undifferentiated Caco-2 cells.

2.2.11 – Confocal Microscopy

Monolayers or excised intestines were rinsed with PBS and fixed in 4% formaldehyde. They were permeabilized with 0.2% Triton-X100 and blocked with 0.2% BSA solution to limit non-specific antibody binding, then incubated for one hour with staining solutions. The staining solutions contained Hoescht 33342 (20 nM, 350 nm/461 nm) to mark nucleic acids, AlexaFluor 488® Phalloidin (5 units/mL, 495 nm/518 nm) to label actin, AlexaFluor 488® Anti-Claudin 1 antibodies (50 µg/mL, 495 nm/518 nm), and/or AlexaFluor® 594 Anti-ZO-1 antibodies (50 µg/mL, 590 nm/617 nm) in PBS with 0.2% BSA. After staining, the monolayers were mounted on slides using ClearMount™ solution and sealed under coverslips using clear nail polish, while intestinal segments were suspended in PBS and mounted to slides using rubber spacers.

Prepared slides were imaged at 63x magnification using a Zeiss LSM 700 confocal microscope with ZEN 2012 SP1 software. Images were captured using a Plan-Apochromat 63x/1.40 Oil DIC objective and an X-Cite Series 120Q laser source exposing at 405, 488, and 555 nm. ImageJ (NIH) image processing software was used to prepare confocal images for publication. Upper and lower thresholds were narrowed

slightly to remove background noise and improve visibility of the signals. All images were processed with the same thresholds and display lookup tables (LUTs), which were linear throughout their ranges. Images were converted from their original 16-bit format to RGB color for saving and arrangement into figures. No other manipulations were performed.

2.2.12 – Mouse Studies

All mouse experiments were approved by the institutional animal care and use committee (IACUC) at Carnegie Mellon University (Pittsburgh, PA, USA) under protocol number PROTO201600017 and performed in accordance with all institutional, local, and federal regulations. C57BL/6 mice were either purchased from Charles River Laboratories (Wilmington, MA, USA) or obtained from an institutionally managed breeding colony. Prior to experiments, mice were housed in cages of no more than five animals, with controlled temperature (25°C), 12 hour light-dark cycles, and free access to food and water. Mice utilized in this study were male and 12-21 weeks old. Mice were fasted 12 hours the night before an experiment to limit the variability caused by food matter and feces in the gastrointestinal tract.

2.2.13 – Intestinal Permeability to Dextran

For dextran permeability studies, fasted mice were anesthetized and their intestines surgically exposed. They received direct injections (2 µL/g volume) of permeation enhancers (200 mg/kg dose of SLS, 32.4 mg/kg PPZ, PBS control) and FITC-DX4 (10 mg/kg). At 0.5, 1.5, and 4 hours post-injection, blood was collected and

centrifuged. The FITC concentration in the serum was measured by reading for fluorescence on the plate reader (485/515 nm) and comparing to a unique calibration curve for each experiment. The relative area under the curve (AUC) was calculated by integrating the serum FITC-DX4 concentration from 0-4 hours after injection.

2.2.14 – Statistics

All data presented as arithmetic mean of the given "n" number of biological replicates (individual animals or number of *in vitro* cell culture wells), and error bars display the standard error of the mean. For statistical significance, two-tailed Student's t-tests were used to calculate p values.

2.3 – Results and Discussion

2.3.1 – FB Essence for Reduced Cell Line Maintenance Costs

We began by exploring whether FB Essence (FBE) could be used to replace fetal bovine serum (FBS) in the ongoing maintenance of the Caco-2 cell line. To do this, we first optimized FBE content for Caco-2 growth and proliferation. Caco-2 cells at passage number 30, previously growing in standard 10% FBS-supplemented media, were split into five groups: one continued in 10% FBS media and the others transferred into flasks with 5%, 10%, 15%, or 20% FBE. At pre-determined passage numbers, cells were examined for their proliferative ability. After two passages (**Figure 2.2a**) and seven passages (**Figure 2.2b**), the cells growing in 15% FBE media outperformed each of the other FBE groups although they still lagged behind the cells in the FBS control media. To this end, the FBE cell flasks required higher passage ratios to maintain the same

schedule as the FBS controls (e.g. a 1:3 split instead of 1:4 or 1:6 to cover the same three day span). Surprisingly, at between seven and nine passages in the FBE media, most of the cells stopped dividing altogether. Only the 15% FBE group survived to ten passages, but even those cells lost the ability to adhere and proliferate (**Figure 2.2c**). This is consistent with the eventual decline in cell growth seen in studies of other FBS alternatives for Caco-2 proliferation[15]. Thus, FBE can be used to supplement media for short-term Caco-2 maintenance, but it should not be used for long-term propagation of the cell line.

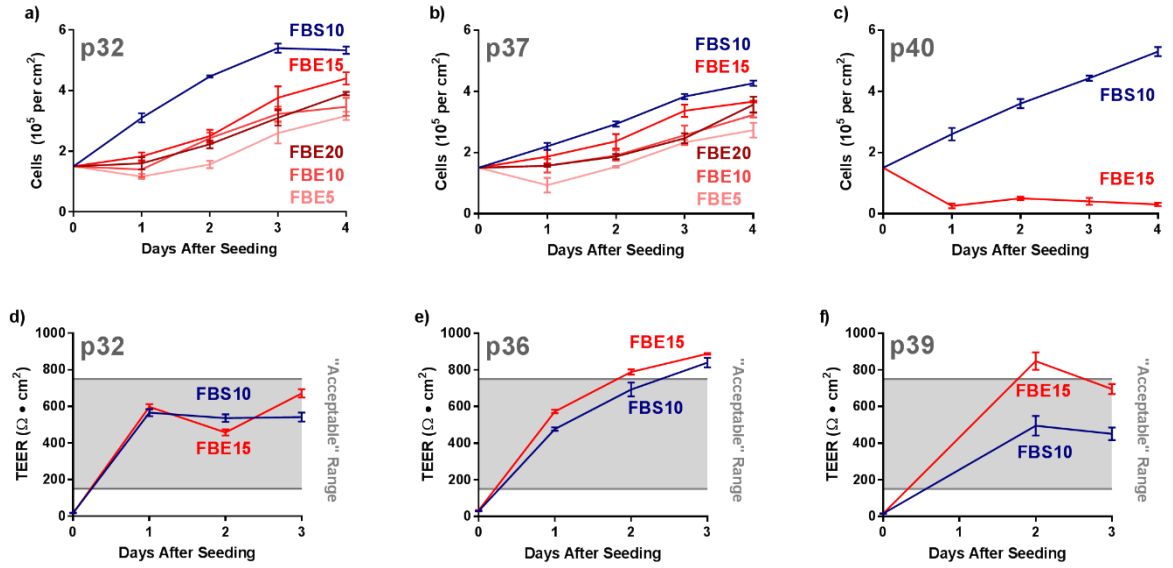

Figure 2.2: **Lower-cost FBS alternative FB Essence (FBE) is of limited use in maintaining Caco-2 cells for intestinal monolayer production.** All graphs compare Caco-2 cells originating from the same population (i.e. growing in the same flask) until the split into different bottles containing different FBS and FBE content media at passage 30 (p30). **(a)** At two passages **(b)** and seven passages after transfer into media containing varying amounts of FBE, cells growing in 15% FBE (FBE15) proliferate at almost the same rate as cells growing in the traditional 10% FBS (FBS10). **(c)** However, by ten passages in the 15% FBE media, the cells cease to grow and divide. **(d)** At two passages, **(e)** six passages, and **(f)** nine passages after transfer, the Caco-2 cells growing in 15% FBE media maintained their ability to form comparable monolayers to cells grown in 10% FBS, as demonstrated by similar transepithelial electrical resistance (TEER). Error bars display s.e.m. (n = 3 for cell proliferation, n = 24 for TEER).

Because 15% FBE was adequate for short-term Caco-2 maintenance, we hypothesized that cells cultured with this serum composition would also be able to differentiate into monolayers, at least for as long as their ability to proliferate persisted. To test this, we examined both the 15% FBE cell population and the 10% FBS control on the established, 3-day HTS Transwell® monolayer system from Corning®. After two (**Figure 2.2d**) and six (**Figure 2.2e**) passages, there was little difference between the two populations, as evidenced by the development of similar transepithelial electrical resistance (TEER). TEER measures the ability of ions to pass through the monolayers and has been shown to correlate inversely with permeability through the tight junctions[21,22]. Thus, higher TEER relates to more complete formation of tight junctions within the monolayers[23,24]. Interestingly, even as their proliferation slowed, the cells cultured in 15% FBE media formed proper monolayers (**Figure 2.2f**). Most likely, this is due to the high seeding density of the HTS system allowing the cells to achieve confluence on the transwell membrane without needing to divide.

Based on their comparable TEER behavior to current Caco-2 models, cells from 15% FBE media could likely be used as a short-term measure for cost saving. However, the decline of cell populations after around 10 passages means that any lab using them would need a continuously maintained, separate line of Caco-2 in FBS or enough cells stored to thaw new populations of cells each month. On top of this complication of operations, the only successful media formulation using FBE required a higher concentration (15%) than the formulation using FBS (10%). As of March 2019, the cost of FBE is approximately half that of FBS. For most labs, the resulting 25% reduction in serum costs would likely not outweigh the cost increases associated with the shortened

life of the cell line or the possibility that FBE alters long-term gene expression in the cell line.

2.3.2 – TRIM as an Alternative to HTS and 21-Day Monolayers

As a second strategy for reducing both time and monetary costs associated with using Caco-2 for *in vitro* screening, we developed a system deemed thrifty, rapid intestinal monolayers (TRIM). As with any new model, we set out to determine how its behavior compared to both established cell culture models and the bodily tissues they are meant to represent. To start, we examined the development of TEER over the course of TRIM formation compared to the same cells differentiating into two established Caco-2 models: Corning® HTS, and 21-day monolayers. TRIM (**Figure 2.3a**) and HTS (**Figure 2.3b**) demonstrated similar behavior, with TEER reaching the acceptable range within 24 hours and persisting for three days, regardless of cell passage number. Similarly, 21-day monolayers achieved high TEER values within 2-3 days after seeding (**Figure 2.3c**), and held them through the rest of the designated junction maturation period, provided they did not become infected during that time. Across each of the systems, TEER was within the acceptable resistance range on the pre-determined experiment day in almost all iterations of monolayer development (**Figure 2.3d**).

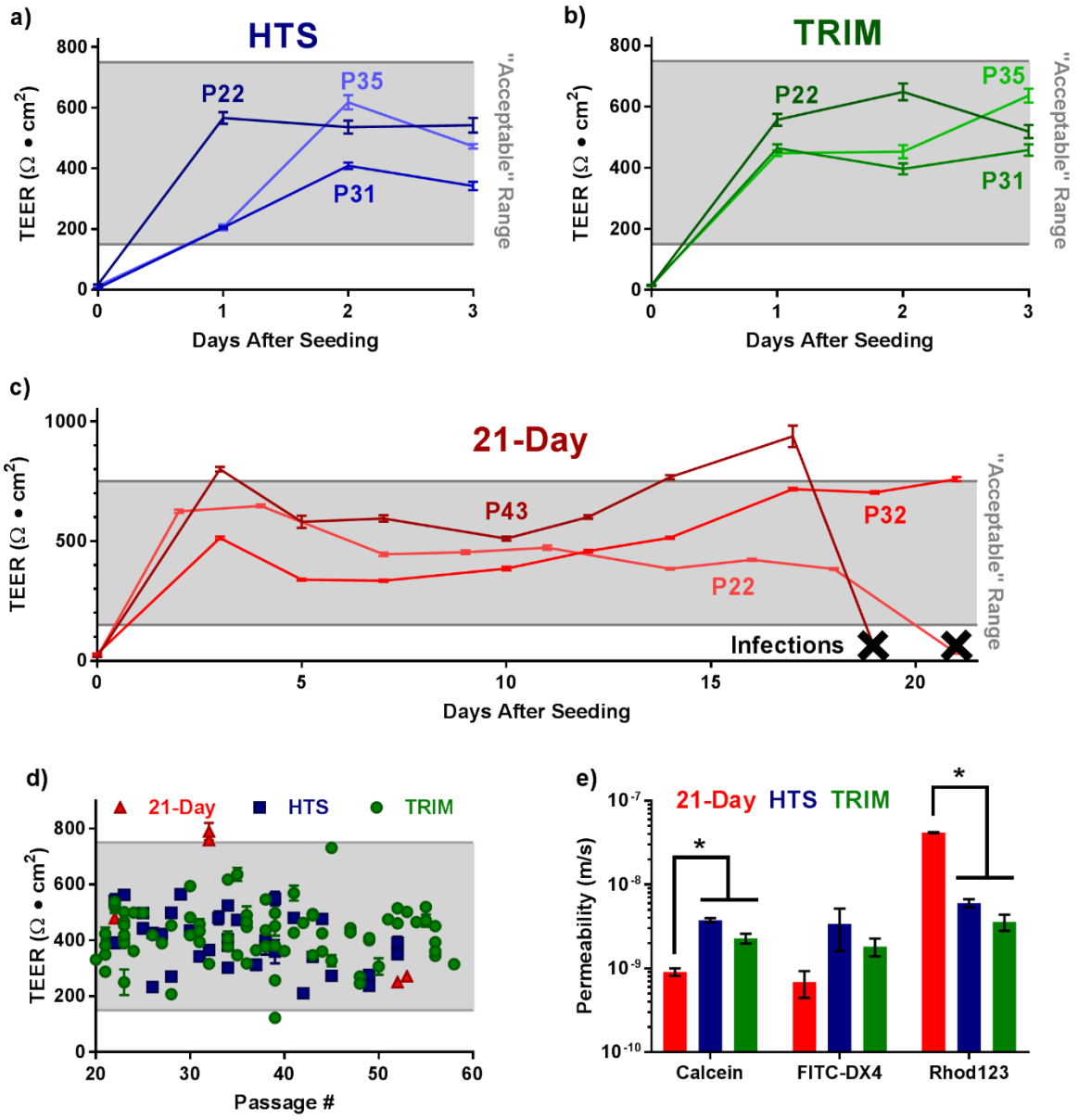

Figure 2.3: **TEER develops at similar rates and to similar final values, but permeability to marker molecules differs between monolayer systems. (a)** In the HTS system, passage number causes early discrepancies in barrier quality, but these differences diminish by the third day. **(b)** In contrast, passage number has little effect on the development of TRIM monolayers. **(c)** 21-day monolayers attain high barrier function by the third day, regardless of passage number, and maintain high TEER as the cells continue to differentiate. However, high rates of infection among 21-day plates leads to failure of many monolayers. **(d)** The vast majority of all monolayers from each of the three systems achieved the "accepted range" of TEER values. Each point represents an entire, 24-well plate of monolayers, and data for the 21-day system is limited due to the high rate of infection. **(e)** Monolayers from the 21-day system exhibit lower paracellular permeability to calcein and 4 kDa FITC-Dextran (FITC-DX4) and higher transcellular permeability to Rhodamine 123 than the 3-day systems. Error bars display s.e.m. (n = 24 for TEER, n = 3 for permeability). * $p < 0.05$ by two-tailed t-test.

In addition to TEER development, apical-to-basal permeability of diffusion marker molecules is a critical experimental characteristic that we wanted to understand in the context of each of these three systems. First, we examined the permeation of two hydrophilic molecules through the tight junctions: calcein (~620 Da) and 4 kDa, FITC-labelled dextran (FITC-DX4). In both cases, paracellular transport was comparable across all three monolayer systems, registering within the same order of magnitude (**Figure 2.3e**), though the tight junctions developed in the 21-day system were slightly better at excluding both molecules. To assess transcellular permeability, we next applied the fluorescent marker rhodamine 123 (Rhod123) to the apical side of monolayers. Rhod123 is sufficiently hydrophobic to diffuse through the cell membrane and is a known P-glycoprotein (P-gp) substrate[13]. Thus, increased Rhod123 transport in the apical to basal direction indicates that less P-gp efflux activity is pumping the marker from the cytosol back into the apical compartment. Permeability of Rhod123 was substantially higher in 21-day monolayers than in HTS or TRIM (**Figure 2.3e**). This has been previously reported with other abbreviated monolayer systems[13] and implies that such monolayers have greater P-gp activity.

2.3.3 – Gene Expression in Monolayer Models

The observed differences in P-gp activity prompted us to question how TRIM development affects gene expression of various proteins when compared to other monolayer models, as well as actual intestines. To begin, we examined the activity of alkaline phosphatase, a brush border enzyme used as a differentiation marker for Caco-2 cells[19,25,26], by measuring conversion of p-nitrophenyl phosphate (p-NPP) to p-

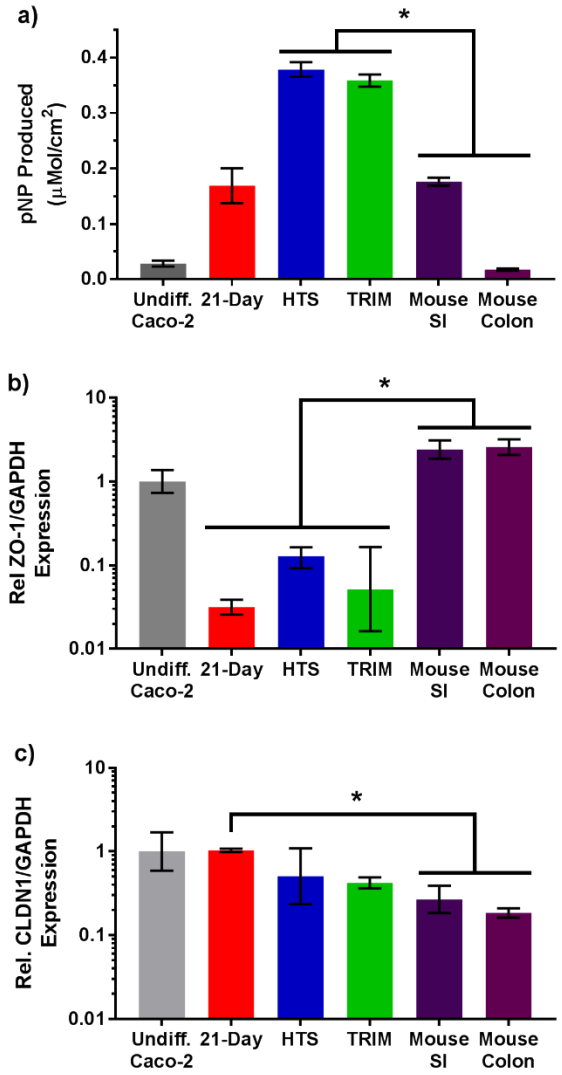

Figure 2.4: Gene expression varies between different monolayer systems and between Caco-2 and intestinal tissue. (a) Activity of alkaline phosphatase, a common differentiation marker for intestinal enterocytes, is significantly higher in 3-day monolayer systems than in 21-day monolayers or mouse intestinal mucosa. **(b)** In all cases, Caco-2 monolayers exhibited less expression of tight junction protein ZO-1 than intestinal cells taken from mouse intestines. **(c)** While claudin-1 expression was similar between 3-day monolayer systems and mouse small intestines, 21-day monolayers exhibited higher CLDN1 levels. Error bars display s.e.m. (n = 3). * $p < 0.05$ by two-tailed t-test.

nitrophenol (p-NP) (**Figure 2.4a**). TRIM exhibited approximately the same enzyme activity as the HTS monolayers, and both were significantly higher than 21-day monolayers and mouse small intestines. Interestingly, colon samples expressed even less enzyme activity, though it should be noted that data for mouse intestinal samples rely on application of published conversion factors for epithelial surface area[20], which introduces some uncertainty as to the absolute values.

Two other proteins of interest in the intestinal epithelium are the tight junction proteins ZO-1, which anchors junctions to the cytoskeleton, and Claudin 1, which partially spans the intercellular junction space[23]. Here, we discovered that ZO-1 expression is consistent between TRIM, HTS, and 21-day monolayers (**Figure 2.4b**), though it is far lower in all three systems than in mouse

colon or intestines. In contrast, expression of Claudin 1 is comparable between TRIM, HTS, and small intestines (**Figure 2 4c**), while 21-day monolayers may slightly overexpress the gene. Taken together, these differences in protein activity and expression show that no single monolayer system provides a completely accurate representation of *in vivo* intestines, and care should be taken in choosing the appropriate assay for a given experiment.

2.3.4 – Imaging Analysis of Monolayer Tight Junctions

Having observed significant differences in the gene expression of tight junction proteins among the five models, we were curious as to how TRIM would compare to the other models in the spatial arrangement of the junction proteins. We used confocal microscopy to visualize nuclei, actin, ZO-1, and Claudin 1 (**Figure 2.5**). Phalloidin and DAPI staining revealed few differences in morphology across the five samples, though the nuclei in the 21-day system were smaller and more irregular than those in the other models. In contrast, the ZO-1 encircling the cells at the tight junctions was noticeably variable. In the 21-day monolayers and excised intestines, the ZO-1 smoothly and regularly ringed the cells, while in both TRIM and HTS monolayers, the ZO-1 displayed ruffling at the edges of the cells. This change in morphology has previously been seen in Caco-2 cells treated with nanostructures to open the tight junctions [27], suggesting a connection between the ruffling observed in the images of TRIM and HTS monolayers and the slightly higher tight junction permeability to calcein and FITC-DX4 observed in this study (**Figure 2.3e**). Finally, as we predicted based on the gene expression experiments in the previous section, the signal for Claudin 1 was strongest in 21-day

monolayers and weakest in the colon, with TRIM showing weak but observable staining around the cell perimeters (**Figure 2.5**). These differences in protein localization and morphology again indicate that TRIM and other monolayer systems each have particular strengths and weaknesses with respect to representing the intestinal epithelium accurately.

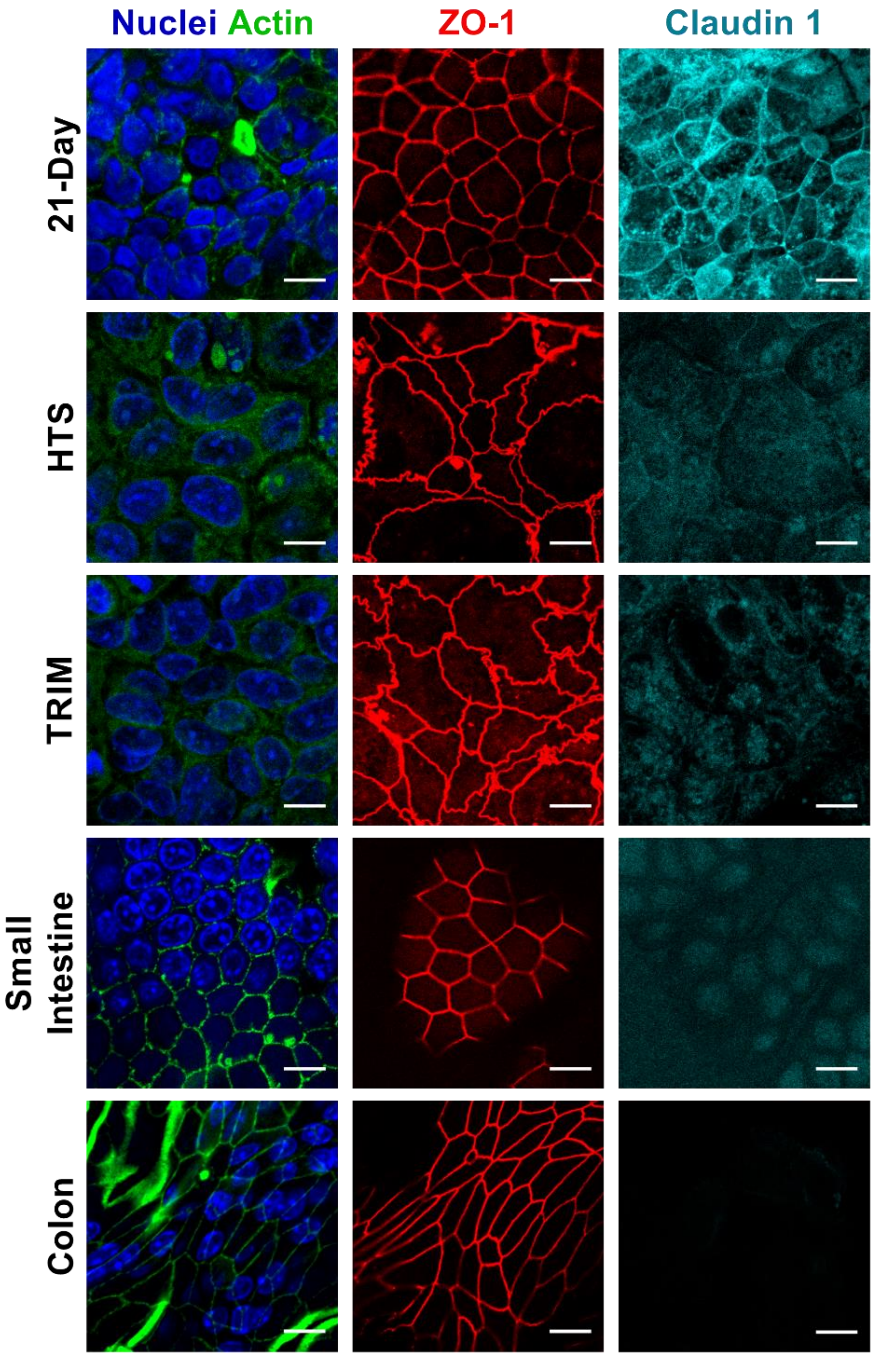

Figure 2.5: 3-day Caco-2 systems develop similar tight junctions, but differ slightly from 21-day systems as observed by confocal microscopy. Among the three types of monolayers, the shape and arrangement of nuclei and actin displayed no notable differences. However, the tight junction protein ZO-1 forms predominantly straight, smooth structures in the 21-day system, while both 3-day systems display ruffling in the ZO-1 pattern. Another tight junction protein, Claudin 1 is much more clearly expressed in the 21-day system than in the 3-day systems. In HTS and TRIM monolayers, as well as both intestinal segments, the Claudin 1 signal is so faint that it is barely indistinguishable from background fluorescence. Scale bars = 10 μm.

2.3.5 – Utility in Permeation Enhancer Screening

Given the observed differences between tight junction expression and morphology, we ultimately asked how the models would differ in their predictions of permeation enhancer efficacy. The monolayers were treated with three permeation enhancers, each known to increase paracellular permeability[21,28–31]: chitosan, 1-phenylpiperazine (PPZ), and sodium lauryl sulfate (SLS). As measured by TEER, 21-day monolayers were consistently less affected by the paracellular permeation enhancers than TRIM or HTS monolayers (**Figure 2.6a**), likely due in part to differences in how tight junction proteins are expressed in each system. This trend was confirmed by increased passage of the diffusion marker calcein through treated TRIM and HTS monolayers (**Figure 2.6b**). The 21-day monolayers did not indicate a significant increase in transport for any of the three permeation enhancers. When evaluated *in*

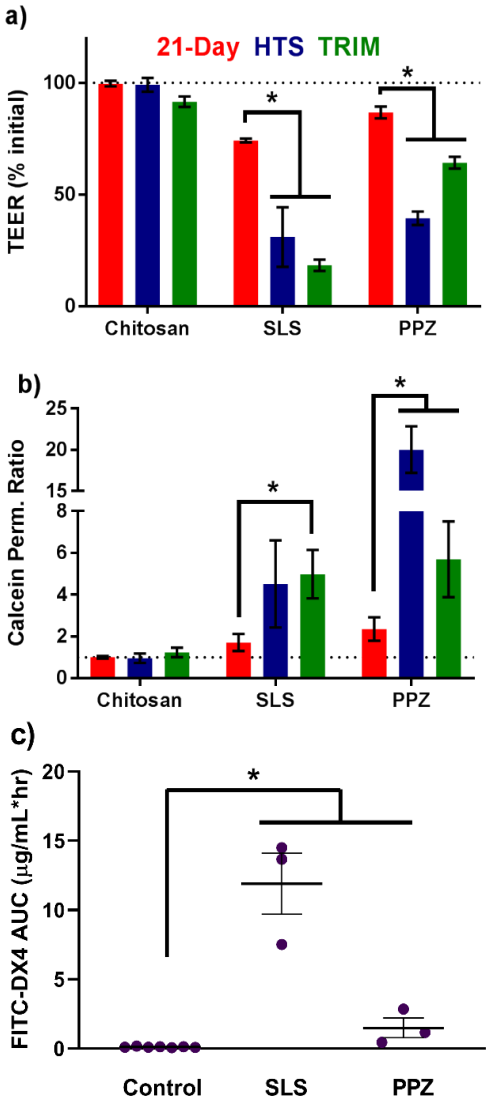

Figure 2.6: **Caco-2 response to chemical permeation enhancers is dependent on the monolayer system used. (a)** By trans-epithelial electrical resistance (TEER), the 3-day monolayer systems indicated greater permeation enhancing power of species tested than did the 21-day monolayers. **(b)** The standard relationship of lower TEER corresponding with higher mass permeability held up across all three monolayer systems. **(c)** As predicted by the 3-day monolayer systems, SLS and PPZ enhanced accumulation of intestinally injected FITC-DX4 in the bloodstream of mice. Error bars display s.e.m. (n = 3 for cells, n = 3-7 for mice). * $p < 0.05$

vivo via direct injection into the intestines of mice, the SLS and PPZ permeation enhancers significantly increased the transport of the FITC-DX4 from the intestines to the bloodstream, as predicted by the behavior of the TRIM and HTS systems. As a result, enhancer-treated mice displayed higher areas under the curve (AUCs) for FITC-DX4 in the bloodstream (**Figure 2.6c**). This indicates that these systems are particularly useful for screening permeation enhancers before advancing to animal models[32].

2.3.6 – Relative Costs of Monolayer Development

Because each of the three monolayer systems examined here have distinct strengths and weaknesses, we anticipate that cost and time input will be an important factor for experimental design in many studies. Based on supply costs as of March 2019, TRIM are the least expensive monolayers to produce, followed by 21-day at 50% higher costs, and HTS at 200% higher (**Table 2.1**). Even for just one graduate student operating at a rate of one experiment per week, this adds up to over $800 per month savings using TRIM over HTS. There is a slight trade off in time input, as TRIM require an extra 12 minutes per plate for collagen

Table 2.1: Cost and time comparisons among 24-well, Caco-2 monolayer systems. Costs are based on prices as of March 2019. Calculations do not include cost or time associated with ongiong maintenance of the cell line.

	21-Day	HTS	TRIM
Transwell Plate	100.94		100.94
Collagen	0.14		0.14
Acetic Acid	0.01		0.01
HTS Plate Kit		338.33	
DMEM	4.32	1.3	3.12
FBS	58.76		
Sodium Butyrate			0.08
MITO+			4.26
Cost Total (USD)	**164.17**	**339.63**	**108.55**
	21-Day	**HTS**	**TRIM**
Collagen Coating	12		12
Preparing Media	10	5	10
Seeding Cells	40	40	40
Media Changes	160	15	15
Time Total (Min)	222	60	77
Time Total (Hours)	**3.7**	**1**	**1.3**

coating (**Table 2.1**), when performed in batches of 5. However, TRIM clock in at just over one hour per plate, while 21-day monolayers require nearly four hours over three weeks. On top of this, 21-day plates are highly prone to infection, as we have shown here (**Figure 2.3c**). The high failure rate further increases the time input to 5-8 hours per successful monolayer plate, greatly exceeding the approximate one hour for HTS and TRIM.

2.4 – Conclusions and Outlook

The ongoing development of faster, less expensive Caco-2 epithelial models is critical to accelerating research for gastrointestinal disease and oral drug delivery. Like many other serum alternatives, FB Essence does not provide a long-term, cost-saving strategy for Caco-2 culture. However, TRIM and HTS monolayer systems offer experimentally comparable and less labor intensive alternatives to 21-day monolayers, especially for research examining intestinal permeability. Furthermore, TRIM can be constructed for less than one third of the cost of HTS monolayers. For the particular characteristics studied here, each system had its own strengths and weaknesses as models of actual intestinal tissue. To this end, Caco-2 monolayers will not always accurately predict the extent of permeability change or gene expression in an actual intestine, but they are critical tools for screening technologies prior to *in vivo* experimentation, thus reducing the number of animals used[32]. Within this realm of cell culture epithelia, TRIM produce valuable results while allowing researchers to trim both money and time inputs from their research.

2.5 – References

(1) Salama, N. N.; Eddington, N. D.; Fasano, A. Tight Junction Modulation and Its Relationship to Drug Delivery. *Adv. Drug Deliv. Rev.* **2006**, *58* (1), 15–28. https://doi.org/10.1016/j.addr.2006.01.003.

(2) Ball, R. L.; Knapp, C. M.; Whitehead, K. a. Lipidoid Nanoparticles for SiRNA Delivery to the Intestinal Epithelium: In Vitro Investigations in a Caco-2 Model. *PLoS One* **2015**, *10* (7), e0133154. https://doi.org/10.1371/journal.pone.0133154.

(3) Zhang, M.; Viennois, E.; Prasad, M.; Zhang, Y.; Wang, L.; Zhang, Z.; Han, M. K.; Xiao, B.; Xu, C.; Srinivasan, S.; et al. Edible Ginger-Derived Nanoparticles: A Novel Therapeutic Approach for the Prevention and Treatment of Inflammatory Bowel Disease and Colitis-Associated Cancer. *Biomaterials* **2016**, *101*, 321–340. https://doi.org/10.1016/j.biomaterials.2016.06.018.

(4) Fisichella, M.; Bérenguer, F.; Steinmetz, G.; Auffan, M.; Rose, J.; Prat, O. "Intestinal Toxicity Evaluation of TiO2 Degraded Surface-Treated Nanoparticles: A Combined Physico-Chemical and Toxicogenomics Approach in Caco-2 Cells." *Part. Fibre Toxicol.* **2012**, *9* (1), 39. https://doi.org/10.1186/1743-8977-9-39.

(5) Yu, H.; Huang, Q. Investigation of the Cytotoxicity of Food-Grade Nanoemulsions in Caco-2 Cell Monolayers and HepG2 Cells. *Food Chem.* **2013**, *141* (1), 29–33. https://doi.org/10.1016/j.foodchem.2013.03.009.

(6) Konsoula, R.; Barile, F. a. Correlation of in Vitro Cytotoxicity with Paracellular Permeability in Mortal Rat Intestinal Cells. *J. Pharmacol. Toxicol. Methods* **2007**, *55* (2), 176–183. https://doi.org/10.1016/j.vascn.2006.06.001.

(7) Artursson, P.; Palm, K.; Luthmanb, K. Caco-2 Monolayers in Experimental and Theoretical Drug Transport Predictions of Drug Transport. *Adv. Drug Deliv. Rev.* **2001**, *46* (96), 27–43.

(8) Sambuy, Y.; De Angelis, I.; Ranaldi, G.; Scarino, M. L.; Stammati, a.; Zucco, F. The Caco-2 Cell Line as a Model of the Intestinal Barrier: Influence of Cell and Culture-Related Factors on Caco-2 Cell Functional Characteristics. *Cell Biol. Toxicol.* **2005**, *21* (1), 1–26. https://doi.org/10.1007/s10565-005-0085-6.

(9) Natoli, M.; Leoni, B. D.; D'Agnano, I.; Zucco, F.; Felsani, A. Good Caco-2 Cell Culture Practices. *Toxicol. Vitr.* **2012**, *26* (8), 1243–1246. https://doi.org/10.1016/j.tiv.2012.03.009.

(10) Chong, Saeho; Dando, Sandra A.; Morrison, R. A. Evaluation of Biocoat Intestinal Epithelium Differentiation Environment (3-Day Cultured Caco-2 Cells) as an Absorption Screening Model with Improved Screening Productivity. *Pharmaceutical Research*. 1997, pp 1835–1837. https://doi.org/10.1023/A:1012160703533.

(11) Lentz, K. A.; Hayashi, J.; Lucisano, L. J.; Polli, J. E. Development of a More Rapid, Reduced Serum Culture System for Caco-2 Monolayers and Application to the Biopharmaceutics Classification System. *Int. J. Pharm.* **2000**, *200* (1), 41–51.

https://doi.org/10.1016/S0378-5173(00)00334-3.

(12) Yamashita, S.; Furubayashi, T.; Kataoka, M.; Sakane, T.; Sezaki, H.; Tokuda, H. Optimized Conditions for Prediction of Intestinal Drug Permeability Using Caco-2 Cells. *Eur. J. Pharm. Sci.* **2000**, *10* (3), 195–204. https://doi.org/10.1016/S0928-0987(00)00076-2.

(13) Yamashita, S.; Konishi, K.; Yamazaki, Y.; Taki, Y.; Sakane, T.; Sezaki, H.; Furuyama, Y. New and Better Protocols for a Short-Term Caco-2 Cell Culture System. *J. Pharm. Sci.* **2002**, *91* (3), 669–679. https://doi.org/10.1002/jps.10050.

(14) Bravo, S. A.; Nielsen, C. U.; Amstrup, J.; Frokjaer, S.; Brodin, B. In-Depth Evaluation of Gly-Sar Transport Parameters as a Function of Culture Time in the Caco-2 Cell Model. *Eur. J. Pharm. Sci.* **2004**, *21* (1), 77–86. https://doi.org/10.1016/S0928-0987(03)00205-7.

(15) Piletz, J. E.; Drivon, J.; Eisenga, J.; Buck, W.; Yen, S.; Mclin, M.; Meruvia, W.; Amaral, C.; Brue, K. Human Cells Grown With or Without Substitutes for Fetal Bovine Serum. *Cell Med.* **2018**, *10*, 1–11. https://doi.org/10.1177/2155179018755140.

(16) Gstraunthaler, G.; Lindl, T.; Valk, J. Van Der. A Plea to Reduce or Replace Fetal Bovine Serum in Cell Culture Media. *Cytotechnology* **2013**, *65*, 791–793. https://doi.org/10.1007/s10616-013-9633-8.

(17) Young, L.; Sung, J.; Stacey, G.; Masters, J. R. Detection of Mycoplasma in Cell Cultures. *Nat. Protoc.* **2010**, *5* (5), 929–934. https://doi.org/10.1038/nprot.2010.43.

(18) Press, B.; Di Grandi, D. Permeability for Intestinal Absorption: Caco-2 Assay and Related Issues. *Curr. Drug Metab.* **2008**, *9* (9), 893–900. https://doi.org/10.2174/138920008786485119.

(19) Ferruzza, S.; Rossi, C.; Scarino, M. L.; Sambuy, Y. A Protocol for Differentiation of Human Intestinal Caco-2 Cells in Asymmetric Serum-Containing Medium. *Toxicol. Vitr.* **2012**, *26*, 1247–1251. https://doi.org/10.1016/j.tiv.2012.01.008.

(20) Casteleyn, C.; Rekecki, A.; Van Der Aa, A.; Simoens, P.; Van Den Broeck, W. Surface Area Assessment of the Murine Intestinal Tract as a Prerequisite for Oral Dose Translation from Mouse to Man. *Lab. Anim.* **2010**, *44* (3), 176–183. https://doi.org/10.1258/la.2009.009112.

(21) Whitehead, K.; Karr, N.; Mitragotri, S. Safe and Effective Permeation Enhancers for Oral Drug Delivery. *Pharm. Res.* **2008**, *25* (8), 1782–1788. https://doi.org/10.1007/s11095-007-9488-9.

(22) Lamson, N. G.; Cusimano, G.; Suri, K.; Zhang, A.; Whitehead, K. A. The PH of Piperazine Derivative Solutions Predicts Their Utility as Transepithelial Permeation Enhancers. *Mol. Pharm.* **2016**, *13* (2), 578–585. https://doi.org/10.1021/acs.molpharmaceut.5b00803.

(23) Suzuki, T. Regulation of Intestinal Epithelial Permeability by Tight Junctions. *Cell.*

Mol. Life Sci. **2013**, *70* (4), 631–659. https://doi.org/10.1007/s00018-012-1070-x.

(24) Srinivasan, B.; Kolli, A. R.; Esch, M. B.; Abaci, H. E.; Shuler, M. L.; Hickman, J. J. TEER Measurement Techniques for In Vitro Barrier Model Systems. *J. Lab. Autom.* **2015**, *20* (2), 107–126. https://doi.org/10.1177/2211068214561025.

(25) Pinto, M.; Robine-Leon, S.; Appay, M.-D.; Kedinger, M.; Triadou, N.; Dussaulx, E.; Lacroix, B.; Simon-Assmann, P.; Haffen, K.; Fogh, J.; et al. Enterocyte-like Differentiation and Polarization of the Human Colon Carcinoma Cell Line Caco-2 in Culture. *Biol. Cell* **1983**, *47* (323), 323–330.

(26) Howell, S.; Kenny, A. J.; Turner, A. J. A Survey of Membrane Peptidases in Two Human Colonic Cell Lines, Caco-2 and HT-29. *Biochem. J.* **1992**, *284*, 595–601.

(27) Kam, K. R.; Walsh, L. a.; Bock, S. M.; Koval, M.; Fischer, K. E.; Ross, R. F.; Desai, T. a. Nanostructure-Mediated Transport of Biologics across Epithelial Tissue: Enhancing Permeability via Nanotopography. *Nano Lett.* **2013**, *13* (1), 164–171. https://doi.org/10.1021/nl3037799.

(28) Vllasaliu, D.; Exposito-Harris, R.; Heras, A.; Casettari, L.; Garnett, M.; Illum, L.; Stolnik, S. Tight Junction Modulation by Chitosan Nanoparticles: Comparison with Chitosan Solution. *Int. J. Pharm.* **2010**, *400* (1–2), 183–193. https://doi.org/10.1016/j.ijpharm.2010.08.020.

(29) Fein, K. C.; Lamson, N. G.; Whitehead, K. A. Structure-Function Analysis of Phenylpiperazine Derivatives as Intestinal Permeation Enhancers. *Pharm. Res.* **2017**, *34* (6), 1320–1329. https://doi.org/10.1007/s11095-017-2149-8.

(30) Yu, Q.; Wang, Z.; Li, P.; Yang, Q. The Effect of Various Absorption Enhancers on Tight Junction in the Human Intestinal Caco-2 Cell Line. *Drug Dev. Ind. Pharm.* **2013**, *39* (4), 587–592. https://doi.org/10.3109/03639045.2012.692376.

(31) Whitehead, K.; Mitragotri, S. Mechanistic Analysis of Chemical Permeation Enhancers for Oral Drug Delivery. *Pharm. Res.* **2008**, *25* (6), 1412–1419. https://doi.org/10.1007/s11095-008-9542-2.

(32) Brake, K.; Gumireddy, A.; Tiwari, A.; Chauhan, H.; Kumari, D. In Vivo Studies for Drug Development via Oral Delivery: Challenges, Animal Models and Techniques. *Pharm. Anal. Acta* **2017**, *08* (09). https://doi.org/10.4172/2153-2435.1000560.

Chapter 3:

The pH of piperazine derivative solutions predicts their utility as transepithelial permeation enhancers

3.1 – Introduction

The successful oral administration of therapeutic macromolecules is often seen as the holy grail of modern drug delivery because of its accessibility, high patient compliance, and ease of administration. Pills or oral liquid formulations are more likely to be taken at proper intervals than their counterparts that must be injected, inhaled, or administered transdermally[1,2]. However, oral drug delivery poses the challenge of low bioavailability due to poor transport of macromolecules across the intestinal epithelium and into the bloodstream. To address this problem and increase the bioavailability of orally delivered molecules, chemical permeation enhancers can be employed to increase the flux of drugs across the intestinal lining[3].

Chemical permeation enhancers increase the transport of macromolecules across the epithelium either by improving their passage through the plasma membranes of barrier cells (transcellular pathway), or by altering the tight junctions between these cells (paracellular pathway)[4]. Some transcellular permeation enhancers increase drug bioavailability by changing behavior of transport proteins on the cell membrane[5]. For example, GW918 inhibits the action of p-glycoprotein, an efflux transporter that pumps absorbed drugs back out of cells, and has been shown to increase the transepithelial

transport of ranitidine by this mechanism[6]. Other transcellular enhancers disrupt the cell membrane in a controlled manner to allow passage of large molecules. For instance, the zwitterionic surfactant palmitoyl ammonio propanesulfonate increases the flux of the hydrophilic diffusion marker calcein through the otherwise hydrophobic cell membranes of intestinal cells[7]. On the other hand, paracellular permeation enhancers are generally species that interact with the variety of proteins that govern the tight junctions. Chitosan, a polysaccharide, increases paracellular flux by inducing the translocation of the junctional adhesion molecule JAM-1[8], while zonula occludens toxin has been shown to disrupt the barrier function of the tight junction proteins occludin and ZO-1[9]. However, the mechanisms of many identified permeation enhancers remain unknown[10].

Previously, a study of fifty-one chemical permeation enhancers with diverse chemical structures demonstrated that two piperazine derivatives were able to achieve strong permeation enhancement and induce minimal cytotoxicity in a Caco-2 model[11]. Interestingly, piperazine derivatives have also been shown to potently deliver siRNA intracellularly, both *in vitro* and *in vivo*[12]. Together with the knowledge that some piperazine derivatives are capable of crossing the blood brain barrier[13] and inhibiting neurotransmitter transport proteins[14], these data suggest that there is something unique about the way piperazine derivatives interface with biological barriers.

Piperazine is a six-membered, organic ring composed of two opposing nitrogens with saturated carbons at the remaining positions. In the previous study on intestinal permeation enhancers, the derivatives 1-phenylpiperazine and 1-methylpiperazine, the only piperazine-based molecules tested, were found to be among the top three chemical permeation enhancers in terms of increasing permeability without damaging

cells[11]. However, it was not clear why the piperazines, on a molecular level, potently enhanced transport or if permeation enhancement is a class effect of piperazine derivatives. To aid in the elucidation of structure-function relationships, this work examines a collection of simple hydrocarbon-substituted piperazine derivatives for their effect on intestinal epithelial permeation enhancement and viability.

3.2 – Methods:

3.2.1 – Materials

Fourteen piperazine derivatives with simple hydrocarbon substituents were examined in this study. Piperazine, 1-methylpiperazine, (S)-(+)-2-methylpiperazine, trans-2,5-dimethylpiperazine, 2,6-dimethylpiperazine, 1-isopropylpiperazine, 1,4-diethylpiperazine, 1-isopropyl-2-methylpiperazine, 2,5-diethylpiperazine, and 1-butylpiperazine were purchased from Sigma-Aldrich® (St. Louis, MO). 1-ethylpiperazine and 1,4-dimethylpiperazine were obtained from TCI America® (Philadelphia, PA). 1-allylpiperazine was purchased from Alfa Aesar® (Ward Hill, MA), and 1,4-diallylpiperazine was purchased from Monomer-Polymer and Dajac Labs (Trevose, PA). Six nitrogenous small molecules were selected to represent a range of primary, secondary, and tertiary amines. 1-aminohexane, 1,6-diaminohexane, ethylbutylamine, 1,2-bis(methylamino)ethane, triethylamine, and 1,2-bis(dimethylamino)ethane were purchased from Sigma-Aldrich®.

For cell culture and *in vitro* experiments, Minimum Essential Medium (MEM), Opti-MEM media, penicillin/streptomycin, trypsin-ethylenediaminetetraacetic acid (trypsin-EDTA), phosphate buffer saline (PBS), fetal bovine serum (FBS), and neutral

10 kDa dextran conjugated to Texas Red fluorescent dye (TR-Dextran10) were purchased from Life Technologies® (Thermo Fisher subsidiary, Carlsbad, CA). Caco-2 cells and methyl thiazole tetrazolium (MTT) kits were purchased from American Type Culture Collection® (ATCC, Manassas, VA). Dulbecco's Modified Eagles Medium (DMEM), Falcon® 225 cm^2 tissue culture flasks, Corning® BioCoat™ HTS 1.0 µm porous support Transwell® plates, Falcon® 24-well plates, Corning® CellBIND® 96-well microplates, basal seeding medium (BSM), Corning® Entero-STIM™ enterocyte differentiation medium (EDM), sodium butyrate, and MITO+ serum extender were obtained from VWR® (Radnor, PA).

3.2.2 – Caco-2 Cell Culture

Caco-2 was cultured in MEM supplemented with 20% FBS, 10 IU/mL of penicillin, and 0.1 mg/mL streptomycin, or in DMEM supplemented with 10% FBS, 10 IU/mL of penicillin, and 0.1 mg/mL streptomycin ("standard medium"). Cultures were incubated at 37°C in a fully humid, 5% CO_2 environment. The cells were subcultured by application of 0.25% trypsin-EDTA and subsequent passaging in 1:3, 1:4, or 1:6 ratios. Cells at passage numbers 25–60 were utilized for further experiments.

For transepithelial electrical resistance (TEER) and diffusion marker permeability experiments, cells were suspended in BSM or DMEM, seeded at a density of 2×10^5 cells per well on BioCoat HTS membrane supports, and incubated for 2 days. The media was then changed to EDM or DMEM supplemented with 2 mM sodium butyrate, and incubated for 1 day. BSM, EDM, and DMEM used for monolayers were additionally supplemented with MITO+ Serum Extender according to the manufacturer's instruction.

The TEER was monitored to confirm proper barrier formation, and only monolayers with initial TEER values of at least 200 $\Omega \cdot cm^2$ were utilized for TEER or calcein permeability experiments.

For MTT experiments, cells were suspended in standard medium, seeded at a density of 1×10^5 cells per well in 96-well plates, and incubated overnight. Before experiments, consistent seeding density was confirmed by eye using a bright field microscope.

3.2.3 – TEER Experiments

HTS inserts containing Caco-2 monolayers were transferred to 24-well plates containing 1 mL EDM per well and allowed to equilibrate for 15 minutes before recording initial resistance values, using a Millicell® voltohmmeter. Piperazine derivatives were dissolved in EDM and applied to the apical chambers, and TEER readings were taken after 10 and 30 minutes. Negative control wells received fresh, unadulterated EDM.

3.2.4 – Diffusion Marker Permeability Experiments

The paracellular diffusion markers were applied at 0.5 mM (calcein) or 0.1 mM (TR-Dextran10), dissolved in EDM or Opti-MEM, to the apical side of fully-formed monolayers with the piperazine treatments. Fresh culture media with the markers was used as a negative control. After one hour, media in the basal chambers was sampled and examined for fluorescence at 495/515 nm (calcein) or 589/615 nm (TR-Dextran10) using a BioTek® Synergy2 plate reader. Application of calibration curves yielded an

amount of mass transferred across each monolayer, which was used in the permeability equation $P_{app} = \frac{\Delta M}{C_a A \Delta t}$, where P_{app} is the apparent permeability through the monolayer, ΔM is the marker mass in the basal compartment, C_a is the apical marker concentration, A is the monolayer area, and Δt is the time between samples.

3.2.5 – MTT Experiments

Cells in a 96-well plate were treated with 100 µL per well of piperazine derivative solutions in standard medium, with negative controls receiving fresh standard medium. Solutions were also added to wells containing no cells in order to control for coloration differences between treatments. The plates were incubated at 37 °C for 30 minutes. Each well then received 10 µL MTT reagent, and the plates were incubated for an additional 3 hours. 100 µL of MTT kit detergent was then added to each well. The plates were wrapped in aluminum foil and held in the dark at room temperature overnight. Sample absorbance was then read at 570 nm using a BioTek® Synergy2 plate reader.

3.2.6 – pH Measurements

For pH measurements, treatments were prepared by dissolving piperazine derivatives into standard media at the concentration of interest. Treatments were sealed and warmed to 37 ± 5 °C, then analyzed with an Orion 3 Star™ pH meter from Thermo Scientific (Beverly, MA). In order to produce culture media at varying pH, standard media was titrated at 37±5 °C with 0.1 M NaOH or 0.1 M HCl to the desired pH.

3.2.7 – pKa Measurements

To determine the pKa of piperazines, 0.01 M piperazine solutions were prepared in ultrapure water from a Barnstead NANOPure® Diamond™ system. The solutions were warmed to 37 ± 5 °C and titrated with 0.1 M HCl or 0.1 M NaOH, subjected to constant stirring. pH measurements were taken after each addition of acid or base, and pKa values calculated using the method outlined by Albert and Serjeant[15].

3.2.8 – Statistics

TEER and diffusion marker permeability experiments were performed in triplicate, while MTT trials were executed in triplicate or quadruplicate. Enhancement Potential (EP), Toxicity Potential (TP), and Overall Potential (OP) values were calculated using arithmetic means of treatment repetitions. Error is displayed as standard error of the mean for each value, and includes any error propagated through calculations.

3.3 – Results and Discussion

3.3.1 – Enhancement Potential of Piperazine Derivatives

To test the hypothesis that piperazine derivatives act as transepithelial permeation enhancers, a group of 14 piperazines was assembled for this study (**Figure 3.1**). Simple hydrocarbon substitutions on piperazine were selected to facilitate the identification of any structure function relationships that may be present. The permeation enhancement potential of each piperazine derivative was determined using transepithelial electrical resistance (TEER) across Caco-2 epithelial cell monolayers as

a surrogate marker for intestinal permeability. Caco-2 is the most common and best-suited cell line for studies of intestinal permeability enhancement due to its ability to differentiate into monolayers that behave similarly to the native epithelial linings[16,17]. These monolayers have good correlation of molecular permeability with typical absorption in human small intestines[18], and develop the same types of tight junction complexes as human intestinal enterocytes [19,20].

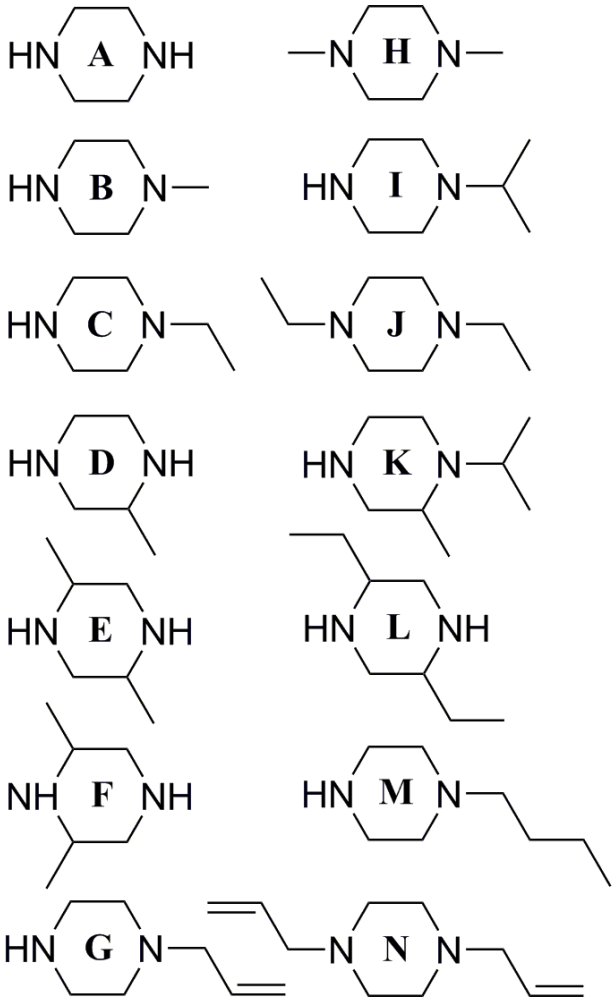

Figure 3.1: Piperazine (A) and thirteen derivatives with hydrocarbon substituents were studied for their potential as transepithelial permeation enhancers. The derivatives were B: 1-methylpiperazine, C: 1-ethylpiperazine, D: (S)-(+)-2-methylpiperazine, E: trans-2,5-dimethylpiperazine, F: 2,6-dimethylpiperazine, G: 1-allylpiperazine, H: 1,4-dimethylpiperazine, I: 1-isopropylpiperazine, J: 1,4-diethylpiperazine, K: 1-isopropyl-2-methylpiperazine, L: 2,5-diethylpiperazine, M: 1-butylpiperazine, and N: 1,4-diallylpiperazine.

TEER measurements, taken across the cell monolayers, relate electrical resistance to molecular permeability by gauging the ability of ions to pass through the paracellular pathways of the epithelium[21]. Throughout this study, TEER data is represented by the normalized parameter, enhancement potential (EP). This parameter was calculated as $EP = 1 - \frac{TEER_p/TEER_i}{TEER_c/TEER_i}$, where $TEER_p$ is the average resistance of monolayers after 30 minutes of treatment with piperazine derivatives,

$TEER_c$ is the average resistance of untreated control monolayers at 30 minutes, and $TEER_i$ is the initial resistance values for the respective monolayers. EP values range from 0 to 1, with higher numbers indicating greater ability to reduce diffusive resistance across the epithelium. In order to confirm a correlation between EP and macromolecular flux across the epithelial layers, eight treatments (untreated; compounds B, E, H, I and J at 30 mM; compounds I and L at 10 mM) representing a broad range of enhancement behavior were selected for co-administration with two fluorescent diffusion markers. Both calcein and 10 kDa dextran showed strong correlation (r^2 values of 0.94 and 0.85, respectively) between permeability through Caco-2 monolayers and EP of the treatments (**Figure 3.2**). This result is in agreement with the literature[10,21], and high EP in the Caco-2 system thereby implies that a treatment will induce improved intestinal permeability to therapeutic macromolecules *in vivo*[22–24].

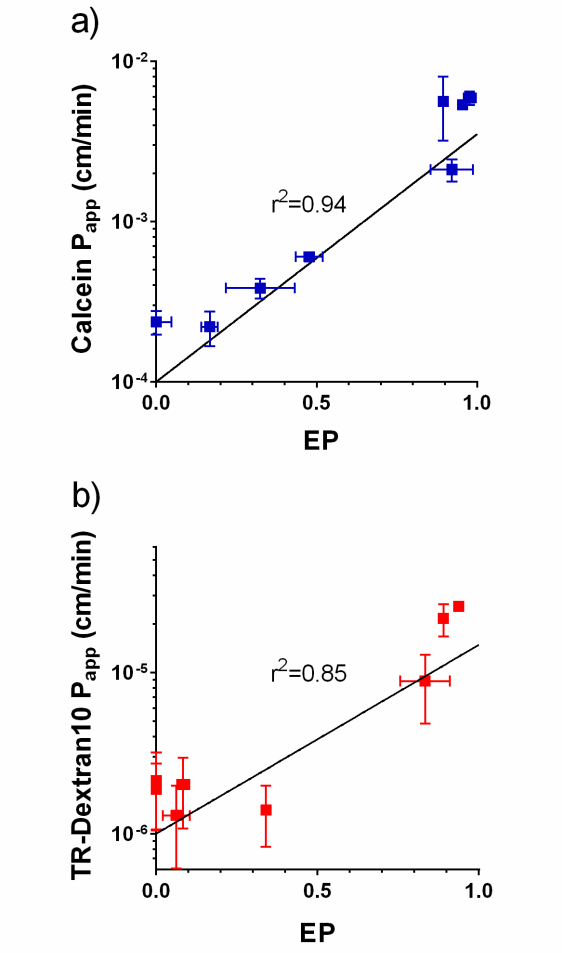

Figure 3.2 TEER was used as a surrogate marker for permeability. The enhancement potential (EP) of piperazine derivatives on Caco-2 monolayers, which was determined by changes in TEER, was strongly correlated with permeability of the paracellular diffusion markers **(a)** calcein (r^2=0.94) and **(b)** 10 kDa dextran (r^2=0.85). Error bars display s.e.m. (n = 3).

EP values were measured for all 14 piperazines at three concentrations: 10 mM, 30 mM, and 100 mM. Potentials spanned the entire possible range from 0 to 1, and showed uniform increase with increasing treatment concentration. Most piperazine derivatives were only mildly effective at a concentration of 10 mM (median EP of 0.19), while approaching maximum possible EP at 30 and 100 mM (median values of 0.91 and 1.00, respectively) (**Figure 3.3a**). A table containing all measured EP values can be found in **Table 3.1**. While the majority of piperazines followed this pattern of low efficacy in 10 mM treatments and high efficacy in 30 and 100 mM treatments, it was noted that species H and N were not highly effective below 100 mM, and species I was effective as low as 10 mM. These discrepancies from the general pattern predicted the existence of a controlling factor, other than concentration, that assisted in determining enhancement potential of the piperazine treatments.

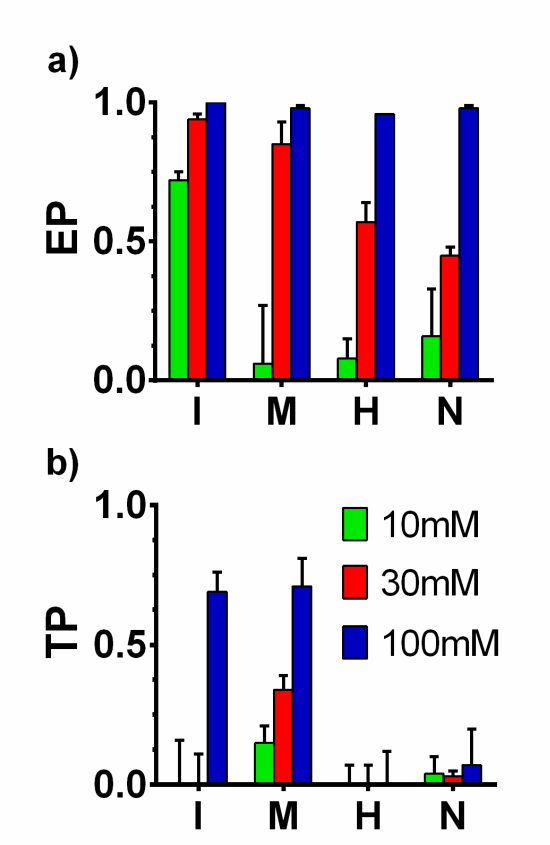

Figure 3.3: Piperazine derivatives induced dose responsive effects on enhancement and toxicity. Dose response behavior at 10, 30, and 100 mM for four of the 14 piperazine derivatives is shown here. I, M, H, and N are described in Figure 1. **(a)** While all compounds were effective enhancers at the highest concentration tested of 100 mM, a smaller number – 12 of 14 – were fully efficacious at 30 mM. Only 1-isopropylpiperazine (I) enhanced permeability at the lowest concentration. **(b)** The lowest concentrations of 10 and 30 mM did not induce toxicity for any piperazines except for 1-butylpiperazine (M). 12 of the 14 piperazines, however, were toxic at 100 mM. Error bars display s.e.m. (n = 3 - 4).

Table 3.1: Measured values and s.e.m. of EP and TP, and calculated OP values, for 14 piperazine derivatives at three concentrations

		10 mM EP	10 mM EP Error	30 mM EP	30 mM EP Error	100 mM EP	100 mM EP Error	10 mM TP	10 mM TP Error	30 mM TP	30 mM TP Error	100 mM TP	100 mM TP Error	10 mM OP	10 mM OP Error	30 mM OP	30 mM OP Error	100 mM OP	100 mM OP Error
A	piperazine	0.07	0.04	1.00	0.00	1.00	0.00	0.06	0.08	0.00	0.15	0.72	0.03	0.01	0.09	1.00	0.15	0.28	0.03
B	1-methylpiperazine	0.10	0.07	1.00	0.02	1.00	0.00	0.00	0.08	0.00	0.12	0.68	0.03	0.10	0.10	1.00	0.12	0.32	0.03
C	1-ethylpiperazine	0.23	0.05	0.98	0.00	1.00	0.01	0.01	0.06	0.00	0.17	0.69	0.08	0.21	0.08	0.98	0.17	0.31	0.08
D	(S)-(+)-2-methylpiperazine	0.19	0.06	0.84	0.08	1.00	0.00	0.00	0.07	0.00	0.08	0.71	0.02	0.19	0.09	0.84	0.11	0.29	0.02
E	trans-2,5-dimethylpiperazine	0.13	0.09	0.94	0.01	1.00	0.00	0.00	0.14	0.00	0.01	0.70	0.05	0.31	0.17	0.94	0.02	0.30	0.05
F	2,6-dimethylpiperazine	0.10	0.03	1.00	0.00	1.00	0.04	0.00	0.14	0.00	0.15	0.79	0.04	0.10	0.14	1.00	0.15	0.21	0.06
G	1-allylpiperazine	0.19	0.02	0.91	0.01	0.99	0.01	0.00	0.02	0.00	0.04	0.63	0.17	0.00	0.03	0.91	0.04	0.36	0.17
H	1,4-dimethylpiperazine	0.08	0.07	0.57	0.07	0.96	0.00	0.00	0.07	0.00	0.07	0.00	0.12	0.08	0.10	0.57	0.10	0.96	0.12
I	1-isopropylpiperazine	0.72	0.03	0.94	0.02	1.00	0.00	0.00	0.16	0.00	0.11	0.69	0.07	0.72	0.16	0.94	0.11	0.31	0.07
J	1,4-diethylpiperazine	0.27	0.10	0.88	0.02	0.98	0.00	0.03	0.02	0.00	0.10	0.43	0.10	0.09	0.11	0.88	0.10	0.55	0.10
K	1-isopropyl-2-methylpiperazine	0.24	0.06	0.45	0.05	0.73	0.02	0.04	0.08	0.00	0.09	0.97	0.07	0.20	0.10	0.45	0.10	0.00	0.07
L	2,5-diethylpiperazine	0.33	0.07	0.90	0.03	0.99	0.01	0.00	0.07	0.11	0.03	0.49	0.14	0.33	0.10	0.79	0.04	0.50	0.14
M	1-butylpiperazine	0.06	0.21	0.85	0.08	0.98	0.01	0.15	0.06	0.34	0.05	0.71	0.10	0.00	0.22	0.51	0.09	0.27	0.10
N	1,4-diallylpiperazine	0.16	0.17	0.45	0.03	0.98	0.01	0.04	0.06	0.03	0.02	0.07	0.13	0.11	0.18	0.42	0.04	0.92	0.13

3.3.2 – Toxicity Potential of Piperazine Derivatives

When assessing permeation enhancers, it is important to differentiate between compounds that increase permeability via a reversible mechanism versus toxic compounds that decrease barrier function by inducing cell death and/or opening holes in the cell monolayer[25]. Therefore, the effect of piperazine derivatives on Caco-2 cell viability was determined by the MTT assay. Toxicity potential (TP) was calculated as $TP = 1 - \frac{A_p - A_b}{A_c - A_b}$, where A_p is the average MTT wavelength absorbance of viable cells in wells treated with piperazine derivatives, A_c is the average absorbance of untreated cells in control wells, and A_b is the average absorbance of wells containing treatment and MTT reagent without cells. TP values ranged from 0 (completely nontoxic) to 0.97 (extremely toxic), and increased with increasing concentration. The piperazine derivatives were generally nontoxic at concentrations of 10 mM and 30 mM (median TP values of 0.00 for both), and severely toxic at 100 mM (median TP of 0.69) (**Figure 3.3b**). A full table of TP values and errors can be found in **Table 3.1**.

3.3.3 – Relationship between Enhancement Potential and Toxicity Potential

Once EP and TP were both determined to increase with increasing concentration, (TP, EP) x-y pairs were plotted for each treatment in order to examine the relationship between efficacy and toxicity (**Figure 3.4a**). The treatments were divided into three regimes based on their combined potential behavior. The lower-left quadrant, representing treatments with low toxicity but low efficacy, was populated primarily by piperazine derivatives tested at 10 mM concentrations. The upper-left quadrant, representing low toxicity and high efficacy, contained primarily 30 mM

treatments. Finally, the upper-right quadrant represents high toxicity and high efficacy, and entirely comprised 100 mM treatments. However, there were some species that differed from these general patterns, showing high efficacy with low toxicity at 10 or 100 mM concentrations.

As a means to balance efficacy and safety of piperazine treatments, an overall potential was calculated as $OP = \begin{cases} EP - TP & if \quad EP > TP \\ 0 & if \quad EP \leq TP \end{cases}$ for each particular piperazine derivative at a specific concentration. The maximum OP of 1 represents an enhancer that fully permeabilized the Caco-2 monolayer (EP of 1) without decreasing viability (TP of 0). In general, a higher OP indicates better potential for therapeutic use, although this metric should be considered together with EP and TP values for a more complete understanding of enhancer behavior. A table containing all OP values and

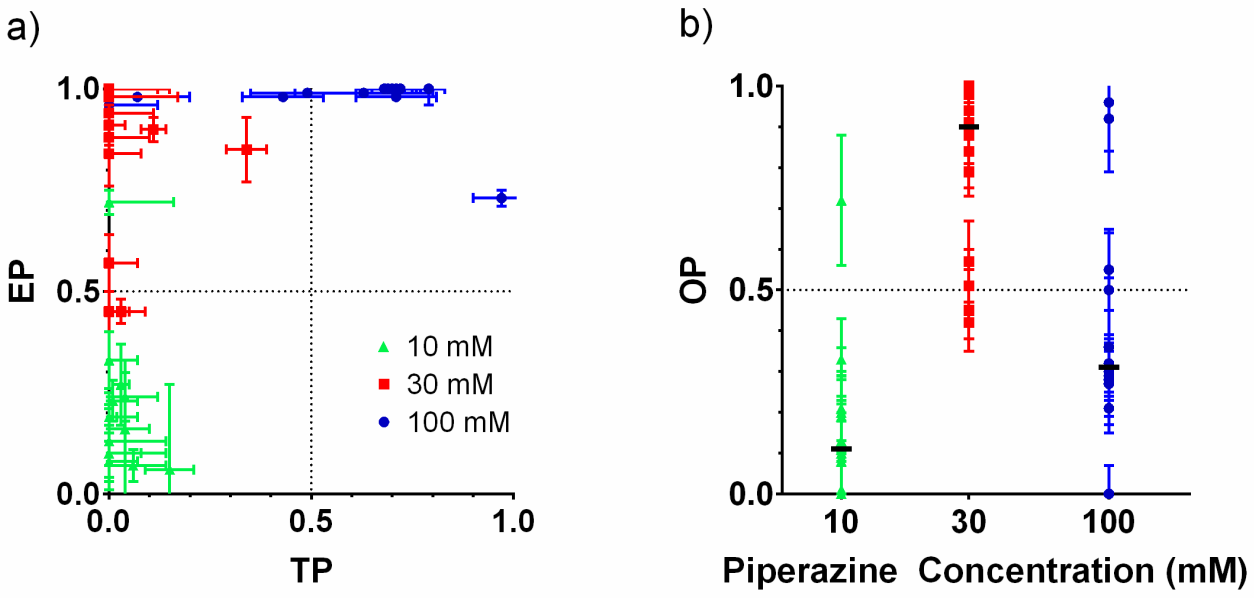

Figure 3.4: Piperazine derivatives generally showed the most potential for use as potent, non-cytotoxic permeation enhancers at a concentration of 30 mM. (a) Most compounds were ineffective and nontoxic at a concentration of 10 mM, but both effective and toxic at 100 mM. The "nontoxic and effective" zone (upper left quadrant) is primarily populated by species at 30 mM concentration. **(b)** Overall potentials (OPs) are shown for each piperazine derivative at each concentration, with 30 mM species showing the highest median OP value (horizontal black bars). Error bars display s.e.m. (n = 3 - 4).

errors can be found in **Table 3.1.** Plotting OP versus piperazine concentration (**Figure 3.4b**) showed that 30 mM treatments had, on average, the highest potentials (median OP of 0.90), followed by 100 mM (median OP of 0.31) and 10 mM (median OP of 0.11) treatments. However, several instances of 10 mM or 100 mM piperazine derivatives exhibiting high overall potentials indicate that one or more factors other than concentration guide potential as a permeation enhancer.

3.3.4 – Effects of Treatment pH on Enhancement Potential and Toxicity Potential

During measurement and calculation of potentials, it was observed that the piperazine derivatives, especially those at higher concentrations, caused color shifts in the culture media, indicating that the piperazine derivatives were altering the media pH from physiological pH (7.4). To confirm that piperazine permeability and cytotoxicity effects were not a simple result of changes in media pH, the EP and TP values for pH-adjusted culture media were determined. Although the pH of cell culture media did affect both of these parameters (**Figure 3.5**), effects were limited to outside of the pH range 6 - 9. Acidic media (pH < 6.0) caused increases in TP, which would not lead to an artificial increase in OP. Under basic conditions,

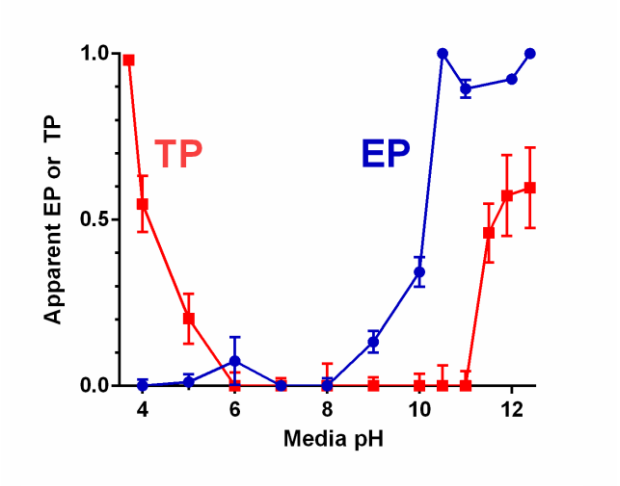

Figure 3.5: EP and TP are both dependent on the pH of the cell culture medium. DMEM was titrated with sodium hydroxide or hydrochloric acid. Media pH less than 6 or greater than 11 increased TP (squares), while a pH greater than 8 increased apparent EP (circles). Error bars display s.e.m. (n = 3 - 4).

however, EP rises significantly at pH values greater than 8, while TP remains fairly low until a pH of 11. Therefore, the pH related increase in OP at pH values above 8 must be factored in when assessing OP values for piperazine treatments falling in the relevant pH range.

3.3.5 – pH and pKa of Piperazine Derivatives

Since treatment pH was shown to be important in the assessment of apparent permeability and cytotoxicity, it was asked whether or not piperazine derivative pKa values or the resulting pH values correlated with permeation enhancement or toxicity behavior. For each of the piperazine derivatives studied, pH and pKa values were determined and are tabulated in **Table 3.2**, as well as fit well with pKa values from available literature[26]**.** The minimum treatment pH was 8.55 for 10 mM 1,4-dimethylpiperazine, while the maximum was 10.31 for 100 mM piperazine. This placed each of the treatments into a media pH regime where the TP was uniformly 0, but EP reached moderate levels at the more basic end of this range. Thus, it is important to compare OP values for higher-pH piperazine treatments with the artificial background OP induced by elevated pH.

Table 3.2: Measured values of pKa and pH at three concentrations for 14 piperazine derivatives								
		10 mM pH	30 mM pH	100mM pH	pKa 1	pKa 1 s.e.m.	pKa 2	pKa 2 s.e.m.
A	piperazine	9.07	9.43	10.31	5.40	0.02	9.59	0.01
B	1-methylpiperazine	8.85	9.12	9.83	4.59	0.04	8.97	0.02
C	1-ethylpiperazine	8.91	9.35	9.93	4.87	0.02	9.10	0.02
D	(S)-(+)-2-methylpiperazine	9.01	9.49	10.20	5.25	0.03	9.53	0.01
E	trans-2,5-dimethylpiperazine	8.95	9.55	10.09	5.16	0.04	9.57	0.03
F	2,6-dimethylpiperazine	8.85	9.46	10.09	5.28	0.01	9.62	0.04
G	1-allylpiperazine	8.76	9.19	9.75	4.34	0.12	9.07	0.05
H	1,4-dimethylpiperazine	8.55	8.88	9.25	4.01	0.05	8.19	0.01
I	1-isopropylpiperazine	8.97	9.41	10.07	5.03	0.06	9.37	0.02
J	1,4-diethylpiperazine	8.63	9.09	9.46	4.43	0.13	8.72	0.03
K	1-isopropyl-2-methylpiperazine	8.90	9.44	10.11	5.04	0.06	9.55	0.07
L	2,5-diethylpiperazine	9.03	9.55	10.24	5.15	0.11	9.63	0.06
M	1-butylpiperazine	8.81	9.31	9.85	4.92	0.05	9.31	0.03
N	1,4-diallylpiperazine	8.57	8.73	9.12	N/A	N/A	7.80	0.05

3.3.6 – pH as a Predictor of Overall Potential

Many piperazine treatments caused changes in permeability beyond what would be predicted as the effect of pH changes alone. **Figure 3.6** shows the relationship between the overall potential (OP) and the piperazine derivative treatment pH. While many treatments did not result in improved potential over the background OP (represented by the dashed line), there is a defined pH range (approximately 8.7 - 9.6) in which most piperazine derivatives exhibited significant improvements in OP. Further, no treatments outside of this pH range exhibited significantly higher OP values than the "expected" background, and many fell below that threshold due to increased toxicity potential.

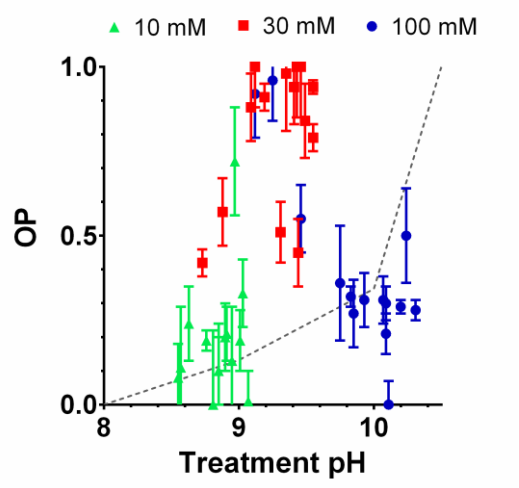

Figure 3.6: The pH of piperazine solutions dictated their overall potential (OP) as permeation enhancers. Piperazine treatments with pH between 8.7 and 9.7 show statistically significant increase in overall potential when compared to the "expected" OP due to pH (denoted by dashed line). No sample outside of this range shows significantly higher OP than the background. Error bars display s.e.m. (n = 3 - 4).

Interestingly, there was also a smaller pH window from 9.1 to 9.6 for which all piperazine treatments, regardless of concentration, exhibited substantially higher OP values than the background. To further define this range of effective treatment pH values, two piperazine derivatives with substantially different concentration-based behaviors were selected for higher-resolution examination. On one hand, 1,4-dimethylpiperazine was moderately effective at 30 mM and highly effective at 100 mM, with no notable toxicity at any concentration. On the other hand, 2,5-dimethylpiperazine was nontoxic and mildly effective at 10 mM, nontoxic and highly effective at 30 mM, and

highly effective but highly toxic at 100 mM. These species were titrated to and tested for toxicity and efficacy at ten concentrations: 1, 3, 7, 10, 15, 20, 25, 30, 70, and 100 mM. In addition, 1,4-dimethylpiperazine was tested at 300 mM, since it did not exhibit toxicity at the previous maximum concentration of 100 mM. When plotted versus pH of the treatments, these two piperazine derivatives showed an increase in TP with increasing pH (**Figure 3.7a**), and distinctly monotonic increases in EP with increasing pH (**Figure**

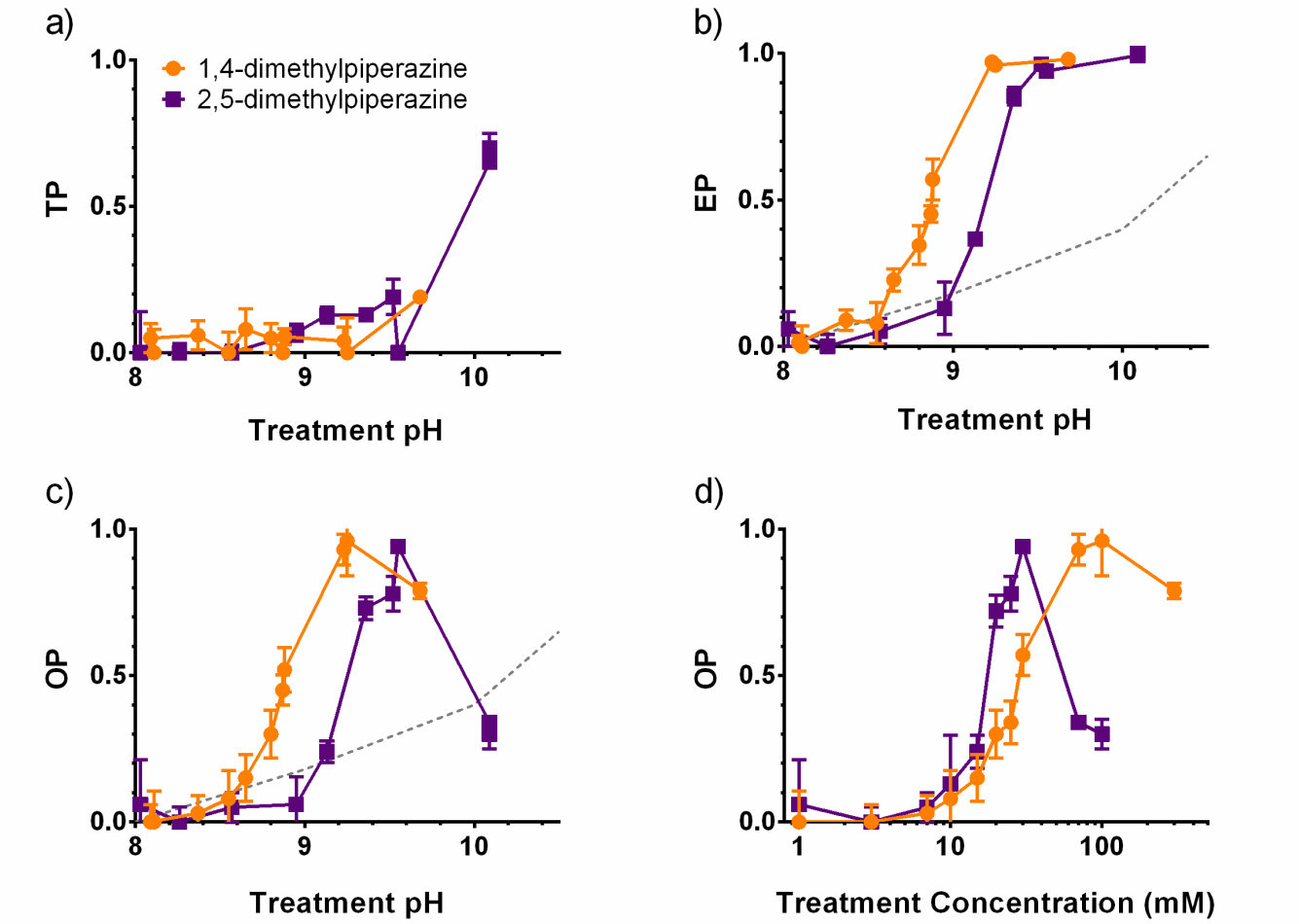

Figure 3.7: Dose response analysis of two selected piperazines confirmed pH-dependent enhancement behavior. Data are shown for 1,4-dimethylpiperazine (circles) and 2,5-dimethylpiperazine (squares) over a range of concentrations [1, 3, 7, 10, 15, 20, 25, 30, 70, and 100 mM, plus 300 mM for only the former]. **(a)** TP and **(b)** EP increase with pH, while significant increase in **(c)** OP over pH-induced background (hashed line) is confined to treatments with pH between 8.7 and 9.7. **(d)** When compared by concentration the two treatments behaved similarly until 15 mM, but diverged at higher concentrations. Error bars display s.e.m. (n = 3 - 4).

3.7b). As seen previously, substantial improvement of piperazine OP (**Figure 3.7c**) over the treatment pH background was confined to a pH range between 8.7 and 9.7. When compared by concentration instead of pH, the two species exhibited similar OP behavior (**Figure 3.7d**) for concentrations at or below 15 mM. However, their behaviors diverge at 20 mM and higher, with 2,5-dimethylpiperazine becoming fully effective as it enters the optimal pH range first, then inducing toxicity at lower concentrations than 1,4-dimethylpiperazine.

3.3.7 – Effects of pKa on Enhancement Potential and Toxicity Potential

To identify possible additional parameters in determining behavior as permeation enhancers, beyond pH, all three potentials were compared to pKa values for each of the piperazine derivatives. Plots of EP, TP, and OP at all three concentrations and for both first and second pKa can be found in **Figure 3.8**. No strong trends existed between potentials of piperazine derivatives as permeation enhancers and their pKa values, although the presence of a lower second pKa may be associated with reduced cytotoxicity of the piperazine derivatives (**Figure 3.8**).

For the fourteen piperazine-based permeation enhancers studied here, it is evident that nontoxic permeation enhancement is a shared effect among this class of molecule. However, the species studied differed significantly in their concentration-dependent behavior, and there was no apparent controlling factor other than pH for combined efficacy and non-toxicity to cells. This is interesting because pH is a parameter of the treatment solution, not of a particular molecule. The pKa of piperazine derivatives is a molecular property that, by definition, is related to pH. However, pKa

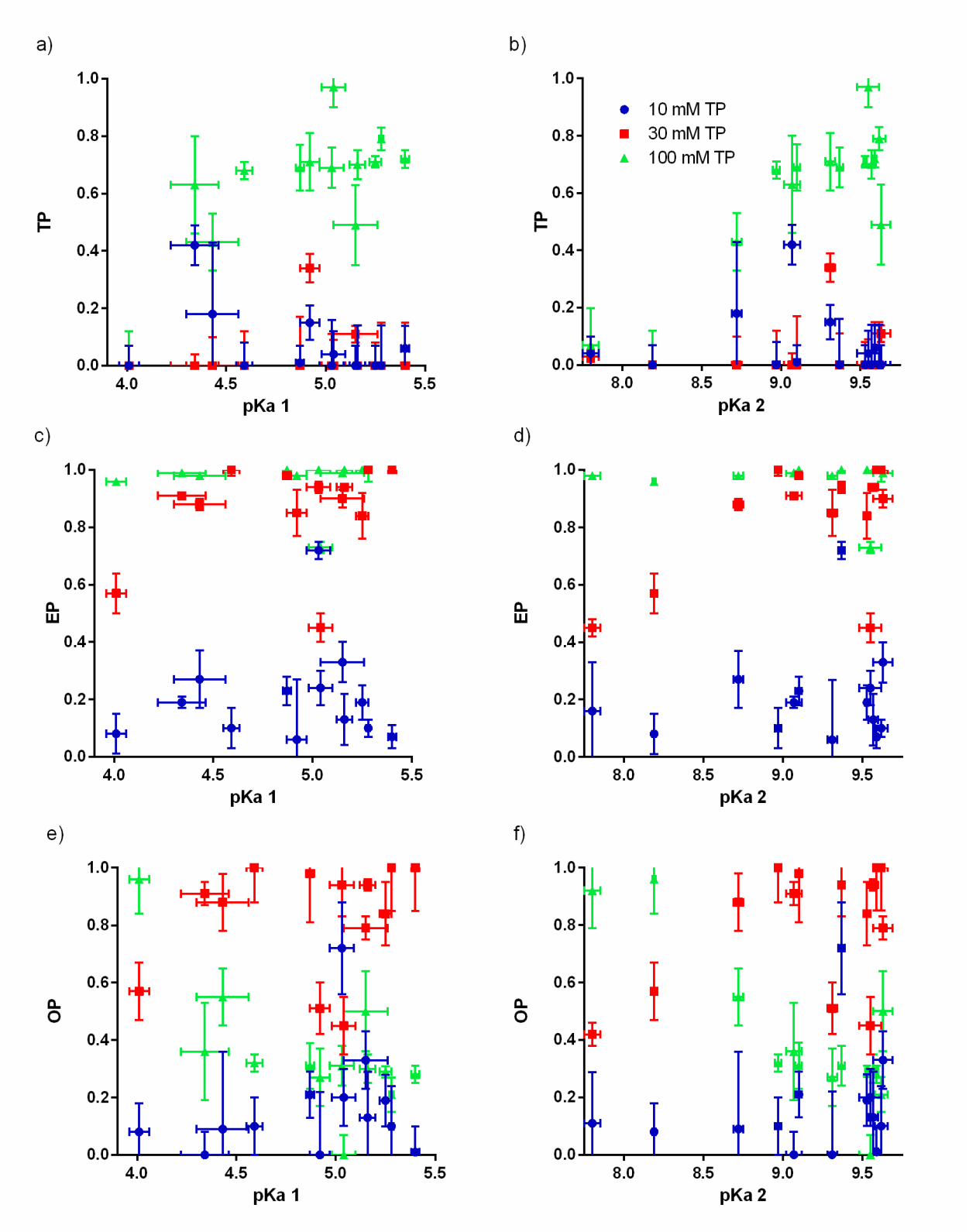

Figure 3.8: No strong relationships exist between potentials of piperazine derivatives as permeation enhancers and their pKas.

values did not correspond with non-cytotoxic efficacy. Although it is not clear why the specific pH range produces the most promising treatments, it is consistent with previous literature that apical pH affects intestinal drug flux[19,21,27,28]. However, no available work has tested permeability effects in the more basic conditions characteristic of the piperazine treatments utilized here.

Given the stability of TEER measurements in the basic range, it is clear that pH alone is not responsible for the enhancement potential of the piperazine derivatives. Instead, the true controlling parameter is likely a molecular property linked to pH, such as protonation status. The permeability of many paracellularly-transported molecules is known to be dependent on protonation or deprotonation of basic or acidic functional groups[19], and can also be affected by pH gradient across the monolayers[21]. Since the piperazine derivatives were shown here to enhance paracellular permeability, they could fall into this regime of requiring specific protonation of their nitrogen atoms in order to effectively interact with the tight junctions. In this case, the identified pH range for optimal permeation enhancement activity would represent the range at which most of the molecules are properly protonated.

3.3.8 – Potentials of Non-Piperazine Amines

Having determined that the pH of piperazine derivative solutions influenced permeation enhancement behavior, further testing was required to determine whether or not such behavior was restricted to piperazines or if it applied to any small molecules in the same pH range. Therefore, six non-piperazine containing amines were selected to screen for potentials as permeation enhancers (**Figure 3.9a**). The amines were tested

at concentrations of 3, 10, and 30 mM in order to target pH values below, within, and above the optimal window determined for piperazines (8.7-9.7), and these pH values can be found in **Table 3.3**. Similarly to piperazine derivatives, high TP (**Figure 3.9b**) was restricted to high concentrations and rose sharply around a pH of 10, while EP (**Figure 3.9c**) increased gradually with increasing pH. Unlike the piperazine treatments, the selected amines showed no clearly-defined, optimal range of pH for maximized OP

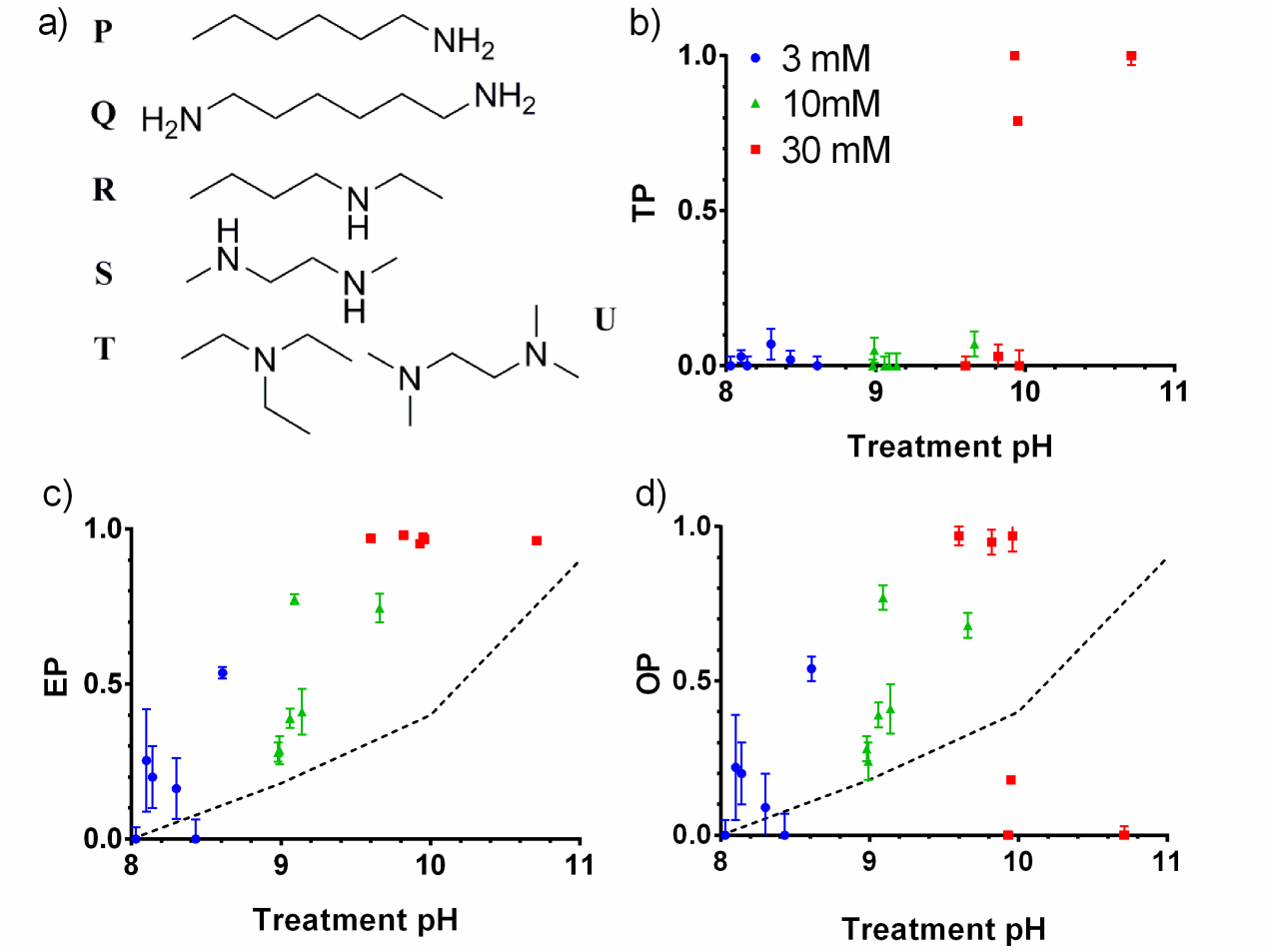

Figure 3.9: Small, nitrogenous molecules display a unique pH-dependent enhancement behavior compared to piperazine derivatives. (**a)** The six small molecule amines tested were P: 1-aminohexane, Q: 1,6-diaminohexane, R: ethylbutylamine, S: 1,2-bis(methylamino)ethane, T: triethylamine, and U: 1,2-bis(dimethylamino)ethane. **(b)** No treatments below a pH of around 10 showed significant TP, while **(c)** EP was generally higher that the pH-induced background (hashed line) and increased with increasing pH. **(d)** The resulting OP also increased with increasing pH until the toxicity cutoff at 10. Error bars represent s.e.m. (n=3-4).

Table 3.3: EP, TP, and OP, and pH values with s.e.m. for non-piperazine amines													
		3mM EP	3mM EP Error	10 mM EP	10 mM EP Error	30 mM EP	30 mM EP Error	3mM TP	3mM TP Error	10 mM TP	10 mM TP Error	30 mM TP	30 mM TP Error
P	1-aminohexane	0.25	0.16	0.77	0.02	0.95	0.00	0.03	0.02	0.00	0.04	1.00	0.00
Q	1,6-diaminohexane	0.54	0.02	0.75	0.05	0.96	0.01	0.00	0.03	0.07	0.04	1.00	0.03
R	ethylbutylamine	0.16	0.10	0.29	0.05	0.97	0.00	0.07	0.05	0.05	0.04	0.79	0.01
S	1,2-bis(methylamino)ethane	0.00	0.06	0.41	0.07	0.97	0.00	0.02	0.03	0.00	0.04	0.00	0.05
T	triethylamine	0.00	0.04	0.28	0.03	0.98	0.00	0.00	0.03	0.00	0.02	0.03	0.04
U	1,2-bis(dimethylamino)ethane	0.20	0.10	0.39	0.03	0.97	0.00	0.00	0.03	0.00	0.03	0.00	0.03
		3mM OP	3mM OP Error	10 mM OP	10 mM OP Error	30 mM OP	30 mM OP Error	3mM pH		10 mM pH		30 mM pH	
P	1-aminohexane	0.17	0.77	0.04	0.00	0.01	0.00	8.10		9.09		9.93	
Q	1,6-diaminohexane	0.04	0.68	0.04	0.00	0.03	0.01	8.61		9.66		10.71	
R	ethylbutylamine	0.11	0.24	0.06	0.18	0.01	0.00	8.30		8.99		9.95	
S	1,2-bis(methylamino)ethane	0.07	0.41	0.08	0.97	0.05	0.00	8.43		9.14		9.96	
T	triethylamine	0.05	0.28	0.04	0.95	0.04	0.00	8.03		8.98		9.82	
U	1,2-bis(dimethylamino)ethane	0.10	0.39	0.04	0.97	0.03	0.00	8.14		9.06		9.60	

(**Figure 3.9d**). Instead, OP tended to remain at or above the pH-induced background (dashed line) until dropping sharply back to 0 at concentrations where significant toxicity was induced. This differs from the trend in OP seen with the piperazine treatments, where OP declined more gradually with increasing pH. Further, most piperazine OP values did not fall to zero, even at the highest concentrations tested. Full tables containing the TP, EP, and OP values for non-piperazine amines can be found in **Table 3.3.** These amines showed enhancement efficacy at lower concentrations than the piperazine derivatives, suggesting that the ring structure may affect how the molecules interact with the tight junction. To the best of our knowledge, this is the first report of simple, linear amines acting as effective permeation enhancers of the intestinal epithelium.

3.3.9 – Concentration-Independent pH Behavior

Given that non-piperazine amines and piperazine derivatives exhibited different relationships between concentration or OP and pH, two piperazine treatments were chosen to investigate the effects of differing treatment pH at the same concentration. 10 mM 1,4-dimethylpiperazine fell below the identified effective pH range for piperazines (pH = 8.5), and was nontoxic but ineffective as a permeation enhancer (OP = 0.08 ± 0.10). Titrating this treatment into the optimal range, to a pH of 9.1, did not yield improved function (OP = 0.00 ± 0.09). In contrast, 30 mM piperazine exhibited a favorable pH (pH = 9.43) and promise as a nontoxic and effective permeation enhancer (OP = 1.00 ± 0.15). However, titrating the treatment to physiological pH of 7.4 yielded a much lower efficacy, leading to a much smaller overall potential (OP = 0.37 ± 0.06). This

reduction in OP is significantly greater in magnitude than the difference between background OP at the two pH points, suggesting that one or more molecular properties that are functions of pH also guide the efficacy as piperazine derivatives as permeation enhancers.

The lumen of the intestines, from which piperazine permeation enhancers and macromolecular drugs would diffuse to the intestinal epithelium, is highly buffered with bicarbonate salts[30,31]. Thus it is unlikely, even with a burst release of the therapeutics from polymer particles, that the local pH near the epithelial tight junctions would increase to the levels seen in the treatments here. To elucidate the effects of this buffering action on piperazine efficacy, the changes in permeation enhancement were examined for piperazine treatments titrated to differing pH values without adjusting concentration. Titrating pH to intestinal conditions appeared to partially reduce efficacy while minimally affecting toxicity. As such, these results may be predictive of the in vivo behavior of permeation enhancers in the near-neutral pH of the small intestines. Especially promising is the potential for utilizing 1,4-substituted piperazines, since the upper concentration limits of their therapeutic windows have not yet been reached, and reductions in efficacy due to pH buffering could therefore be mediated with higher doses.

3.4 – Conclusions and Future Outlook

Chemical permeation enhancement is a promising means for improving the oral bioavailability of macromolecular drugs, and many effective species have been

identified to date. However, development of these species into therapeutics has been hindered in most cases by accompanying toxicity to intestinal cells. Successful implementation of intestinal permeation enhancers will therefore require thorough knowledge of the mechanisms by which they improve macromolecular flux. This work provides a step toward fully understanding the action and therapeutic windows of simple piperazine derivatives as transepithelial permeation enhancers.

The search for structure function relationships as controlling factors in piperazine derivative efficacy or toxicity elucidated only loose trends among the species studied. Two of the three piperazine derivatives with 1,4- substitution (H and N in **Figure 1**) were much better tolerated than all of the other species, showing no toxicity at the highest concentration tested. While these two species also required the highest concentration to achieve full permeation enhancement efficacy, the lack of detected damage to the cells indicates that their therapeutic windows could extend to considerably higher concentrations. It is unclear if the unique behavior of these two molecules was directly due to their structure (containing two tertiary amines while each of the other derivatives contains at least one secondary amine), or due to another molecular property that is linked to degree of amine substitution. It was noted that H and N had the lowest pKa values of the collection and caused less pH increase per unit concentration than the other derivatives, behaviors that have also been noted in previous research of piperazine chemical behavior[26]. The 1,4- substituted piperazines are also particularly attractive for therapeutic application because they contain only tertiary amines. Secondary amines, like those found in the other twelve species examined here, have been shown to react with food-derived nitrates in the stomach to form N-nitrosamines[29],

which exhibit both toxicity and carcinogenicity in rats. Thus, 1,4- substituted piperazines may be advantageous for use in oral drug delivery systems.

To further the goals of oral macromolecular delivery, this research has investigated the enhancement and toxicity behaviors of a small library of piperazine derivatives using the Caco-2 model of the intestinal epithelium. It was determined that non-cytotoxic permeation enhancement was a class effect of the piperazine derivatives studied, as each species showed efficacy at one or more concentrations. However, cell responses to piperazine treatments were not solely governed by concentration, and the pH of the treatment solutions was found to dictate efficacy. Further investigation of non-piperazine amines showed that they were efficacious as permeation enhancers, though their efficacy occurred at pH values distinct from piperazine derivatives. Collectively, these data underscore the importance of pH-dependent molecular parameters in determining the efficacy of intestinal permeation enhancers. Several of the piperazine derivatives identified herein show significant potential for use in oral macromolecular delivery systems, and future work will focus on their extension *in vivo*.

3.5 – References

(1) Agrawal, U.; Sharma, R.; Gupta, M.; Vyas, S. P. Is Nanotechnology a Boon for Oral Drug Delivery? *Drug Discov. Today* **2014**, *19* (10), 1530–1546. https://doi.org/10.1016/j.drudis.2014.04.011.

(2) Mrsny, R. J. Oral Drug Delivery Research in Europe. *J. Control. Release* **2012**, *161* (2), 247–253. https://doi.org/10.1016/j.jconrel.2012.01.017.

(3) Hamman, J. H.; Enslin, G. M.; Kotze, A. F. Oral Delivery of Peptide Drugs. *Biodrugs* **2005**, *19* (3), 166–177.

(4) Aungst, B. J. Intestinal Permeation Enhancers. *J. Pharm. Sci.* **2000**, *89* (4), 429–442. https://doi.org/10.1002/(SICI)1520-6017(200004)89:4<429::AID-JPS1>3.0.CO;2-J.

(5) Friend, D. R. Drug Delivery to the Small Intestine. *Curr. Gastroenterol. Rep.* **2004**, *6* (5), 371–376. https://doi.org/10.1007/s11894-004-0052-z.

(6) Bourdet, D. L.; Pollack, G. M.; Thakker, D. R. Intestinal Absorptive Transport of the Hydrophilic Cation Ranitidine: A Kinetic Modeling Approach to Elucidate the Role of Uptake and Efflux Transporters and Paracellular vs. Transcellular Transport in Caco-2 Cells. *Pharm. Res.* **2006**, *23* (6), 1178–1187. https://doi.org/10.1007/s11095-006-0204-y.

(7) Whitehead, K.; Mitragotri, S. Mechanistic Analysis of Chemical Permeation Enhancers for Oral Drug Delivery. *Pharm. Res.* **2008**, *25* (6), 1412–1419. https://doi.org/10.1007/s11095-008-9542-2.

(8) Sonaje, K.; Chuang, E. Y.; Lin, K. J.; Yen, T. C.; Su, F. Y.; Tseng, M. T.; Sung, H. W. Opening of Epithelial Tight Junctions and Enhancement of Paracellular Permeation by Chitosan: Microscopic, Ultrastructural, and Computed-Tomographic Observations. *Mol. Pharm.* **2012**, *9* (5), 1271–1279. https://doi.org/10.1021/mp200572t.

(9) Schmidt, E.; Kelly, S. M.; van der Walle, C. F. Tight Junction Modulation and Biochemical Characterisation of the Zonula Occludens Toxin C-and N-Termini. *FEBS Lett.* **2007**, *581* (16), 2974–2980. https://doi.org/10.1016/j.febslet.2007.05.051.

(10) Hu, Y. J.; Wang, Y. D.; Tan, F. Q.; Yang, W. X. Regulation of Paracellular Permeability: Factors and Mechanisms. *Mol. Biol. Rep.* **2013**, *40* (11), 6123–6142. https://doi.org/10.1007/s11033-013-2724-y.

(11) Whitehead, K.; Karr, N.; Mitragotri, S. Safe and Effective Permeation Enhancers for Oral Drug Delivery. *Pharm. Res.* **2008**, *25* (8), 1782–1788. https://doi.org/10.1007/s11095-007-9488-9.

(12) Whitehead, K. a.; Dorkin, J. R.; Vegas, A. J.; Chang, P. H.; Veiseh, O.; Matthews, J.; Fenton, O. S.; Zhang, Y.; Olejnik, K. T.; Yesilyurt, V.; et al. Degradable Lipid Nanoparticles with Predictable in Vivo SiRNA Delivery Activity. *Nat. Commun.* **2014**, *5*, 1–10. https://doi.org/10.1038/ncomms5277.

(13) Bali, a; Reddy, a C. D. K. Synthesis and Evaluation of Meta Substituted 1-

(Aryloxypropyl)-4- (Chloroaryl) Piperazines as Potential Atypical Antipsychotics. *Med. Chem. Res.* **2013**, *22* (1), 382–391. https://doi.org/10.1007/s00044-012-0038-6.

(14) Severinsen, K.; Kraft, J. F.; Koldso, H.; Vinberg, K. a; Rothman, R. B.; Partilla, J. S.; Wiborg, O.; Blough, B.; Schiott, B.; Sinning, S. Binding of the Amphetamine-like 1-Phenyl-Piperazine to Monoamine Transporters. *ACS Chem Neurosci* **2012**, *3* (9), 693–705. https://doi.org/10.1021/cn300040f.

(15) Albert, A.; Serjeant, E. P. Determination of Ionization Constants by Potentiometric Titration Using a Glass Electrode. In *The Determination of Ionization Constants: A Laboratory Manual*; Chapman and Hall: London, 1984; pp 14–38. https://doi.org/10.1007/978-94-009-5548-6_2.

(16) Pinto, M.; Robine-Leon, S.; Appay, M.-D.; Kedinger, M.; Triadou, N.; Dussaulx, E.; Lacroix, B.; Simon-Assmann, P.; Haffen, K.; Fogh, J.; et al. Enterocyte-like Differentiation and Polarization of the Human Colon Carcinoma Cell Line Caco-2 in Culture. *Biol. Cell* **1983**, *47* (323), 323–330.

(17) Sambuy, Y.; De Angelis, I.; Ranaldi, G.; Scarino, M. L.; Stammati, a.; Zucco, F. The Caco-2 Cell Line as a Model of the Intestinal Barrier: Influence of Cell and Culture-Related Factors on Caco-2 Cell Functional Characteristics. *Cell Biol. Toxicol.* **2005**, *21* (1), 1–26. https://doi.org/10.1007/s10565-005-0085-6.

(18) Press, B.; Di Grandi, D. Permeability for Intestinal Absorption: Caco-2 Assay and Related Issues. *Curr. Drug Metab.* **2008**, *9* (9), 893–900. https://doi.org/10.2174/138920008786485119.

(19) Volpe, D. A. Variability in Caco-2 and MDCK Cell-Based Intestinal Permeability Assays. *J. Pharm. Sci.* **2008**, *97* (2), 712–725. https://doi.org/10.1002/jps.21010.

(20) Shen, L.; Weber, C. R.; Raleigh, D. R.; Yu, D.; Turner, J. R. Tight Junction Pore and Leak Pathways: A Dynamic Duo. *Annu. Rev. Physiol.* **2011**, *73*, 283–309. https://doi.org/10.1146/annurev-physiol-012110-142150.

(21) Yamashita, S.; Furubayashi, T.; Kataoka, M.; Sakane, T.; Sezaki, H.; Tokuda, H. Optimized Conditions for Prediction of Intestinal Drug Permeability Using Caco-2 Cells. *Eur. J. Pharm. Sci.* **2000**, *10* (3), 195–204. https://doi.org/10.1016/S0928-0987(00)00076-2.

(22) Yee, S. In Vitro Permeability across Caco-2 Cells (Colonic) Can Predict in Vivo (Small Intestinal) Absorption in Man - Fact or Myth. *Pharmaceutical Research*. 1997, pp 763–766. https://doi.org/10.1023/A:1012102522787.

(23) Artursson, P.; Palm, K.; Luthmanb, K. Caco-2 Monolayers in Experimental and Theoretical Drug Transport Predictions of Drug Transport. *Adv. Drug Deliv. Rev.* **2001**, *46* (96), 27–43.

(24) Artursson, P.; Karlsson, J. Correlation between Oral Drug Absorption in Humans and Apparent Drug Permeability Coefficients in Human Intestinal Epithelial (CACO-2) Cells. *Biochem. Biophys. Res. Commun.* **1991**, *175* (3), 880–885. https://doi.org/10.1016/0006-291X(91)91647-U.

(25) Konsoula, R.; Barile, F. a. Correlation of in Vitro Cytotoxicity with Paracellular

Permeability in Caco-2 Cells. *Toxicol. Vitr.* **2005**, *19* (5), 675–684. https://doi.org/10.1016/j.tiv.2005.03.006.

(26) Khalili, F.; Henni, A.; East, A. L. L. PKa Values of Some Piperazines at (298, 303, 313, and 323) K. *J. Chem. Eng. Data* **2009**, *54*, 2914–2917. https://doi.org/10.1021/je900005c.

(27) Konishi, Y. K.; Kubo, K. K.; Shimizu, M. S. Structural EŠects of Phenolic Acids on the Transepithelial Transport of Fluorescein in Caco-2 Cell Monolayers. **2014**, *67* (9), 2014–2017.

(28) Nagahara, N.; Tavelin, S.; Artursson, P. Contribution of the Paracellular Route to the PH-Dependent Epithelial Permeability to Cationic Drugs. *J. Pharm. Sci.* **2004**, *93* (12), 2972–2984. https://doi.org/10.1002/jps.20206.

(29) Hinuma, K.; Matsuda, J.; Tanida, N.; Hori, S.; Tamura, K. N-Nitrosamines in the Stomach with Special Reference to in Vitro Formation , and Kinetics after Intragastric or Intravenous Administration in Rats Experiment I : In Vitro Formation Formation of NAs In Vitro Formation of NAs Was Examined By. *Japanese Soc. Gastroenterol.* **1990**, *25* (4), 417–424.

(30) Sheng, J. J.; McNamara, D. P.; Amidon, G. L. Toward an In Vivo Dissolution Methodology: A Comparison of Phosphate and Bicarbonate Buffers. *Mol. Pharm.* **2009**, *6* (1), 29–39. https://doi.org/10.1021/mp800148u.

(31) Tsume, Y.; Langguth, P.; Carcia-Arieta, A.; Amidon, G. L. In Silico Prediction of Drug Dissolution and Absorption with Variation in Intestinal PH for BCS Class II Weak Acid Drugs: Ibuprofen and Ketoprofen. *Biopharm. Drug Dispos.* **2012**, *33* (7), 366–377. https://doi.org/10.1016/j.micinf.2011.07.011.Innate.

Chapter 4:

Identification of the strawberry-derived permeation enhancer pelargonidin from a library of fruit, vegetable, and herb extracts

4.1 – Introduction

Oral protein delivery has long been hindered by low bioavailability due to poor drug transport through the intestinal epithelium and into the bloodstream. Paracellular permeability enhancers hold potential to improve absorption of large, orally-administered drugs[1–4], and there have been many efforts in the past to discover molecules that manipulate intestinal tight junctions. However, as with the family of piperazines examined in **Chapter 3**, almost all have been hampered by toxicity or permanent intestinal damage inflicted by the permeation enhancers[5–7]. Thus, there is an ongoing need to develop permeation enhancers that are well-tolerated by the intestinal epithelium and can be translated into clinical use. To address this critical gap, we flipped the paradigm for current permeation enhancer research. Rather than identifying efficacious compounds then screen them for efficacy, we instead began with a massive chemical library known to be in constant, safe contact with the intestines: foods.

Food chemicals represent a diverse bank of species that are well-tolerated by intestinal cells. Over thousands of years, humans and plants have coevolved via mutualism: plants (especially fruits, vegetables, and herbs) provide a source of nutrition for humans, while humans disperse seeds through harvest, preparation, and

defecation[8]. Given this cooperation, edible plants and their molecular building blocks do not typically induce toxic or immunogenic responses from the intestine. Further, many plant-derived compounds (e.g. tannins, flavonoids) are known to be bioactive in other aspects, inducing anti-inflammatory, anti-microbial, or anti-cancer effects[9–14].

Many compounds from edible foods have also been shown to affect paracellular permeability of *in vitro* intestinal models[15–22]. For example, capsianosides, commonly found in certain varieties of peppers, increase epithelial permeability by interfering with the actin cytoskeleton that anchors the tight junction proteins[21]. Additionally, a peptide from a popular culinary mushroom in Japan can assemble pores through tight junctions and improve paracellular passage of hydrophilic marker molecules[23,24]. However, it is not yet known which food-derived chemical families are best able to interact with tight junction proteins. Furthermore, such studies of food-based effects on intestinal permeability have typically been performed by food scientists or cell biologists, not from the perspective of drug delivery research. Thus, we set out to screen a side-by-side comparison of permeation enhancing ability among a large library of food extracts.

Here, we examine a library of 106 fruits, vegetables, and herbs for both toxicity and permeation enhancing ability. From this library, strawberry was identified as the most potent, nontoxic, reversible permeation enhancer. We then used an established, iterative separation-screening method[25–28] to narrow down extracts until a pure, active chemical was obtained. By probing the absorption enhancing activity of that compound, pelargonidin, in mice, we demonstrate that it can substantially improve oral uptake of model macromolecules and the protein insulin.

4.2 – Methods

4.2.1 – Materials

Penicillin/streptomycin, trypsin-ethylenediaminetetraacetic acid (trypsin-EDTA), phosphate buffer saline (PBS), fetal bovine serum (FBS), rat tail Collagen I, PrestoBlue® viability kit, and calcein were purchased from Life Technologies® (Thermo Fisher subsidiary, Carlsbad, CA, USA). Caco-2 cells were purchased from American Type Culture Collection® (ATCC, Manassas, VA, USA). Dulbecco's Modified Eagles Medium (DMEM), Falcon® 225 cm^2 tissue culture flasks, Corning® HTS 1.0 µm porous support Transwell® plates, Falcon® 24-well plates, Corning® CellBIND® 96-well microplates, sodium butyrate, MITO+ serum extender, Aimstrip® Plus blood glucose strips, blood glucose monitor, gentisic acid, furoic acid, ellagic acid, kaempferol, naringin, vanillic acid, protocatechuic acid, ferulic acid, caffeic acid, lactone hexose, resveratrol, and luteolin were obtained from VWR® (Radnor, PA, USA). FITC-labelled dextrans, Amberlite™ XAD7 resin, bovine pancreas insulin, catechin, epicatechin, polydatin, myricitrin, myricetin, hesperetin, myrtenol, and gallic acid were purchased from Sigma-Aldrich® (St. Louis, MO, USA). C18 bulk silica gel SMT-Bod-C18 was purchased from Separation Methods Technologies (Newark, DE, USA). Callistephin and procyanidin B1 were obtained from Alkemist Labs (Costa Mesa, CA, USA). Epicatechin gallate and pelargonidin were from ChromaDex (Irvine, CA, USA). Genistein, glucogallin, and sarsasapogenin were purchased from Toronto Research Chemicals (North York, ON, Canada).

4.2.2 – Preparation of Crude Food Extract Library

Food samples were obtained from local supermarkets or grown from nursery seed/stock in KAW's vegetable garden, totaling 106 fruits, vegetables, and herbs (see **Table 4.1** for full list). After removing inedible portions, the samples were blended with 125% by weight distilled water on medium-high speed for three minutes using a household blender. The resulting slurry was transferred to 50 mL conical tubes and centrifuged for 30 minutes at 1500 RPM. The resulting liquid was centrifuged to remove insoluble components, and the supernatant filtered through standard coffee filters to remove any large particulate matter, isolating water-soluble components that are compatible with aqueous cell culture assays. The extracts were then adjusted to neutral pH (7) with 1 M NaOH, and lyophilized. The resulting powders were stored at -80°C until use, when they were dissolved at 15 mg/mL in cell culture media immediately before testing with cell-based assays.

4.2.3 – Cell Culture

Caco-2 lines were confirmed mycoplasma free by direct DNA staining with Hoechst 33342[29]. Cells were cultured in DMEM supplemented with 10% FBS, 100 IU/mL of penicillin, 0.1 mg/mL streptomycin, and 0.25 µg/mL Amphotericin B ("Caco-2 media"). Cultures were incubated at 37°C in a fully humid, 5% CO_2 environment. The cells were subcultured with 0.25% trypsin-EDTA and subsequent passaging every 3 to 4 days at ratios between 1:3 and 1:8. Cells at passage numbers 20–50 were utilized for further experiments.

4.2.4 – PrestoBlue® Assay

Caco-2 cells were seeded in a clear-bottom, black, 96-well plate at a concentration of 10^4 cells/well. After incubating the plate overnight at 37°C, the media in the wells was aspirated and replaced with the treatment solutions (15 mg/ml, 100 µL/well). After three hours of exposure, the extracts were aspirated. PrestoBlue® reagent (10 µL/well) and Caco-2 media (90 µL/well) were added to the wells. Thirty minutes later, a BioTek® Synergy2 automated plate reader was used to measure the fluorescent signal produced by viable cells. The viability of each treatment is expressed as the ratio of the fluorescence intensity of the untreated cells to that of the untreated cells.

4.2.5 – Caco-2 Permeability Experiments

For transepithelial electrical resistance (TEER) and diffusion marker permeability experiments, HTS[30–32] and TRIM models of rapid, 3-day Caco-2 intestinal epithelial monolayers were employed. Caco-2 cells were suspended in DMEM supplemented with MITO+ serum extender (basal seeding medium, BSM), seeded at a density of 2×10^5 cells per well on collagen-coated HTS membrane supports, and incubated for 24-48 hours. The media was then changed to DMEM supplemented with MITO+ and 2 mM sodium butyrate (enterocyte differentiation medium, EDM), and incubated for 48 hours. The TEER was monitored to confirm proper barrier formation, and only monolayers with initial TEER values of at least 150 $\Omega\cdot cm^2$ were utilized for TEER or molecular permeability experiments.

HTS inserts containing Caco-2 monolayers were transferred to 24-well plates containing 1 mL DMEM per well and allowed to equilibrate for 30 minutes before recording initial resistance values using a Millicell® voltohmmeter. Treatments were suspended in EDM (15 mg/mL unless otherwise specified) and applied to the apical chambers, and negative control wells received fresh EDM. TEER readings were taken after 15, 30, 60, 120, and 180 minutes. After 180 minutes, treatments were removed (mimicking the natural flow of material out of the intestines) and the monolayers rinsed once with warm PBS before returning to EDM in both the apical and basal chambers for a 24-hour recovery period.

For molecular permeability, calcein was applied at 0.5 mM into the apical side of the monolayers with the fruit treatments. After one hour, media in the basal chambers was sampled and examined for fluorescence at 495/515 nm using the plate reader. Application of calibration curves yielded the amount of marker transferred across each monolayer, which was used in the permeability equation $P_{app} = \frac{\Delta M}{C_a A \Delta t}$, where P_{app} is the apparent permeability through the monolayer, ΔM is the amount of calcein in the basal compartment, C_a is the apical calcein concentration, A is the monolayer area, and Δt is the time between samples. Permeability measurements are expressed as the ratio of each monolayer's permeability at 3 hours of treatment to its permeability before treatment, normalized to any change in untreated control monolayers during that time.

4.2.6 – Amberlite™ Separation of Strawberry Extracts

Polyphenols were isolated via a previously published method [33]. Briefly, a strawberry extract produced by extracting lyophilized fruit with ethanol, then drying via

rotary evaporation and lyophilization. The material was dissolved in methanol and adsorbed onto Amberlite™ XAD 7 HP (acrylate ester) resin. The methanol was removed from the resin and evaporated to dryness, yielding unabsorbed material, which comprises a wide variety of compounds. The beads were then washed with water, which was collected and lyophilized to produce a sample composed primarily of sugars and organic acids. Next, the beads were washed with ethanol to collect the remainder of the adsorbed material. The ethanol was removed via rotary evaporation, and any remaining water was lyophilized away to yield a solid, powdered polyphenol extract.

4.2.7 - Mouse Studies

All mouse experiments were approved by the institutional animal care and use committee (IACUC) at Carnegie Mellon University (Pittsburgh, PA, USA) under protocol number PROTO201600017, and were performed in accordance with all institutional, local, and federal regulations. C57BL/6 mice were either purchased from Charles River Laboratories (Wilmington, MA, USA) or obtained from an institutionally managed breeding colony. Prior to experiments, mice were housed in cages of no more than six animals, with controlled temperature (25°C), 12 hour light-dark cycles, and free access to food and water. Mice utilized in this study were female and 8-16 weeks (18-24 g weight range). The free-to-use PS power calculator (Vanderbilt) was used to determine the minimal sample size for which statistical power was greater than or equal to 0.8. (Generally, n=5-6). Mice were fasted 8-12 hours the night before an experiment to limit the variability caused by food matter and feces in the GI tract. Fasting also served to stabilize the animals' blood sugar for insulin activity experiments, with a starting blood

glucose range of approximately 70 to 120 mg/dL. Oral gavages were administered at a volume of 10 mL solution per kg of mouse body weight (10 μL/g). Intestinal and subcutaneous injections were administered at a volume of 1 ml/kg (1 μL/g).

4.2.8 – Intestinal Permeability to Dextrans

For dextran efficacy studies, fasted mice were orally gavaged with treatment solutions (600 mg/kg STRB PPh or 40 mg/kg pelargonidin), then gavaged one hour later with 600 mg/kg FITC-DX4. Three hours after the dextran gavage, blood was collected and centrifuged. The serum was removed and examined for FITC concentration by reading for fluorescence on the plate reader and comparing to a unique calibration curve for each experiment. For larger macromolecule studies, 40 kDa dextran (FITC-DX40) was substituted at the same 600 mg/kg concentration.

4.2.9 – Intestinal Insulin Delivery

Following ten hours of fasting, mice were orally gavaged with PBS (for control) or strawberry treatments (600 mg/kg STRB PPh or 40 mg/kg pelargonidin). One hour later, their initial blood sugar was measured and the animals were placed under anesthesia. Their intestines were surgically exposed, and insulin was injected at the predetermined dose (1 unit per kg body weight unless otherwise specified) into the duodenum. The mice were closed and secured with tissue adhesive, then kept under anesthesia as their blood sugar levels were monitored each hour for five hours. An endpoint at five hours was enforced for all experiments, as the combined effects of the anesthesia,

dehydration, and reduced blood sugar prevented reliable survival beyond that point. For comparison to the current standard of insulin delivery, subcutaneous injections were given at 1 U/kg to additional mice, into the scruff on their necks. To determine areas above the curve for each mouse, trapezoidal integration was used to sum the area between known points on the blood glucose curve and the starting blood glucose value for the individual animal.

4.2.10 – Chromatography

Medium pressure liquid chromatography (MPLC) was performed using a Buchi Sepacore® system. Glass columns were hand-packed with reverse-phase (C18) silica gel and each run utilized a gradient from 10% acetonitrile to 100% acetonitrile in 0.1% aqueous trifluoroacetic acid (TFA). Run α was implemented for a coarse separation of the strawberry polyphenol extract (**Table 4.1**). Eluent absorption at 280 nm was

Table 4.1: Parameters for chromatography runs.
In each case, solvent A is 0.1 % TFA in water and solvent B is acetonitrile

MPLC Run α
Column: 26 x 460 mm
Starting mass: 1 g Pph

Time (min)	% A	% B
0.00	90	10
4.87	90	10
7.57	80	20
11.25	80	20
13.53	70	30
17.50	70	30
28.40	60	40
39.12	60	40
46.93	0	100
51.00	0	100

MPLC Runs β, γ, δ, ε
Column: 15 x 920 mm
Starting mass:
β: 0.06 g
γ: 0.04 g
δ: 0.07 g
ε: 0.12 g

Time (min)	% A	% B
0.00	90	10
6.05	90	10
14.93	85	20
20.98	80	20
28.65	0	100
32.31	0	100

UPLC
Acquity UPLC Column
Starting material:
10 µLMPLC fraction

Time (min)	% A	% B
0.00	90	10
1.00	85	15
3.50	80	20
6.00	0	100
7.00	0	100

monitored to track phenol group migration[34]. Fractions were collected, concentrated via rotary evaporation, and re-applied to a longer, narrower column for runs β, γ, δ, and ε. Fractions were collected and re-concentrated for testing in cell culture.

Each MPLC fraction was analyzed by ultra performance liquid chromatography (UPLC) using a Waters Acquity UPLC® system and Acquity UPLC C18 Column. Each run began with a 10 µLinjection of concentrated MPLC eluent. The gradient began at 10% acetonitrile in 0.1% aqueous TFA, then proceeded to 100% acetonitrile (**Table 4.1**). Eluent was monitored by a photodiode array (PDA) detector, allowing each sample to be recorded for both the 280 nm absorbance trace over time and absorbance spectra of characteristic polyphenol peaks.

4.2.11 – Statistics

All data presented as arithmetic mean of the given “n” number of biological replicates (individual animals or number of *in vitro* cell culture wells), and error bars display the standard error of the mean. For statistical significance, two-tailed Student’s t-tests were used to calculate p values.

4.3 – Results

4.3.1 – Food Extracts are Tolerated by Intestinal Cells

To first examine the hypothesis that food-derived compounds would be well tolerated by intestinal cells, we examined the library of 106 food extracts for toxicity in Caco-2 cells using the PrestoBlue® viability assay. Caco-2 cells were incubated for three hours with the fruit treatments, then thirty minutes with the PrestoBlue® reagent, and the resulting cell viability is expressed as the ratio of treated cells' fluorescent signal to that of untreated cells. Exact viability measurements for each extract are listed in **Table 4.2**. The prediction that edible material would yield nontoxic extracts for intestinal cell systems was generally supported (**Figure 4.1**); of over 100 extracts tested, only 23 showed statistically significant reductions in viability by the highly concentrated, 15 mg/mL treatments.

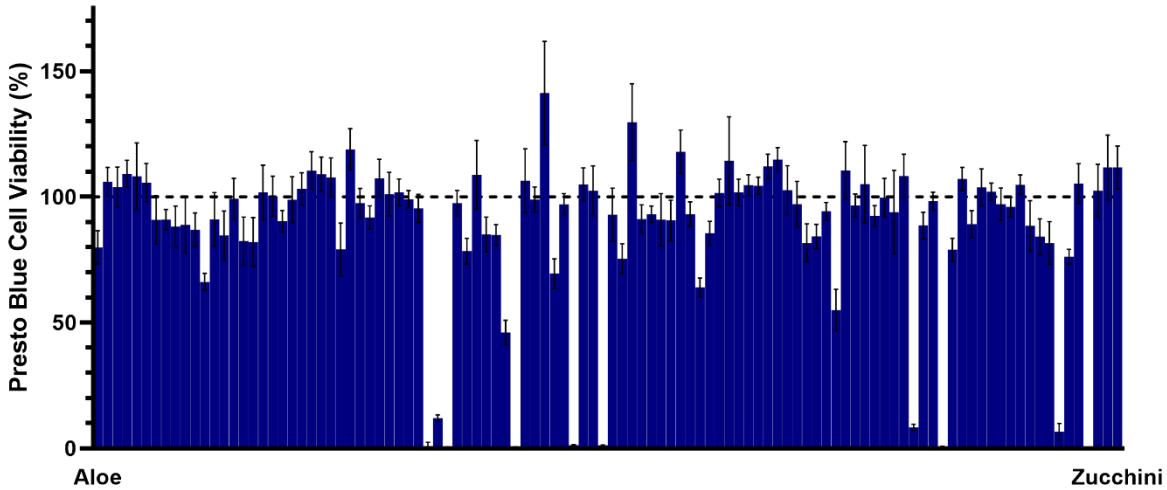

Figure 4.1: Crude food extracts are generally well-tolerated by Caco-2 cells. Extracts are arranged alphabetically along the x axis, and a full table of toxicity values is provided in **Table 4.1**. The viability measurements of cells treated with a vast majority of the extracts were not statistically distinguishable from those of untreated control cells. Error bars display s.e.m., n = 8.

Of the apparently toxic extracts, most fell within a few categories that may explain their behavior. For example, several fruits known to contain protease enzymes (including kiwi, pineapple, and papaya) appeared to be toxic to the cells. However, based on visual observation, we believe that the proteases were not killing the cells, but simply lifting them from the culture plate in the same manner as trypsin during the cell culture passaging process. Next, while rinds from citrus fruits are often used as flavorings and garnishes, they are seldom eaten on their own or in large volume. Finally, many of the more pungent extracts (e.g. garlic, ginger, rosemary) also tended to reduce cell viability, likely related again to the relatively small portion of food intake that these herbs and spices generally comprise.

Table 4.1: Presto viability, TEER, and calcein permeability screening results for crude food extracts. Viability ("Via.") columns are all presented with respect to untreated control cells. Some apparently toxic extracts were not tested for TEER or calcein permeability. Lower values for "TEER % 3 h" denote more efficacious permeation enhancers. "TEER Rec." denotes whether the average TEER value for the treated monolayers returned to at least 80% of their original value within 24 hours after removal of the extracts. "Calcein Class" indicates whether the extract (P)ermeabilized the monolayers or (C)losed tight junctions to a statistically significant extent, or caused (I)nsignificant differences from control. * $p < 0.05$ by Student's two-tailed t-test with respect to untreated control.

Extract	Via. %	Via. s.e.m.	*		TEER % 3 h	TEER s.e.m.	TEER Rec.	Calcein Ratio	Calcein s.e.m.	Calcein Class
Aloe	79.9	6.6	Yes		2.6	2.7	No	28.6	3.2	P
Apple, Granny Smith	106.0	5.6	No		73.1	6.9	Yes	1.3	0.2	I
Apple, Red Delicious	103.9	7.9	No		110.3	13.4	Yes	0.8	0.1	I
Asparagus	109.1	5.3	No		30.5	9.7	No	1.8	1.1	I
Avocado	108.2	13.2	No		98.4	8.5	Yes	1.5	0.4	I
Banana	105.6	7.6	No		90.0	3.7	Yes	0.7	0.1	I
Basil	90.9	9.6	No		13.4	1.3	No	9.5	2.3	P
Beans, Green	90.9	4.0	No		51.6	6.4	Yes	1.3	0.3	I
Beet	88.2	8.2	No		2.8	0.6	No	52.5	18.2	P
Blackberry	88.9	11.0	No		106.9	8.5	Yes	0.8	0.1	I
Blueberry	86.9	6.8	No		93.9	6.2	Yes	0.5	0.2	I
Breadfruit	66.2	3.4	Yes							

Table 4, continued										
Extract	**Via. %**	**Via. s.e.m.**	*****		**TEER % 3 h**	**TEER s.e.m.**	**TEER Rec.?**	**Calcein Ratio**	**Calcein s.e.m.**	**Calcein Class**
Broccoli	91.0	10.7	No		76.8	12.0	Yes	0.7	0.0	C
Brussels Sprouts	84.6	9.8	No		90.8	4.9	Yes	0.8	0.1	I
Cabbage, Red	99.2	8.1	No		73.6	10.9	Yes	1.1	0.2	I
Cactus Pear	82.4	9.6	No		101.9	1.8	Yes	0.7	0.1	I
Cantaloupe	82.0	9.7	No		106.5	8.5	Yes	1.0	0.2	I
Carrots, Orange	101.7	10.9	No		97.6	3.1	Yes	1.4	0.7	I
Carrots, Purple	100.2	7.9	No		115.4	11.5	Yes	1.8	1.2	I
Celery	90.3	4.3	No		87.0	7.4	Yes	1.0	0.1	I
Chayote	98.8	9.2	No		20.1	1.6	Yes	4.7	0.6	P
Cherry, Red	103.2	6.4	No		95.4	1.7	Yes	0.9	0.1	I
Cherry, White	110.4	7.4	No		95.6	1.3	Yes	0.9	0.1	I
Chokeberry	108.9	6.8	No		32.9	2.4	No	0.8	0.1	I
Cilantro	107.7	7.7	No		60.9	11.5	No	0.9	0.1	I
Corn	79.1	10.5	No		99.5	25.2	Yes	1.1	0.1	I
Cranberry	118.9	8.2	No		16.3	1.6	No	5.2	0.3	P
Cucumber	97.5	5.8	No		54.7	14.8	Yes	1.7	0.3	I
Currant, Black	91.8	4.5	No		22.6	2.5	No	1.9	0.3	I
Currant, Red	107.4	7.4	No		20.3	0.5	No	2.6	0.3	P
Dill	101.1	8.6	No		43.7	6.2	No	1.6	0.1	P
Dragonfruit	101.8	5.3	No		87.5	11.6	Yes	0.9	0.1	I
Eggplant	99.1	3.4	No		92.1	6.7	Yes	0.9	0.1	I
Fennel	95.4	5.6	No		36.2	10.8	Yes	2.4	0.8	P
Galangal	1.0	1.4	Yes							
Garlic	12.0	1.2	Yes		18.5	3.3	No	5.5	1.1	I
Ginger	-0.1	-0.8	Yes		1.6	1.1	No	125.6	59.3	I
Grapefruit	97.5	5.1	No		95.3	10.1	Yes	0.9	0.1	I
Grapefruit Rind	78.4	5.1	Yes							
Grapes, Green	108.8	13.6	No		70.0	2.9	Yes	0.9	0.2	I
Grapes, Red Seedless	85.0	6.9	No		16.7	0.6	Yes	6.2	0.7	P
Guava	84.8	4.2	Yes							
Horseradish	46.1	4.9	Yes							

Table 4, continued										
Extract	**Via. %**	**Via. s.e.m.**	*****		**TEER % 3 h**	**TEER s.e.m.**	**TEER Rec.?**	**Calcein Ratio**	**Calcein s.e.m.**	**Calcein Class**
Huckleberry, Garden	0.4	0.2	Yes							
Jalapeno	106.4	12.6	No		57.7	12.6	Yes	1.7	0.6	I
Jaltomato	98.9	4.9	No		42.2	0.6	Yes	1.7	0.1	P
Jicama	141.2	20.5	No		91.7	5.8	No	0.9	0.1	I
Kiwi	69.4	5.9	Yes							
Lemon	97.0	4.3	No		14.7	0.9	No	6.8	0.7	P
Lemon Rind	1.3	0.2	Yes							
Lettuce	104.9	6.6	No		65.1	7.8	Yes	2.6	0.9	I
Lime	102.4	9.8	No		78.0	16.0	Yes	2.7	0.8	P
Lime Rind	1.2	0.2	Yes							
Mango	92.9	10.6	No		101.5	4.2	Yes	1.7	0.2	I
Mushroom	75.4	5.9	Yes		42.6	2.4	No	2.5	0.5	I
Name	129.7	15.3	No		68.9	14.6	Yes	1.0	0.6	I
Nectarine	91.2	5.6	No		57.7	5.0	Yes	3.0	0.7	P
Okra	93.1	3.3	No		120.7	20.2	Yes	0.8	0.1	I
Onion, Red	90.9	10.3	No		75.2	7.8	Yes	1.0	0.1	I
Onion, Yellow	90.6	8.0	No		71.7	6.3	Yes	1.3	0.1	I
Orange	117.9	8.7	No		108.7	5.0	Yes	0.5	0.2	I
Orange Otricoli	93.1	4.9	No		48.3	3.8	Yes	1.2	0.1	I
Orange Rind	64.0	3.7	Yes							
Papaya	85.5	4.8	Yes							
Parsley	101.5	5.4	No		30.7	8.6	Yes	5.0	0.7	P
Parsnip	114.3	17.5	No		95.7	13.6	Yes	1.1	0.1	I
Passionfruit	101.8	5.3	No		41.9	7.3	Yes	2.4	0.3	P
Peach	104.7	4.1	No		111.4	10.6	Yes	0.3	0.2	I
Peach, White	104.4	3.4	No		120.8	9.2	Yes	0.5	0.3	I
Pear, Anjou	112.1	4.9	No		90.5	9.3	Yes	2.7	0.4	I
Pear, Asian	114.8	4.8	No		87.7	20.0	Yes	3.9	2.1	I
Pepino	102.6	9.7	No		29.7	3.3	Yes	2.3	0.2	P
Pepper, Green Bell	97.1	9.1	No		43.5	3.5	No	1.9	0.2	P
Pepper, Red Bell	81.7	7.5	Yes		88.5	1.8	Yes	0.9	0.2	I
Peppermint	84.2	4.8	No		41.3	11.3	Yes	3.6	0.9	P

Table 4, continued										
Extract	**Via. %**	**Via. s.e.m.**	*****		**TEER % 3 h**	**TEER s.e.m.**	**TEER Rec.?**	**Calcein Ratio**	**Calcein s.e.m.**	**Calcein Class**
Persimmon	94.3	3.5	No		89.6	14.2	Yes	1.6	0.7	I
Pineapple	55.0	8.3	Yes							
Plum, Purple	110.5	11.3	No		40.9	3.5	Yes	1.6	0.2	I
Plum, Yellow	96.5	4.5	No		63.4	3.6	Yes	1.1	0.1	I
Pomegranate	105.1	15.4	No		104.1	9.1	Yes	0.9	0.1	I
Pomelo	92.4	4.1	No		72.4	14.3	Yes	0.8	0.4	I
Pomelo Rind	99.6	7.7	No		61.8	6.9	Yes	0.8	0.4	I
Potato, Baking	93.9	16.6	No		36.7	2.9	Yes	4.4	2.0	I
Potato, Blue	108.2	8.7	No		30.3	3.0	Yes	5.2	2.2	I
Potato, Red	8.3	1.3	Yes		3.7	0.6	No	28.4	2.5	P
Quince	88.6	5.3	No		75.9	15.2	No	1.5	0.9	I
Raspberry	98.2	3.6	No		120.6	5.6	Yes	0.3	0.1	C
Rosemary	0.6	0.3	Yes							
Spinach	79.0	4.6	Yes							
Starfruit	107.1	4.6	No		13.7	1.5	Yes	5.1	0.6	P
Strawberry	89.1	5.3	No		17.8	2.9	Yes	7.9		P
Strawberry, White	103.8	7.3	No		60.6	17.3	Yes	1.6	0.2	P
Sugar Cane	102.0	3.5	No		101.8	11.1	Yes	4.1	3.3	I
Sweet Potato	97.0	6.5	No		99.3	4.7	Yes	1.0	0.4	I
Sweet Potato, Purple	96.0	3.8	No		78.0	5.4	No	1.2	0.2	I
Thyme	104.8	3.8	No		29.5	4.4	Yes	1.8	0.1	P
Tomato, Black	88.4	10.0	No		100.5	5.9	Yes	0.6	0.1	C
Tomato, Red	84.1	7.2	No		89.3	10.2	Yes	4.2	0.3	P
Tomato, Yellow	81.6	8.5	No		102.4	7.6	Yes	1.4	1.0	I
Tumeric	6.7	3.2	Yes							
Turnip	76.2	2.9	Yes							
Watermelon	105.3	7.9	No		117.6	8.0	Yes	0.5	0.2	I
Wonderberry	0.0	0.5	Yes							
Yautia	102.4	10.5	No		91.8	10.8	No	0.7	0.1	C
Yucca	111.7	12.8	No		104.7	12.5	Yes	0.9	0.5	I
Zucchini	111.7	8.5	No		81.8	8.1	Yes	0.8	0.1	I

4.3.2 – Food Extracts Cause a Wide Variety of Permeability Responses

We next examined permeation enhancement efficacy of the extracts by measuring transepithelial electrical resistance (TEER) on differentiated Caco-2 cell monolayers. Since TEER values represent the resistance of the cell monolayers to paracellular ion passage, a reduction in TEER corresponds to increased paracellular permeability of the layers. Conversely, increased TEER signals a tightening of the junctions and lower paracellular permeability. After recording initial resistance values for each monolayer, the media on top of each monolayer was gently replaced with a treatment (15 mg/mL fruit extract in media), while control wells received fresh media. TEER values were monitored for three hours following treatment addition, and are reported as percent resistance of one treatment's monolayers to their initial resistances, normalized to the same value for the control monolayers.

From the extracts tested, we observed a wide variety of TEER-manipulating behaviors, especially among those samples that were well-tolerated by the cells (**Figure 4.2a**). Raspberry and blueberry yielded high TEER values through the entire treatment, corresponding to a strengthening of tight junction integrity. By contrast, culinary aloe, red grapes, and strawberries substantially reduced TEER and increased permeability of the cell layers (**Figure 4.2b**)**.** However, among these three most active permeation enhancers, only the effects of red grapes and strawberries were reversible after a 24-hour recovery period; the Caco-2 monolayers treated with aloe did not regain barrier function after treatment removal, indicating permanent cell damage.

To confirm the trends implicated by TEER, we also assessed apparent permeability of calcein through the Caco-2 monolayers (**Figure 4.2c**). Due to its strong

negative charge at physiological pH (=7.4), calcein must transport paracellularly, through the tight junctions. Calcein was added into media on top of the cells for one hour before treatment addition to provide a baseline value of each monolayer's untreated permeability. Media from below the cells was then sampled for calcein and replaced with fresh media each hour in order to maintain sink conditions. Permeation ratios are reported as final permeability (t = 2 h to t = 3 h after treatment addition) divided by baseline permeability (pre-treatment leakiness) of treated monolayers, normalized to the same values for untreated controls. As in TEER experiments, aloe,

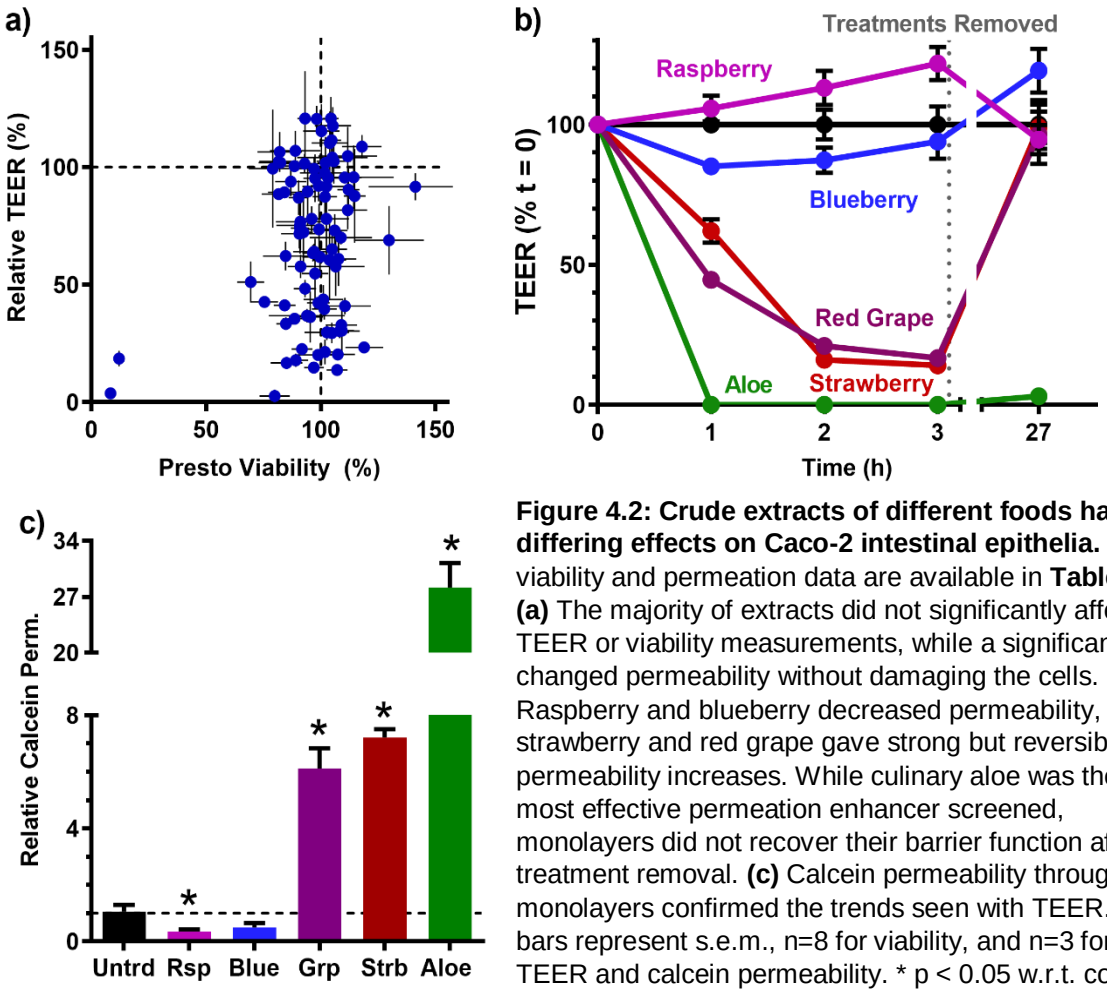

Figure 4.2: Crude extracts of different foods have differing effects on Caco-2 intestinal epithelia. Full viability and permeation data are available in **Table 4.1**. **(a)** The majority of extracts did not significantly affect TEER or viability measurements, while a significantly changed permeability without damaging the cells. **(b)** Raspberry and blueberry decreased permeability, while strawberry and red grape gave strong but reversible permeability increases. While culinary aloe was the most effective permeation enhancer screened, monolayers did not recover their barrier function after treatment removal. **(c)** Calcein permeability through the monolayers confirmed the trends seen with TEER. Error bars represent s.e.m., n=8 for viability, and n=3 for TEER and calcein permeability. * $p < 0.05$ w.r.t. control.

strawberry, and red grape were identified as potential permeability enhancers, while raspberry and blueberry strengthened the barrier function of Caco-2 tight junctions.

Though we are primarily interested in increasing epithelial permeability for this study, our identification of fruits that reduce permeability is nonetheless interesting. For example, intestinal epithelial barrier function plays a key role in the pathology of inflammatory bowel diseases (IBD). When inflamed, the epithelium becomes leaky (i.e. increases in paracellular permeability), allowing antigen proteins and bacteria to move through enlarged gaps between enterocytes and stimulate immune cells[35]. In response, the immune cells secrete additional pro-inflammatory cytokines, which induce further leakiness of the epithelial layer and a dangerous positive feedback loop that furthers the progression of the disease. Despite the importance of the epithelial barrier dysfunction in IBD, there are currently no FDA-approved drugs designed to bolster barrier function[36]. The potential for a raspberry-derived therapeutic to treat the epithelial leakiness of IBD (by tightening intestinal tight junctions) was spun out of this work and is being pursued by Kyle Cochran, a fellow PhD candidate in the Whitehead Lab.

4.3.3 – Food Color is an Indication of Permeation Enhancing Efficacy

Among the screening results from the crude extract library, an intriguing trend emerged: different colored varieties of the same fruits and vegetables sometimes yielded drastically different permeability responses. This was not true for all sets of varieties tested; in the cases of apples (red and green), cherries (red and white), and peaches (standard and white), none of the extracts were effective permeation

enhancers. However, for tomatoes, grapes, strawberries, and potatoes, there was a visible pattern: the red varieties of those foods were all effective permeation enhancers, while the white, green, or yellow varieties did not substantially affect monolayer permeability (**Figure 4.3**). Interestingly, each of those crops are known to produce a family of molecules, called polyphenols, which often contribute to plant coloration[37–40]. Based on this connection, we decided to examine this family as the next step in our iterative isolation process. Because strawberry was the most efficacious yet reversible permeabilizing extract (monolayers treated with red potato did not recover their barrier function), we proceeded to examine the strawberry polyphenols as our set of target molecules.

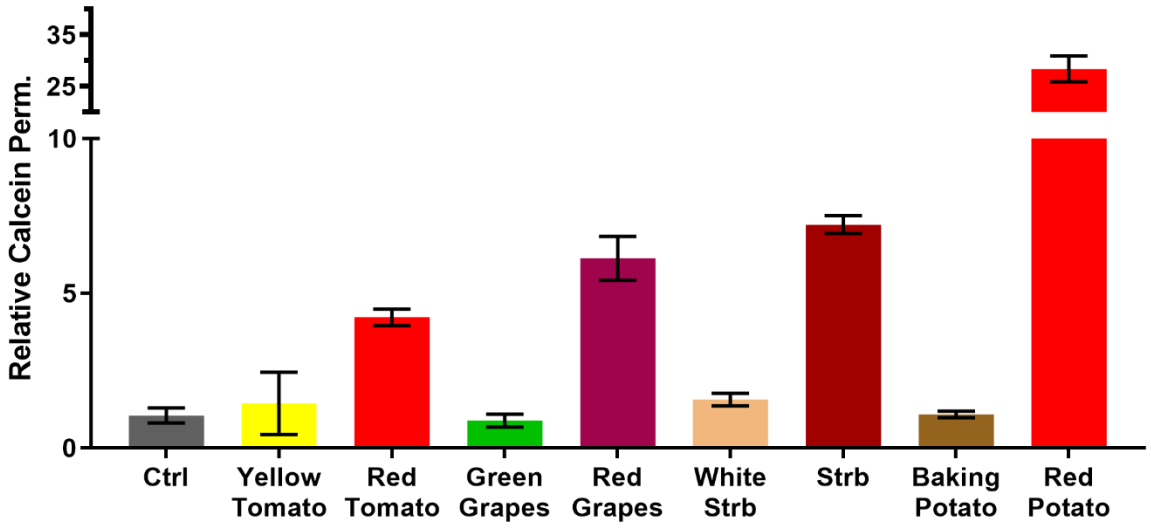

Figure 4.3: Crude extract color predicts permeation enhancing efficacy for some foods. Calcein permeability through monolayers treated with four different types of fruits and vegetables indicated that only those varieties with red coloration were effective permeation enhancers. All monolayers recovered their barrier function after treatment, with the exception of those exposed to red potato extract. Error bars represent s.e.m., * $p < 0.05$ w.r.t. control.

4.3.4 – Strawberry Polyphenols are Potent Permeation Enhancers

Polyphenols are a diverse group of molecules that are characterized by containing multiple phenol functional groups[41]. They are found in a wide variety of foods, and are highly abundant strawberries[42–45], with some examples shown in **Figure 4.4a**. Our strawberry polyphenol (STRB PPh) extraction method was adopted from a lab specializing in phenolic natural product research[33], and is summarized in **Figure 4.4b**. Briefly, strawberries were lyophilized, ground, extracted with ethanol, and filtered, which yielded an extract with similar properties to the crude strawberry extract. This was taken and applied to Amberlite™ XAD7 resin, which selectively adsorbs phenol groups. A series of sequential wash steps removed all of the non-phenolic material, then the polyphenols were eluted with ethanol and dried, yielding approximately 3.5 grams of extract per kilogram of strawberries for biological testing.

When applied to Caco-2 monolayers, the non-phenolic material caused little change in permeability (**Figure 4.4c**). However, the polyphenols achieved approximately the same increases in calcein permeability at one third the concentration of the crude extract. To confirm that this permeation enhancement in Caco-2 correlates to improved macromolecular bioavailability through intestinal tissues, we next orally dosed mice with strawberry polyphenols (600 mg STRB PPh per kg of animal), followed by 4 kDa, FITC-labelled dextran (FITC-DX4). FITC-DX4 is a non-digestible, fluorescent macromolecule commonly used to probe the permeability of the intestinal epithelium in animal models, and its size approximates a large peptide or small protein. After three hours, the serum fluorescence was measured to determine the blood FITC-DX4 concentration. As expected, the strawberry polyphenols increased FITC-DX4

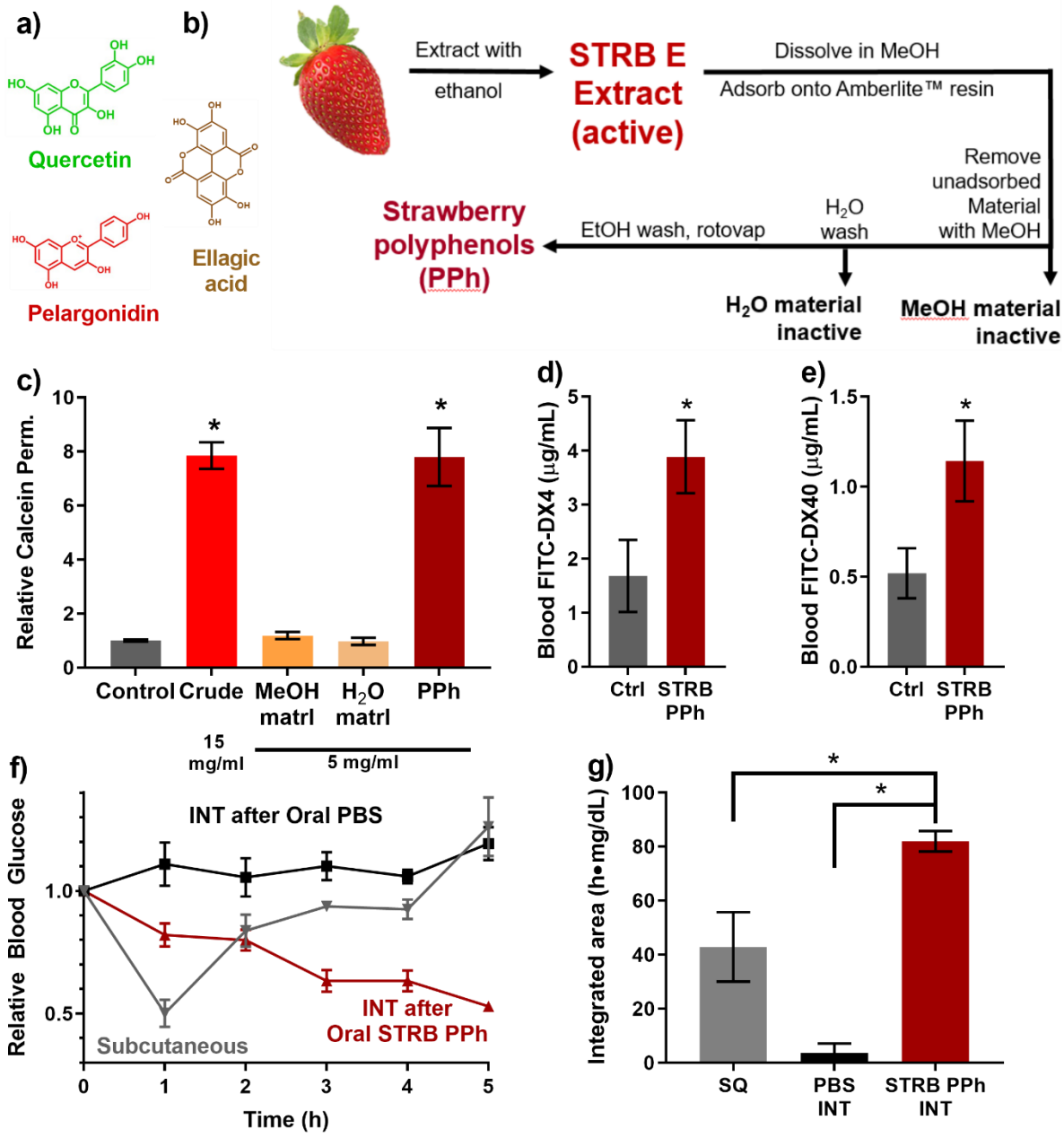

Figure 4.4: Polyphenols are responsible for strawberry's permeation enhancing activity. (**a**) A selection of polyphenols known to exist in strawberries. (**b**) Polyphenols were extracted from strawberry via adsorption to Amberlite™ resin and a sequence of washing steps. (**c**) Only the polyphenol fraction of the strawberries acted as a permeation enhancer, achieving the same calcein permeability as crude strawberry extract with a much smaller dose. (**d**) Treatment with strawberry polyphenols doubled the uptake of 4 kDa dextran (FITC-DX4) and (**e**) 40 kDa dextran in mice. **(f)** One hour following oral gavage strawberry polyphenols to mice, an intestinal injection of 1 U/kg insulin induced sustained reductions in blood glucose levels. A 1 U/kg subcutaneous insulin dose induced a pronounced but brief response. **(g)** Integrated areas above the curves from (f) show that oral delivery with STRB PPh in approximately twice the total pharmacodynamic effect as subcutaneous injection. Error bars represent s.e.m., n = 3 for calcein permeability and n = 5 for mice. * $p < 0.05$ w.r.t. control.

absorption across the intestinal barrier by more than 100% (**Figure 4.4d**). The same double in uptake efficiency was seen when 40 kDa FITC-dextran (FITC-DX40) was delivered orally (**Figure 4.4e**), indicating that the strawberry polyphenols can be used to orally deliver a wide size range of macromolecule drugs.

As a proof-of-concept that improved dextran absorption would correlate with improved oral protein delivery, we next examined transport of functional insulin across the mouse epithelium. We chose insulin for these studies because it is a modestly-sized (5.8 kDa) and relatively inexpensive protein that is not orally bioavailable in normal animals. Furthermore, its bioactivity is easily assessed by monitoring the depression of blood glucose levels that results from increased insulin concentration in the bloodstream. Mice received an oral dose of strawberry polyphenols, followed by an injection of 1 U/kg dose of insulin directly into the small intestine, circumventing possible digestion in the stomach. Blood glucose levels were monitored each hour and normalized to each mouse's blood sugar before the procedure. Mice that received insulin and strawberry polyphenols experienced a substantial reduction in blood glucose compared to mice that received insulin after just a saline gavage (**Figure 4.4f**). Further, the STRB PPh and intestinal insulin combination sustained hypoglycemia several hours longer than the same 1 U/kg dose of subcutaneous insulin, the current gold standard of administration.

To compare the total insulin bioactivity between these administration methods, we integrated the areas between each mouse's glucose curve and its starting blood sugar value. The areas above the curve (AACs) show that pharmacodynamic activity of intestinal insulin in polyphenol-treated mice is approximately double that of

subcutaneous insulin (**Figure 4.4g**), yielding a relative bioactivity value of 191%. Importantly, the sustained activity of the polyphenol-assisted intestinal insulin indicates that this administration route may be advantageous for drugs that require extended release profiles. Additionally, this successful protein absorption across the intestinal epithelium confirmed that strawberry polyphenols are efficacious enhancers and should be further pursued and refined for this purpose.

4.3.5 – Chromatography Indicates One Active Strawberry Polyphenol

To continue the iterative separation-activity cycle of compound isolation, we turned to chromatography for better resolution of the strawberry polyphenol extract into discrete fractions. Specifically, we employed reverse-phase medium pressure liquid chromatography (MPLC) using a trifluoroacetic acid (TFA)-doped water and acetonitrile mobile phase. Each MPLC run was assigned a Greek letter identifier, moving consecutively through the alphabet, and gradient information from each run is listed in **Section 4.2.10**. The first MPLC run (α) yielded fractions that were divided into seven groups, based on fraction color and ultra performance liquid chromatography (UPLC) traces of the eluents (**Figure 4.5a**). Four of these produced enough material to support a second tier of MPLC runs, yielding fractions for the β, γ, δ, and ε groups, respectively. Interestingly, UPLC traces identified two pure compounds that each appeared in multiple Greek letter groups. These were pooled together to yield the samples denoted as Compound η and Compound θ.

Next, we took each of the 22 fractions and compounds from MPLC and screened them for bioactivity on Caco-2 monolayers. Most fractions were screened at a concentration of 1 mg/mL, though some (β2, γ1, δ2, ε1, and ε3) did not yield enough material and were tested at lower concentrations (entire fraction). By calcein permeability, the vast majority of the samples did not substantially affect epithelial permeability (**Figure 4.5b**). However, one fraction, ε3, was an exceptional permeation enhancer. Interestingly, ε3's late elution from the columns identifies it as one of the less hydrophilic members of the polyphenol family. It was also deep red in color and a very small fraction, yielding less than three milligrams from one gram of polyphenol starting material. While the small mass promisingly indicated the fraction's high potency, it also complicated efforts to properly discern its molecular identity.

To expedite our identification of the permeation enhancing compound in fraction ε3, we assembled a library of known phenolic compounds from strawberry. As with the fractions, we screened these for their bioactivity on Caco-2 cells at 1 mg/mL concentration (**Figure 4.5c**). By calcein permeability, only one of these compounds was an effective permeation enhancer: pelargonidin. Pelargonidin and its glucoside, callistephin, are primarily responsible for the red coloration in strawberries[39,45]. The vast majority of the pigment is present in the glycosylated form, due to its improved solubility for storage in aqueous vacuoles[46,47]. However, our screening showed that callistephin was not an effective permeation enhancer (**Figure 4.5c**), and that only the non-glycosylated pelargonidin improved epithelial permeability. This is consistent with the observations that the effective fraction, ε3, yielded a small mass of deep red, fairly

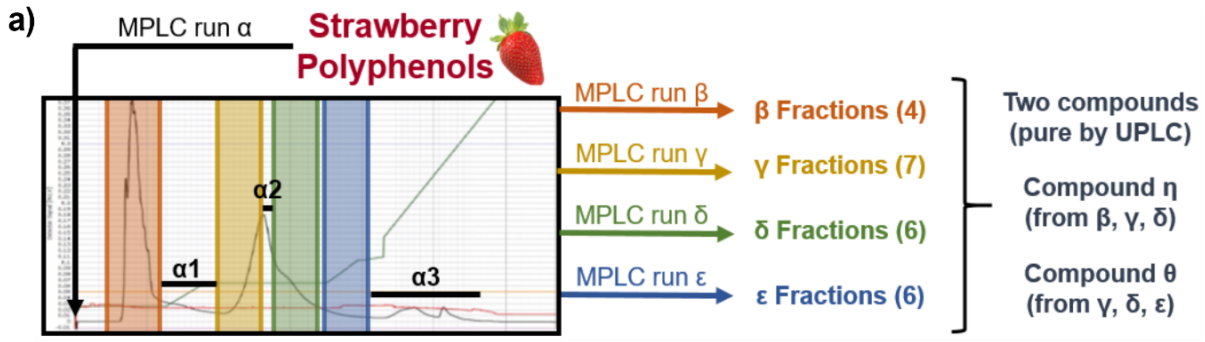
a)
MPLC run α
Strawberry Polyphenols
α1
α2
α3
MPLC run β
β Fractions (4)
MPLC run γ
γ Fractions (7)
MPLC run δ
δ Fractions (6)
MPLC run ε
ε Fractions (6)
Two compounds (pure by UPLC)
Compound η (from β, γ, δ)
Compound θ (from γ, δ, ε)

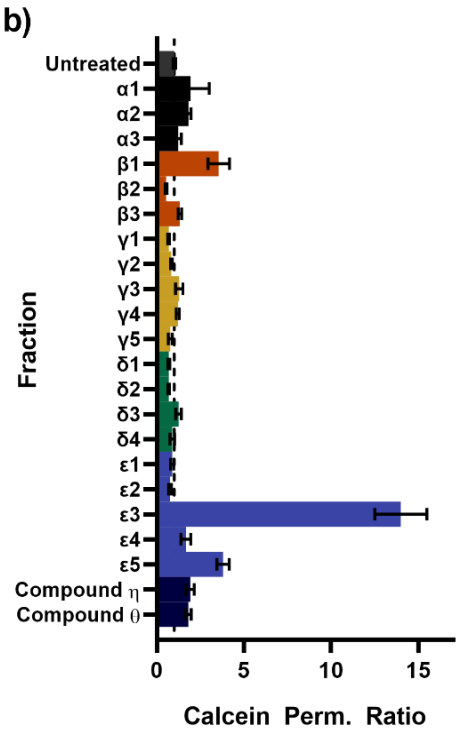
b)
Fraction
Untreated
α1
α2
α3
β1
β2
β3
γ1
γ2
γ3
γ4
γ5
δ1
δ2
δ3
δ4
ε1
ε2
ε3
ε4
ε5
Compound η
Compound θ
0
5
10
15
Calcein Perm. Ratio

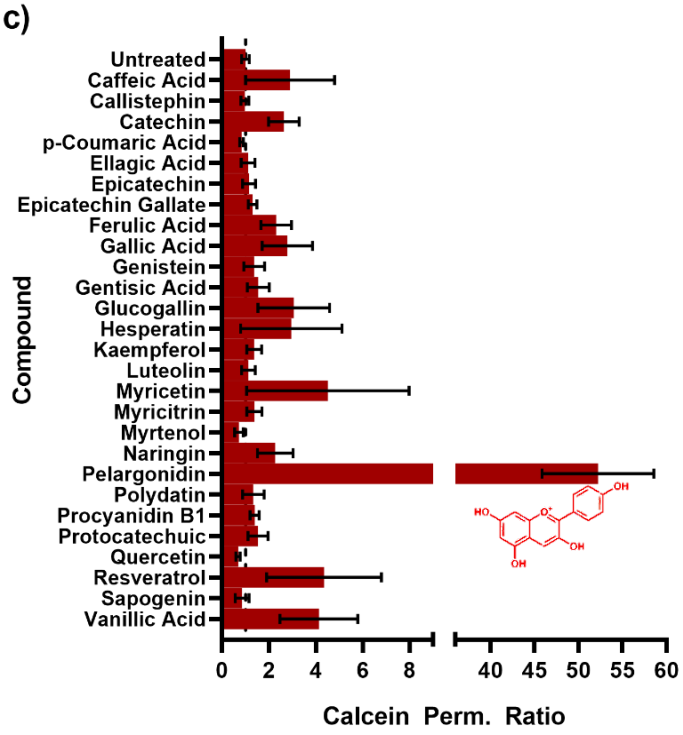
c)
Compound
Untreated
Caffeic Acid
Callistephin
Catechin
p-Coumaric Acid
Ellagic Acid
Epicatechin
Epicatechin Gallate
Ferulic Acid
Gallic Acid
Genistein
Gentisic Acid
Glucogallin
Hesperatin
Kaempferol
Luteolin
Myricetin
Myricitrin
Myrtenol
Naringin
Pelargonidin
Polydatin
Procyanidin B1
Protocatechuic
Quercetin
Resveratrol
Sapogenin
Vanillic Acid
0
2
4
6
8
40
45
50
55
60
Calcein Perm. Ratio

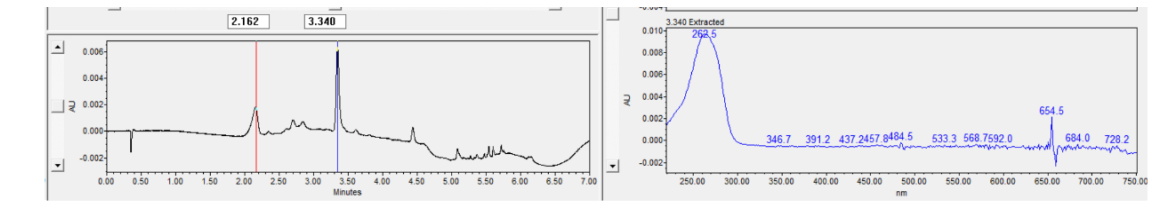
d) Fraction ε3
2.162
3.340
3.340 Extracted
262.5
654.5
346.7
391.2
437.2
457.8
484.5
533.3
568.7
592.0
684.0
728.2
Minutes
nm

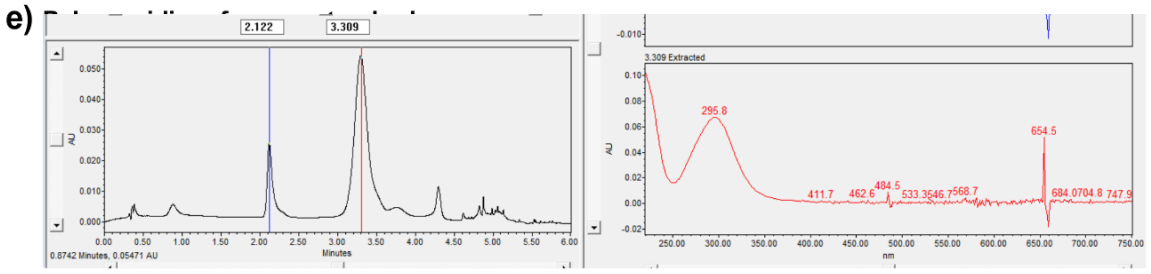
e)
2.122
3.309
3.309 Extracted
295.8
654.5
411.7
462.6
484.5
533.3
546.7
568.7
684.0
704.8
747.9
0.8742 Minutes, 0.05471 AU
Minutes
nm

Figure 4.5: Chromatography indicates that pelargonidin is the primary permeation enhancer in strawberries. (a) Two tiers of MPLC were used to separate the STRB PPh extract into fractions. The first run, α, yielded three fractions for direct biological testing (α1-α3) and four sets of material for the second tier of MPLC runs. These runs yielded the β, γ, δ, and ε fractions, as well as pure compounds η and θ. **(b)** When screened for activity on Caco-2 monolayers, only the ε3 fraction was an effective permeation enhancer. **(c)** Similarly, of a large group of phenolic compounds known to occur in strawberries, only the pigment molecule pelargonidin significantly increased the permeability of calcein across cell monolayers. **(d)** UPLC traces for fraction ε3 and **(e)** pelargonidin contain the same characteristic peaks in absorbance (at 280 nm) at approximately 2.1 and 3.3 minutes (left graphs) as well as similar absorption spectra (right graphs), indicating that they are likely chemically identical. Error bars represent s.e.m., n = 3 for calcein experiments.

hydrophobic material. To further support the similarity between ε3 and pelargonidin, we ran a sample of each on UPLC and compared the trace at 280 nm, as well as the absorbance spectra of the peaks (**Figures 4.5d** and **4.5e**). While it should be noted that the pelargonidin standard was run with almost an order of magnitude more material, the UPLC elution time readouts were nonetheless consistent. Both samples displayed characteristic peaks in 280 nm absorbance at approximately 2.1 and 3.3 minutes into the run, as well as similar UV-vis light absorption spectra. While this evidence is sufficient for us to conclude that pelargonidin is the primary permeation enhancer in strawberries, ongoing work aims to further probe its bioactivity and irrefutably confirm the identity of the ε3 fraction via NMR analysis.

4.3.6 – Pelargonidin Enables Oral Protein Delivery in Mice

In addition to strawberries, pelargonidin can be found in each of the previously-discussed red foods: tomatoes[37], red grapes[38,48], and red potatoes[40]. With this knowledge and our chromatography based evidence, we set out to demonstrate and characterize pelargonidin as a reversible, food-derived permeation enhancer. First, we examined dose dependent permeability response in Caco-2 monolayers. Reductions in

TEER (**Figure 4.6a**) and improvements in calcein permeability (**Figure 4.6b**) both increased with higher concentrations of (commercially purchased) pelargonidin treatment. It should be noted that the highest concentration, 1 mg/mL pelargonidin, opened the tight junctions beyond their ability to recover barrier function, underscoring the potency of this molecule at low concentrations. However, both lower concentrations of pelargonidin, 0.33 mg/mL and 0.67 mg/ml, induced substantial yet reversible permeabilization of the monolayers.

We then asked whether the pelargonidin-induced improvements in Caco-2 monolayer permeability would translate into successful oral administration of proteins and other macromolecules. To test this, we administered pelargonidin (40 mg/kg), then FITC-DX4 orally to mice, then examined the content of the fluorescent dextran in their blood. As expected, pelargonidin treatment doubled FITC-DX4 absorption across the intestinal barrier (**Figure 4.6c)** when compared to a phosphate-buffered saline (PBS) gavage. Based on this improved oral bioavailability of FITC-DX4, we again sought to determine if a protein drug translocate across the pelargonidin-treated intestinal epithelium. We orally gavaged mice with pelargonidin, then intestinally administered a 1 U/kg dose of insulin. Mice receiving insulin after pelargonidin treatment showed a significant reduction in blood glucose when compared to mice that received the drug after a saline control (**Figure 4.6d**). Further, the pelargonidin and insulin combination sustained hypoglycemia several hours longer than the same 1 U/kg dose of subcutaneous insulin. The areas above the curve (AACs) demonstrate that pharmacodynamic activity of pelargonidin-assisted intestinal insulin is approximately 130% that of subcutaneous insulin (**Figure 4.6e**). From this, we can conclude that

pelargonidin is an effective intestinal permeation enhancer that holds promise for future development and clinical translation.

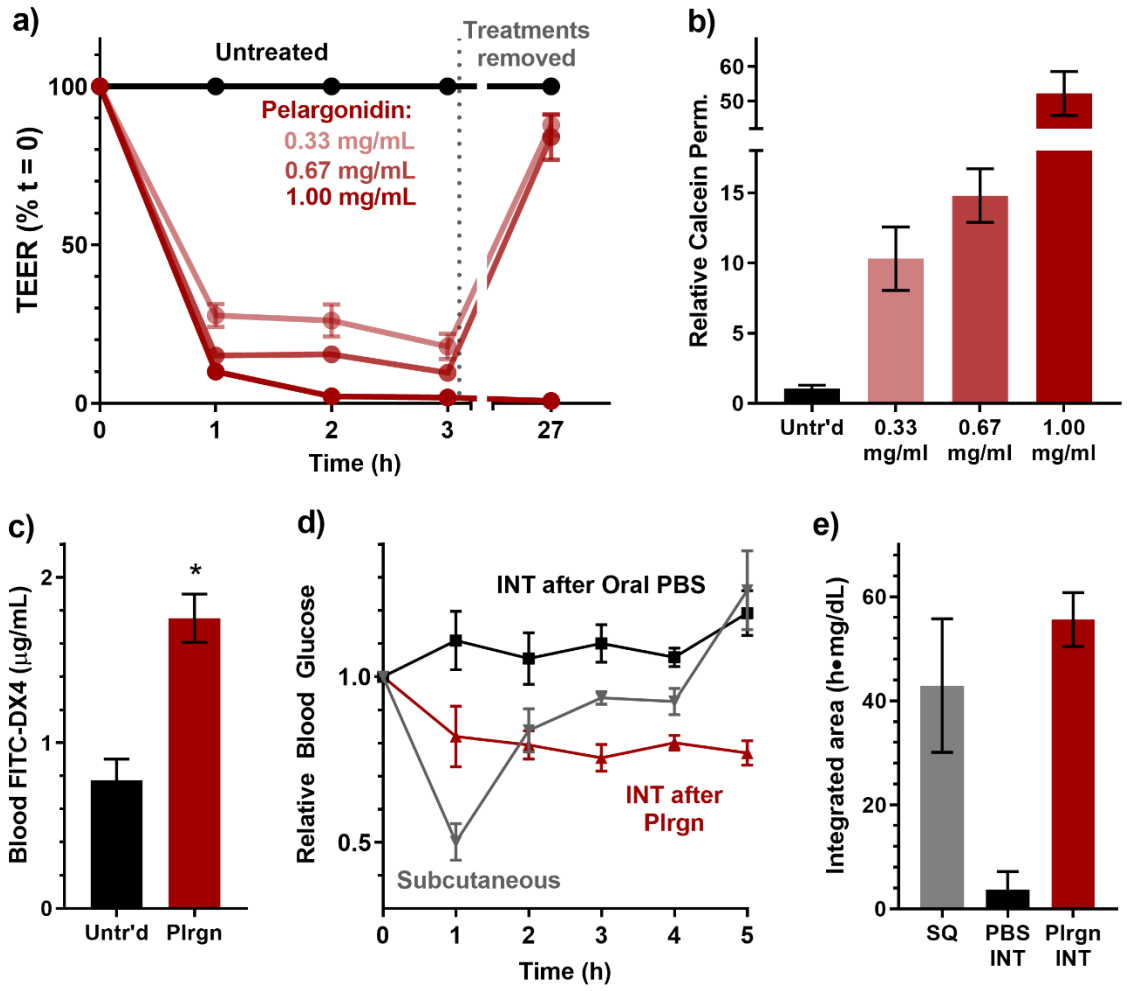

Figure 4.6: Pelargonidin is a reversible, efficacious permeation enhancer for oral protein delivery. (a) By TEER, pelargonidin gave a dose-dependent opening of the tight junctions between 0.33 and 1.00 mg/mL. However, only the two lower concentrations recovered their barrier function within 24 hours. **(b)** The dose dependence was also evident in pelargonidin's improvement of calcein permeability through the monolayers. **(c)** Treatment with pelargonidin doubled 4 kDa dextran absorption in mice, when compared to mice receiving just saline control. **(d)** One hour following oral gavage of pelargonidin in mice, an intestinal injection of 1 U/kg insulin induced sustained reductions in blood glucose levels. A 1 U/kg subcutaneous insulin dose induced a dramatic but transient. **(e)** Integrated areas above the curves from (d) show that oral delivery with pelargonidin resulted in 1.3 fold pharmacodynamic effect when compared to subcutaneous. **(e)** Error bars represent s.e.m., n = 3 for Caco-2 experiments and n = 5 for mouse experiments. * $p < 0.05$ w.r.t. untreated control

4.4 – Conclusions and Outlook

Oral administration of protein drugs, especially insulin, has the potential to broadly improve patient experience, compliance, and clinical outcomes for a wide array of maladies. However, successful clinical translation of oral delivery systems will require sufficiently high bioavailability of the drugs without damaging intestinal tissues. To address this need, we began here with the hypothesis that food-derived extracts would provide a well-tolerated, chemically diverse library from which one or more permeation enhancers could be identified. We demonstrated from this extensive library of crude extracts demonstrated that most foods do not appreciably change intestinal permeability. Of the few that do, strawberry was the most potent permeation enhancer, and demonstrated increased potency as extracts were refined and screened for oral drug delivery capabilities in both cell culture and in mice. Most notably, the compound pelargonidin approximately doubled bioavailability of the model macromolecule dextran and yielded approximately 130% bioactivity of intestinally administered insulin. These conclusive *in vivo* results demonstrate the ability of pelargonidin to effectively increase epithelial permeability, enabling the oral delivery of macromolecular drugs. Future investigations will include oral delivery of other active protein drugs, comprehensive safety studies in mice, and translation to higher animal models before moving to treat humans in the clinic.

3.5 – References

(1) Van Itallie, C. M.; Anderson, J. M. Claudins and Epithelial Paracellular Transport. *Annu. Rev. Physiol.* **2006**, *68*, 403–429. https://doi.org/10.1146/annurev.physiol.68.040104.131404.

(2) Friend, D. R. Drug Delivery to the Small Intestine. *Curr. Gastroenterol. Rep.* **2004**, *6* (5), 371–376. https://doi.org/10.1007/s11894-004-0052-z.

(3) Nagahara, N.; Tavelin, S.; Artursson, P. Contribution of the Paracellular Route to the PH-Dependent Epithelial Permeability to Cationic Drugs. *J. Pharm. Sci.* **2004**, *93* (12), 2972–2984. https://doi.org/10.1002/jps.20206.

(4) Claude, P. Morphological Factors Influencing Transepithelial Permeability: A Model for the Resistance of the Zonula Occludens. *J. Membr. Biol.* **1978**, *39* (2–3), 219–232. https://doi.org/10.1007/BF01870332.

(5) Aungst, B. J. Intestinal Permeation Enhancers. *J. Pharm. Sci.* **2000**, *89* (4), 429–442. https://doi.org/10.1002/(SICI)1520-6017(200004)89:4<429::AID-JPS1>3.0.CO;2-J.

(6) Ward, P. D.; Tippin, T. K.; Thakker, D. R. Enhancing Paracellular Permeability by Modulating Epithelial Tight Junctions. *Pharm. Sci. Technol. Today* **2000**, *3* (10), 346–358. https://doi.org/10.1016/S1461-5347(00)00302-3.

(7) Zhang, J.; Zhu, X.; Jin, Y.; Shan, W.; Huang, Y. Mechanism Study of Cellular Uptake and Tight Junction Opening Mediated by Goblet Cell-Specific Trimethyl Chitosan Nanoparticles. *Mol. Pharm.* **2014**, *11* (5), 1520–1532. https://doi.org/10.1021/mp400685v.

(8) Eriksson, O. Evolution of Angiosperm Seed Disperser Mutualisms: The Timing of Origins and Their Consequences for Coevolutionary Interactions between Angiosperms and Frugivores. *Biol. Rev.* **2016**, *91* (1), 168–186. https://doi.org/10.1111/brv.12164.

(9) Espín, J. C.; García-Conesa, M. T.; Tomás-Barberán, F. a. Nutraceuticals: Facts and Fiction. *Phytochemistry* **2007**, *68* (22–24), 2986–3008. https://doi.org/10.1016/j.phytochem.2007.09.014.

(10) Tsuji, P. A.; Stephenson, K. K.; Wade, K. L.; Liu, H.; Fahey, J. W. Structure-Activity Analysis of Flavonoids: Direct and Indirect Antioxidant, and Antiinflammatory Potencies and Toxicities. *Nutr. Cancer* **2013**, *65* (7), 1014–1025.

(11) Li, X.; Wang, T.; Zhou, B.; Gao, W.; Cao, J.; Huang, L. Chemical Composition and Antioxidant and Anti-Inflammatory Potential of Peels and Flesh from 10 Different Pear Varieties (Pyrus Spp.). *Food Chem.* **2014**, *152*, 531–538. https://doi.org/10.1016/j.foodchem.2013.12.010.

(12) Tairirai, C.; Viljoen, A. M.; Hamman, J. H. Effect of Dietary Fruits, Vegetables, and a Herbal Tea on the in Vitro Transport of Cimetidine: Comparing the Caco-2

Model with Porcine Jejunum Tissue. *Pharm. Biol.* **2012**, *50* (2), 254–263.

(13) Madhavi, D. L.; Bomser, J.; Smith, M. a L.; Singletary, K. Isolation of Bioactive Constituents from Vaccinium Myrtillus (Bilberry) Fruits and Cell Cultures. *Plant Sci.* **1998**, *131* (1), 95–103. https://doi.org/10.1016/S0168-9452(97)00241-0.

(14) Khan, N.; Syed, D. N.; Pal, H. C.; Mukhtar, H.; Afaq, F. Pomegranate Fruit Extract Inhibits UVB-Induced Inflammation and Proliferation by Modulating NF-KB and MAPK Signaling Pathways in Mouse Skin. *Photochem. Photobiol.* **2012**, *88* (5), 1126–1134. https://doi.org/10.1111/j.1751-1097.2011.01063.x.

(15) Amasheh, M.; Schlichter, S.; Amasheh, S.; Mankertz, J.; Zeitz, M.; Fromm, M.; Schulzke, J. D. Quercetin Enhances Epithelial Barrier Function and Increases Claudin-4 Expression in Caco-2 Cells. *J. Nutr.* **2008**, *138* (6), 1067–1073.

(16) Chen, W.; Lu, Z.; Viljoen, A.; Hamman, J. Intestinal Drug Transport Enhancement by Aloe Vera. *Planta Med.* **2009**, *75* (6), 587–595. https://doi.org/10.1055/s-0029-1185341.

(17) Lim, S.-L.; Lim, L.-Y. Effects of Citrus Fruit Juices on Cytotoxicity and Drug Transport Pathways of Caco-2 Cell Monolayers. *Int. J. Pharm.* **2006**, *307* (1), 42–50. https://doi.org/10.1016/j.ijpharm.2005.09.017.

(18) Vreeburg, R. A. M.; van Wezel, E. E.; Ocaña-Calahorro, F.; Mes, J. J. Apple Extract Induces Increased Epithelial Resistance and Claudin 4 Expression in Caco-2 Cells. *J. Sci. Food Agric.* **2011**, *92*, 439–444.

(19) Rabbani, G. H.; Teka, T.; Saha, S. K.; Zaman, B.; Majid, N.; Khatun, M.; Wahed, M. a.; Fuchs, G. J. Green Banana and Pectin Improve Small Intestinal Permeability and Reduce Fluid Loss in Bangladeshi Children with Persistent Diarrhea. *Dig. Dis. Sci.* **2004**, *49* (3), 475–484. https://doi.org/10.1023/B:DDAS.0000020507.25910.cf.

(20) Tsukura, Y.; Mori, M.; Hirotani, Y.; Ikeda, K.; Amano, F.; Kato, R.; Ijiri, Y.; Tanaka, K. Effects of Capsaicin on Cellular Damage and Monolayer Permeability in Human Intestinal Caco-2 Cells. *Biol. Pharm. Bull.* **2007**, *30* (10), 1982–1986. https://doi.org/10.1248/bpb.30.1982.

(21) Hashimoto, K.; Kawagishi, H.; Nakayama, T.; Shimizu, M. Effect of Capsianoside, a Diterpene Glycoside, on Tight-Junctional Permeability. *Biochim. Biophys. Acta - Biomembr.* **1997**, *1323* (2), 281–290. https://doi.org/10.1016/S0005-2736(96)00196-4.

(22) Shimizu, M. Modulation of Intestinal Functions by Food Substances. *Nahrung* **1999**, *43* (3), 154–158. https://doi.org/10.1002/(SICI)1521-3803(19990601)43:3<154::AID-FOOD154>3.0.CO;2-A.

(23) Watanabe, H.; Narai, A.; Shimizu, M. Purification and CDNA Cloning of a Protein Derived from Flammulina Velutipes That Increases the Permeability of the Intestinal Caco-2 Cell Monolayer. *Eur. J. Biochem.* **1999**, *262* (3), 850–857. https://doi.org/10.1046/j.1432-1327.1999.00440.x.

(24) Narai, A.; Watanabe, H.; Iwanaga, T.; Tomita, T.; Shimizu, M. Effect of a Pore-Forming Protein Derived from Flammulina Velutipes on the Caco-2 Intestinal Epithelial Cell Monolayer. *Biosci. Biotechnol. Biochem.* **2004**, *68* (11), 2230–2238. https://doi.org/JST.JSTAGE/bbb/68.2230 [pii].

(25) Tsao, R.; Deng, Z. Separation Procedures for Naturally Occurring Antioxidant Phytochemicals. *J. Chromatogr. B Anal. Technol. Biomed. Life Sci.* **2004**, *812* (1–2 SPEC. ISS.), 85–99. https://doi.org/10.1016/j.jchromb.2004.09.028.

(26) Maldoni, B. Alkaloids: Isolation and Purification. *J. Chem. Educ.* **1991**, *68* (8), 700–703.

(27) Bohlmann, J.; Keeling, C. I. Terpenoid Biomaterials. *Plant J.* **2008**, *54* (4), 656–669. https://doi.org/10.1111/j.1365-313X.2008.03449.x.

(28) Chang, L. C.; Kinghorn, A. D. Flavonoids as Cancer Chemopreventive Agents. In *Bioactive Compounds from Natural Sources: Isolation, Characterisation and Biological Properties*; Tringali, C., Ed.; Taylor & Francis: New York, NY, 2001; pp 159–178.

(29) Young, L.; Sung, J.; Stacey, G.; Masters, J. R. Detection of Mycoplasma in Cell Cultures. *Nat. Protoc.* **2010**, *5* (5), 929–934. https://doi.org/10.1038/nprot.2010.43.

(30) Chong, Saeho; Dando, Sandra A.; Morrison, R. A. Evaluation of Biocoat Intestinal Epithelium Differentiation Environment (3-Day Cultured Caco-2 Cells) as an Absorption Screening Model with Improved Screening Productivity. *Pharmaceutical Research*. 1997, pp 1835–1837. https://doi.org/10.1023/A:1012160703533.

(31) Yamashita, S.; Konishi, K.; Yamazaki, Y.; Taki, Y.; Sakane, T.; Sezaki, H.; Furuyama, Y. New and Better Protocols for a Short-Term Caco-2 Cell Culture System. *J. Pharm. Sci.* **2002**, *91* (3), 669–679. https://doi.org/10.1002/jps.10050.

(32) Gupta, V.; Doshi, N.; Mitragotri, S. Permeation of Insulin, Calcitonin and Exenatide across Caco-2 Monolayers: Measurement Using a Rapid, 3-Day System. *PLoS One* **2013**, *8* (2). https://doi.org/10.1371/journal.pone.0057136.

(33) Li, C.; Trombley, J. D.; Schmidt, M. A.; Hagerman, A. E. Preparation of an Acid Butanol Standard from Fresh Apples. *J. Chem. Ecol.* **2010**, *36* (5), 453–460. https://doi.org/10.1007/s10886-010-9784-4.

(34) Escarpa, A.; González, M. C. High-Performance Liquid Chromatography with Diode-Array Detection for the Determination of Phenolic Compounds in Peel and Pulp from Different Apple Varieties. *J. Chromatogr. A* **1998**, *823* (1–2), 331–337. https://doi.org/10.1016/S0021-9673(98)00294-5.

(35) Triantafillidis, J. K.; Merikas, E.; Georgopoulos, F. Current and Emerging Drugs for the Treatment of Inflammatory Bowel Disease. *Drug Des. Devel. Ther.* **2011**, *5*, 185–210. https://doi.org/10.2147/DDDT.S11290.

(36) Pastorelli, L.; Salvo, C. De; Mercado, J. R.; Vecchi, M.; Pizarro, T. T. Central Role

of the Gut Epithelial Barrier in the Pathogenesis of Chronic Intestinal Inflammation: Lessons Learned from Animal Models and Human Genetics. *Front. Immunol.* **2013**, *4* (SEP), 1–22. https://doi.org/10.3389/fimmu.2013.00280.

(37) Martí, R.; Roselló, S.; Cebolla-Cornejo, J. Tomato as a Source of Carotenoids and Polyphenols Targeted to Cancer Prevention. *Cancers (Basel).* **2016**, *8* (6), 1–28. https://doi.org/10.3390/cancers8060058.

(38) Ananga, A.; Georgiev, V.; Ochieng, J.; Phills, B.; Tsolov, V. Production of Anthocyanins in Grape Cell Cultures: A Potential Source of Raw Material for Pharmaceutical, Food, and Cosmetic Industries. *Mediterr. Genet. Code - Grapevine Olive* **2013**, 247–287. https://doi.org/10.5772/54592.

(39) Kosińska-Cagnazzo, A.; Diering, S.; Prim, D.; Andlauer, W. Identification of Bioaccessible and Uptaken Phenolic Compounds from Strawberry Fruits in in Vitro Digestion/Caco-2 Absorption Model. *Food Chem.* **2015**, *170*, 288–294. https://doi.org/10.1016/j.foodchem.2014.08.070.

(40) Zhang, Y.; Cheng, S.; De Jong, D.; Griffiths, H.; Halitschke, R.; De Jong, W. The Potato R Locus Codes for Dihydroflavonol 4-Reductase. *Theor. Appl. Genet.* **2009**, *119* (5), 931–937. https://doi.org/10.1007/s00122-009-1100-8.

(41) Tsao, R.; Yang, R. Optimization of a New Mobile Phase to Know the Complex and Real Polyphenolic Composition: Towards a Total Phenolic Index Using High-Performance Liquid Chromatography. *J. Chromatogr. A* **2003**, *1018* (1), 29–40. https://doi.org/10.1016/j.chroma.2003.08.034.

(42) Milder, I. E. J.; Arts, I. C. W.; van de Putte, B.; Venema, D. P.; Hollman, P. C. H. Lignan Contents of Dutch Plant Foods: A Database Including Lariciresinol, Pinoresinol, Secoisolariciresinol and Matairesinol. *Br. J. Nutr.* **2005**, *93* (3), 393–402. https://doi.org/10.1079/BJN20051371.

(43) Määttä-Riihinen, K. R.; Kamal-Eldin, A.; Törrönen, A. R. Identification and Quantification of Phenolic Compounds in Berries of Fragaria and Rubus Species (Family Rosaceae). *J. Agric. Food Chem.* **2004**, *52* (20), 6178–6187. https://doi.org/10.1021/jf049450r.

(44) Larsen, M.; Poll, L. Odor Thresholds of Some Important Aroma Compounds in Strawberries. *Zeitschrift fuer Leb. und -forsch.* **1992**, *195* (2), 120–123.

(45) Seeram, N. P.; Lee, R.; Scheuller, H. S.; Heber, D. Identification of Phenolic Compounds in Strawberries by Liquid Chromatography Electrospray Ionization Mass Spectroscopy. *Food Chem.* **2006**, *97* (1), 1–11. https://doi.org/10.1016/j.foodchem.2005.02.047.

(46) Giampieri, F.; Tulipani, S.; Alvarez-Suarez, J. M.; Quiles, J. L.; Mezzetti, B.; Battino, M. The Strawberry: Composition, Nutritional Quality, and Impact on Human Health. *Nutrition* **2012**, *28* (1), 9–19. https://doi.org/10.1016/j.nut.2011.08.009.

(47) Tumbas Šaponjac, V.; Gironés-Vilaplana, A.; Djilas, S.; Mena, P.; Ćetković, G.;

Moreno, D. A.; Čanadanović-Brunet, J.; Vulić, J.; Stajčić, S.; Vinčić, M. Chemical Composition and Potential Bioactivity of Strawberry Pomace. *RSC Adv.* **2015**, *5* (7), 5397–5405. https://doi.org/10.1039/c4ra14296a.

(48) Xie, S.; Zhao, T.; Zhang, Z.; Meng, J. Reduction of Dihydrokaempferol by Vitis Vinfera Dihydroflavonol 4-Reductase to Produce Orange Pelargonidin-Type Anthocyanins. *J. Agric. Food Chem.* **2018**, *66* (13), 3524–3532. https://doi.org/10.1021/acs.jafc.7b05766.

Chapter 5:

Anionic nanoparticles enable oral protein delivery by enhancing intestinal permeability

5.1 – Introduction

During the course of examining the crude fruit library in **Chapter 4**, we made a peculiar observation regarding some of the samples: those that were near their solubility limit and precipitated during the experiments caused strange behavior in the cell culture models. Further, simply filtering the samples through a standard, kitchen coffee filter produced completely different results. We hypothesized that some colloidal factor characteristic of the treatments was affecting the permeability of the Caco-2 monolayers, and began to consider the possibility of using a nanoparticle as a physical disrupter of the tight junctions.

As a potentially safer and more effective alternative to chemical permeation enhancers, some strategies for physically manipulating the epithelial barrier have been examined in preclinical trials. For example, polymer films with surface nanotopography open tight junctions in intestinal cell cultures, improving the transepithelial diffusion of model proteins[1]. Other studies have shown that ultrasound, through the physical process of cavitation, can temporarily disrupt the intestinal epithelial barrier to systemically deliver protein drugs[2]. Together, these studies suggest that physical means of intestinal permeabilization may offer improved safety profiles when used alone or, potentially, in combination with chemical approaches.

Here, we describe a serendipitous discovery that small, negatively charged particles act as physicochemical permeation enhancers that facilitate the oral delivery of protein. Specifically, the nanoparticles described here act not by moving across the intestinal epithelium as delivery vehicles, but by binding intestinal surface receptors that mediate the opening of tight junctions. This stands in contrast to previous studies for oral insulin delivery using nanoparticles, which primarily fall into two categories: insulin-loaded particles for transcytotic uptake[3–7] or insulin-loaded, chemical permeation enhancer-doped particles[8,9].

With this surprising revelation that the mere presence of nanoparticles can open tight junctions, we set out to establish the breadth of this effect, its therapeutic potential, and its mechanism. We discovered that small (<100 nm), anionic nanoparticle treatments improve absorption of model drugs across both Caco-2 monolayers and mouse intestines *in vivo*. Further, the oral delivery of two therapeutically-relevant protein drugs, insulin and exenatide, became possible when they were co-administered with silica nanoparticles in mice. Mechanistically, the nanoparticles increase intestinal permeability by binding integrins and activating myosin light chain kinase. Finally, we eliminate several safety concerns typical of permeation enhancers by showing their effect is reversible and does not cause necrosis or inflammation of intestinal tissue.

5.2 – Methods

5.2.1 – Materials

Thirteen commercially available nanoparticles were used in this study. Nine were purchased from nanoComposix (San Diego, CA, USA): nonfunctionalized silica (20, 50,

100, 200, 500 and 1200 nm), 50 nm amine functionalized silica, nonfunctionalized silver, and gold. Four were purchased from Microspheres-Nanospheres (Cold Spring, NY, USA): 50 nm polystyrene, 50 nm carboxyl functionalized silica, and silica internally doped with FITC (50 nm) or Rhodamine B (20 nm).

For cell culture and *in vitro* experiments, penicillin/streptomycin, trypsin-ethylenediaminetetraacetic acid (trypsin-EDTA), phosphate buffer saline (PBS), fetal bovine serum (FBS), rat tail Collagen I, calcein, DAPI, Hoechst 33342, Alexa Fluor® 488 tagged phalloidin, and Alexa Fluor® 594 tagged anti-ZO-1 antibodies were purchased from Life Technologies® (Thermo Fisher subsidiary, Carlsbad, CA, USA). Caco-2 cells and methyl thiazole tetrazolium (MTT) kits were purchased from American Type Culture Collection® (ATCC, Manassas, VA, USA). Dulbecco's Modified Eagles Medium (DMEM), Falcon® 225 cm^2 tissue culture flasks, Corning® HTS 1.0 µm porous support Transwell® plates, Falcon® 24-well plates, Corning® CellBIND® 96-well microplates, sodium butyrate, and MITO+ serum extender were obtained from VWR® (Radnor, PA, USA). FITC-labelled dextrans, Type II mucin from porcine stomach, myosin light chain kinase inhibitor peptide 18 (PIK), Eriochrome® Black T indicator (EBT), EDTA, anti-integrin αV, and anti-integrin β1 antibodies were purchased from Sigma-Aldrich® (St. Louis, MO, USA).

For mouse experiments, bovine pancreas insulin, bovine serum albumin (BSA), and metoclopramide hydrochloride were purchased from Sigma-Aldrich®. Exenatide, aprotinin, Aimstrip® Plus blood glucose strips, and blood glucose monitor were obtained from VWR®. Human insulin ELISA kits were purchased from LifeTechnologies®. Exenatide ELISA kits were purchased from Peninsula Laboratories (San Carlos, CA,

USA). Mouse sized (M) capsules and dosing kit were supplied by Torpac® (Fairfield, NJ, USA), and Eudragit® L100-55 enteric coating polymers were a gift of Evonik (Essen, Germany).

5.2.2 – Particle Characterization

Nanoparticles were diluted in deionized, 0.22 µm filtered water to a solids concentration of 1 mg/mL (w/v) for all DLS and zeta potential characterization. Suspension parameters were measured using a Malvern Zetasizer Nano (Malvern Instruments, UK), using the instrument software's pre-programmed material properties. Data reported for size and zeta potential are the averages of three technical replicate runs. All other particle characteristics reported were supplied by nanoComposix in particle batch certificates of analysis.

5.2.3 – Caco-2 Cell Culture

Caco-2 lines were confirmed mycoplasma free by direct DNA staining with Hoechst 33342[10]. Cells were cultured in DMEM supplemented with 10% FBS, 100 IU/mL of penicillin, 0.1 mg/mL streptomycin, and 0.25 µg/mL Amphotericin B ("Caco-2 media"). Cultures were incubated at 37°C in a fully humid, 5% CO_2 environment. The cells were subcultured with 0.25% trypsin-EDTA and subsequent passaging every 3 to 4 days at ratios between 1:3 and 1:8. Cells at passage numbers 20–50 were utilized for further experiments. The free-to-use PS power calculator (Vanderbilt) was used to determine the minimal sample size for which statistical power was greater than or equal to 0.8, generally n = 3-4 for Caco-2 based experiments.

5.2.4 – Toxicity Assays

For the MTT viability assay, Caco-2 cells were seeded in a clear, 96-well plate at a concentration of 10^5 cells/well. After incubating the plate overnight at 37°C, the media in the wells was aspirated and replaced with treatment solutions (100 µL/well, 0.2% w/v particles). After three hours of exposure, treatments were removed and cells were rinsed with warm PBS. MTT reagent (10 µL/well) and Caco-2 media (100 µL/well) were added to the wells. Three hours later, detergent reagent was added (100 µL/well), and the plate was incubated at room temperature, overnight, in the dark. A BioTek® Synergy2 automated plate reader was used to measure the absorbance of the MTT product in each well. The viability of each treatment is expressed as the ratio of its wells' absorbance values to the absorbance values of untreated wells.

For the LDH release viability assay, Caco-2 cells were seeded in a 96-well plate at a concentration of 10^4 cells/well. After incubating the plate overnight at 37°C, the media in the wells was aspirated and replaced with treatment solutions (100 µL/well, 0.2% w/v particles). After three hours of exposure, 50 µL of media from each well was transferred to a new, clear plate and combined with 50 µL/well LDH reaction mixture. Thirty minutes later, stop solution was added (50 µL/well), and the plate was read for absorbance at 680 nm (background signal) and 490 nm (formazan product of LDH activity). Viability percentages are provided by comparing the formazan absorbance of particle-treated cells to that of untreated (negative control) and completely lysed (positive control) cells.

5.2.5 – Caco-2 Permeability Experiments

For transepithelial electrical resistance (TEER) and diffusion marker permeability experiments, an established model[11–13] of rapid, 3-day Caco-2 intestinal epithelial monolayers was employed. Caco-2 cells were suspended in DMEM supplemented with MITO+ serum extender (basal seeding medium, BSM), seeded at a density of 2×10^5 cells per well on collagen-coated HTS membrane supports, and incubated for 24-48 hours. The media was then changed to DMEM supplemented with MITO+ and 2 mM sodium butyrate (enterocyte differentiation medium, EDM), and incubated for 48 hours. The TEER was monitored to confirm proper barrier formation, and only monolayers with initial TEER values of at least 150 $\Omega\cdot cm^2$ were utilized for TEER or molecular permeability experiments.

HTS inserts containing Caco-2 monolayers were transferred to 24-well plates containing 1 mL DMEM per well and allowed to equilibrate for 30 minutes before recording initial resistance values using a Millicell® voltohmmeter. Nanoparticle treatments were suspended in EDM (0.2 % w/v unless otherwise specified) and applied to the apical chambers, and negative control wells received fresh EDM. TEER readings were taken after 15, 30, 60, 120, and 180 minutes. After 180 minutes, treatments were removed and the monolayers rinsed once with warm PBS before returning to EDM in both the apical and basal chambers for a 24-hour recovery period.

For molecular permeability, fluorescent paracellular diffusion markers were applied at 0.5 mM (calcein) or 0.2 mM (FITC-DX4), into the apical side of the monolayers with the nanoparticle treatments. After one hour, media in the basal chambers was sampled and examined for fluorescence at 495/515 nm (calcein) or

485/515 nm (FITC-DX4) using the plate reader. Application of calibration curves yielded the amount of mass transferred across each monolayer, which was used in the permeability equation $P_{app} = \frac{\Delta M}{C_a A \Delta t}$, where P_{app} is the apparent permeability through the monolayer, ΔM is the marker mass in the basal compartment, C_a is the apical marker concentration, A is the monolayer area, and Δt is the time between samples. Permeability measurements are expressed as the ratio of each monolayer's permeability at 3 hours after treatment addition to its permeability before treatment, normalized to any change in untreated control monolayers during that time.

5.2.6 – Integrin Blockade and MLCK Inhibition

For the integrin blockade, Caco-2 monolayers were incubated for an hour before treatment with 1:10 diluted anti-integrin αV and 1:40 diluted (25 μg/mL) anti-integrin β1 antibodies. Particle treatments were added without removing the antibodies, and all changes in permeability were normalized to monolayers treated with the antibodies but no particles. For MLCK inhibition, the same procedure was employed, adding 0.33 mM (0.44 mg/mL) PIK to the cell media instead of the antibodies.

5.2.7 – Particle Translocation Across Mucus Layers

Type II mucin isolated from pig stomach was employed to create the *in vitro* mucus models, as it is the primary component of intestinal mucus[14]. Mucus was simulated by dissolving 5% (w/v) mucin in PBS, sonicating, then applying to Transwell® permeable membrane supports (1 μm pore size) to give a 2 mm deep layer. The supports were placed into a basal plate containing 1 mL of PBS in each well, and

fluorescent particle suspensions were added to the apical surface of the mucus. Samples were taken from the basal wells over time with PBS replenishment, and read for Rhodamine B (540/625 nm) or FITC (485/515 nm) on the plate reader to determine the fraction of particles transported across the barrier.

5.2.8 – Particle-Mucus Interactions

Mucin binding studies were based on previous mucus-binding studies by multiple groups[15,16]. Briefly, Type II mucin was dissolved in distilled water to a concentration of 10 mg/mL, stirring overnight at room temperature and sonicating to aid dissolution. The solution was then centrifuged for 30 minutes at 850 x g to remove any undissolved solids. Nanoparticles were added to the mucin solution at 1 mg/mL particles, then kept at 37°C with gentle stirring for the remainder of the experiment. At each time point, a sample of nanoparticle and mucin solution was collected and immediately examined for nanoparticle size via dynamic light scattering. Data shown are the averages of three DLS measurements on each sample.

5.2.9 – Mouse Studies

All mouse experiments were approved by the institutional animal care and use committee (IACUC) at Carnegie Mellon University (Pittsburgh, PA, USA) under protocol number PROTO201600017, and were performed in accordance with all institutional, local, and federal regulations. C57BL/6 mice were either purchased from Charles River Laboratories (Wilmington, MA, USA) or obtained from an institutionally managed breeding colony. Prior to experiments, mice were housed in cages of no more than six

animals, with controlled temperature (25°C), 12 hour light-dark cycles, and free access to food and water. Mice utilized in this study were female and 8-16 weeks (dextran and intestinal insulin, 18-24 g weight range) or 24-30 weeks (insulin capsules, 30-39 g weight range to ensure capsule passage through the GI tract) old, though only mice within 6 weeks of age are directly compared to one another (i.e. placed on the same graph) for consistency. The free-to-use PS power calculator (Vanderbilt) was used to determine the minimal sample size for which statistical power was greater than or equal to 0.8. (Generally, n=5-6). Mice were fasted 8-12 hours the night before an experiment to limit the variability caused by food matter and feces in the GI tract. Fasting also served to stabilize the animals' blood sugar for insulin activity experiments, with a starting blood glucose range of approximately 70 to 120 mg/dL. Oral gavages were administered at a volume of 10 mL solution per kg of mouse body weight (10 μL/g). Intestinal and subcutaneous injections were administered at a volume of 1 ml/kg (1 μL/g).

5.2.10 – Intestinal Permeability to Dextran

For dextran efficacy studies, fasted mice were orally gavaged with 100 mg/kg nanoparticle solutions (10 mg/kg concentration), then gavaged two hours later with a 60 mg/kg solution of FITC-DX4, at a dose of 600 mg/kg (for a timing study with 50 nm nonfunctionalized silica, this time step was varied between zero and twenty-four hours). Three hours after the dextran gavage, blood was collected and centrifuged. The serum was removed and examined for FITC concentration by reading for fluorescence on the plate reader (485/515 nm) and comparing to a unique calibration curve for each

experiment. For larger macromolecule studies, 40,000 MW dextran (FITC-DX40) was substituted at the same 600 mg/kg concentration. For permeability recovery, one group of mice was held for twenty-four hours, rather than two hours, between particle and FITC-DX4 gavages.

5.2.11 – Intestinal Insulin Delivery

Following ten hours of fasting, mice were orally gavaged with PBS (for control) or nanoparticle suspensions (100 mg/kg unless otherwise specified). Two hours later, their initial blood sugar was measured and the animals were placed under anesthesia. Their intestines were surgically exposed, and insulin was injected at the predetermined dose (1 unit per kg body weight unless otherwise specified) into the duodenum. The mice were closed and secured with tissue adhesive, then kept under anesthesia as their blood sugar levels were monitored each hour for five hours. An endpoint at five hours was enforced for all experiments, as the combined effects of the anesthesia, dehydration, and reduced blood sugar prevented reliable survival beyond that point. For comparison to the current standard of insulin delivery, subcutaneous injections were given at 1 U/kg to additional mice, into the scruff on their necks. To determine areas above the curve for each mouse, trapezoidal integration was used to sum the area between known points on the blood glucose curve and the starting blood glucose value for the individual animal.

To determine specific insulin concentrations, blood samples were collected and separated via centrifugation. The serum was subjected to ELISA analysis per the instructions of the kit manufacturer, and the kit exhibited reliable detection of the bovine

insulin used. To calculate areas under the concentration curve for each mouse, trapezoidal integration was used to sum the area between known points on the serum concentration curve and the pre-administration serum concentration for the individual animal.

5.2.12 – Oral Insulin Delivery with Capsules

Dry capsule contents for 675 U/kg insulin doses were produced by combining insulin, the protease inhibitor aprotinin, and inactive bovine serum albumin (BSA) filler at a 3:1:1 ratio in aqueous solution, then lyophilizing. Filler for negative control capsules contained just lyophilized aprotinin and BSA (0:1:4). 40 U/kg and 10 U/kg capsule fillers were created by diluting the high-dose insulin powder with the negative control powder. Size M capsules were filled with 2-3 mg filler, and their exact weights recorded. Each capsule was then dip coated 3 times in a 7% (w/v in ethanol) solution of Eudragit® L100-55, drying completely under gentle airflow following each coat. The total dry weight of polymer added to each capsule ranged from 0.4 to 0.8 mg.

Following a ten-hour fasting period, large (> 30 g) mice were orally gavaged with PBS (controls) or 100 mg/kg 50 nm silica nanoparticles, then injected subcutaneously with 1 mg/kg metoclopramide hydrochloride (to stimulate gastric emptying) and orally administered capsules two hours later. Capsules were chosen so small variations in filler weight matched small variations in mouse weight, giving insulin doses within 10% of the designated average dose. The capsules were immediately flushed into the stomach with an additional gavage of PBS or 100 mg/kg silica. Blood glucose was measured every two hours for a total of ten hours, and normalized to each mouse's

reading before capsule administration. From the blood glucose measurements, areas above the curve were calculated as previously described. These areas were used to calculate dose-corrected relative bioactivity as follows:

$$\underset{Bioactivity}{Relative} = \left(\frac{\beta \frac{U}{kg}\ AAC\ -\ 0\ \frac{U}{kg}\ Capsule\ AAC}{\beta \frac{U}{kg}} \right) \Bigg/ \left(\frac{1\ \frac{U}{kg}\ SQ\ AAC - 0\ \frac{U}{kg}\ SQ\ AAC}{1 \frac{U}{kg}} \right) \times 100\%$$

where β is the insulin dose in U/kg of the capsule treatment being examined, and SQ is subcutaneous injection.

For exenatide delivery using oral capsules, the same scheme was used. Capsule filler was 75:25:1 BSA : aprotinin : exenatide by mass. In the place of blood glucose measurements, blood was collected from each mouse at the predetermined times, and the serum was examined for exenatide concentration via ELISA. Areas under the concentration curve were calculated using trapezoidal integration to sum the area between known points on the serum concentration curve and the pre-administration serum concentration for the individual animal. The ratio of these areas is reported as the bioavailability.

5.2.13 – Confocal Microscopy

Monolayers were rinsed with PBS to remove treatments and fixed in 4% paraformaldehyde. They were permeabilized with 0.2% Triton-X100 and blocked with 0.2% BSA solution to limit non-specific antibody binding, then incubated for one hour with staining solutions. The staining solution contained DAPI (12 µg/mL, 358 nm/461 nm) to mark nucleic acids, AlexaFluor 488® conjugated phalloidin (5 units/mL, 495 nm/518 nm) to bind actin, and AlexaFluor® 594 conjugated Anti-ZO-1 antibodies (50

μg/mL, 590 nm/617 nm) in 0.2% BSA. For monolayers that were treated with FITC-doped particles (490 nm/525 nm) the staining solution was prepared without phalloidin. After staining, the monolayers were mounted on slides using ClearMount™ solution (Invitrogen - Carlsbad, CA, USA) and sealed under coverslips using clear nail polish.

Following treatment with FITC-doped particles (490 nm/525 nm), intestines were gently rinsed with PBS to remove fecal debris and fixed in 4% paraformaldehyde. They were permeabilized with 0.2% Triton-X100 and blocked with 0.2% BSA solution to limit non-specific antibody binding, then incubated for one hour with DAPI (12 μg/mL, 358 nm/461 nm) in 0.2% BSA. After staining, the intestines were gently sliced into small section and mounted onto slides in 0.6 mL PBS, using rubber spacers to prevent the coverslip from crushing the tissue.

Prepared slides were imaged at 10x (intestines) or 63x (monolayers) magnification using a Zeiss LSM 700 confocal microscope with ZEN 2012 SP1 software. Images were captured using a Plan-Apochromat 63x/1.40 Oil DIC objective and an X-Cite Series 120Q laser source exposing at 405, 488, and 555 nm. Since all samples were fixed, images were captured at room temperature and represent a single time point. Images were approximately 101.5 μm x 101.5 μm and were captured with a lateral resolution of approximately 0.3 μm. Z stack images were taken in 0.4 μm slices. No additional processing or averaging was performed to enhance the resolution of the images.

ImageJ (NIH) image processing software was used to prepare confocal images for publication. Upper and lower thresholds were narrowed slightly to remove background noise and improve visibility of the signals. All images were processed with

the same thresholds and display lookup tables (LUTs), which were linear throughout their ranges. Images were converted from their original 16-bit format to RGB color for saving and arrangement into figures. No other manipulations were performed. Z-stack images were converted to side perspective using the Orthogonal Views tool or assembled into video files using the Stacks tool in ImageJ.

To determine the ratio of nuclei to ZO-1 rings, ten locations were randomly selected from three monolayers each for both untreated and 50 nm, nonfunctionalized silica-treated cells. All monolayers were seeded from the same population of cells onto the same Transwell® plate. ZO-1 and DAPI were imaged for each location, and the resulting images randomized to blind the counter to their treatment status. Each image was then counted for number of nuclei or number of ZO-1 rings. The samples were then matched with their identities, and the corresponding nuclei to ZO-1 ratios calculated for each sample and each treatment.

5.2.14 – Histology

Three particle-treated and three untreated control mice were sacrificed following FITC-DX4 absorption experiments, and their small intestines were immediately excised. The organs were fixed for 24 hours in 4% paraformaldehyde, then transferred to 70% ethanol for shipment to Mass Histology Services (Worcester, MA, USA). There, paraffin sections were prepared and stained with hematoxylin and eosin for histological examination. A semi-quantitative analysis of tissue health, inflammation, and immune cell infiltration for each specimen was also prepared by a certified veterinary pathologist.

5.2.15 – Statistics

All data presented are accompanied by an indication of which statistical test was used to determine significance. For experiments in which the direction of effect was known, but the magnitude of the effect was being measured (e.g. permeability increases), one-tailed, Student's t-tests (*) were applied. For experiments determining if two treatments cause distinct responses from the biological subjects (e.g. difference between same number of two discrete particle sizes), two-tailed, Student's t-tests (†) were used to calculate relevant p values. In experiments where the same treatment was examined to different degrees (e.g. dose responses), statistics provided are the results of one-way ANOVA (#). All figures display the arithmetic mean of the given "n" number of biological replicates (individual animals or number of *in vitro* cell culture wells), and error bars display the standard error of the mean.

5.3 – Results and Discussion

5.3.1 – Nanoparticle library of varied sizes and surface chemistries

A collection of nanoparticles was purchased to probe the effect of size, surface charge, and chemistry on intestinal barrier function. We confirmed the supplier-provided particle properties using dynamic light scattering (DLS) and zeta potential measurements (**Table 5.1**). Particle diameters ranged from 20 nm to 1200 nm. Non-functionalized silica particles had the most negative zeta potentials (ranging from -41 to -84 mV), followed by carboxyl-functionalized silica, silver, and gold particles. Polystyrene particles were negligibly charged, and amine-functionalized particles had positive zeta potential (+16 mV).

Table 5.1: DLS size and zeta potential data for nanoparticles in water at neutral pH. Values for particle number and surface area per mass were obtained from specification sheets provided by the supplier. FITC = fluorescein isothiocyanate. RhodB = rhodamine B. n.f. = non-functionalized; PVP = 40,000 MW polyvinylpyrrolidone capping agent.

Core		Surface chem	Nomenclature	Z-average diameter		Zeta potential	Particles per mass	Surface area
Size (*nm*)	Material			*d.nm*	*PDI*	*(mV)*	*#/mg*	*cm^2/mg*
1200	silica	n.f.	**1200 nm SiO^-**	1173*	0.05*	-84.0	5.41E+08	23
500	silica	n.f.	**500 nm SiO^-**	536	0.08	-68.9	5.88E+09	52
200	silica	n.f.	**200 nm SiO^-**	209	0.02	-57.6	1.09E+11	137
100	silica	n.f.	**100 nm SiO^-**	90	0.05	-41.2	9.61E+11	280
50	silica	n.f.	**50 nm SiO^-**	49	0.04	-41.4	7.81E+12	554
20	silica	n.f.	**20 nm SiO^-**	26	0.05	-57.6	7.89E+13	1212
50	silica	COOH	**50 nm SiO-COO^-**	46	0.15	-27.3	n/a	n/a
50	silver	PVP	**50 nm Ag^-**	54	0.14	-21.4	1.47E+12	109
50	gold	PVP	**50 nm Au^-**	61	0.09	-16.3	7.64E+11	59
50	polystyrene	n.f.	**50 nm PS**	58	0.06	0.2	n/a	n/a
50	silica	NH_2	**50 nm SiO-NH_3^+**	49	0.44	15.6	7.24E+12	547
50	FITC-silica	n.f.	**50 nm FITC-SiO^-**	56	0.20	-27.2	n/a	n/a
20	RhodB-silica	n.f.	**20 nm RhodB-SiO^-**	23	0.20	-24.3	n/a	n/a

***** Values based on T.E.M. measurements and provided by manufacturer due to poor quality of DLS results with large particles.

5.3.2 – Anionic particles increased Caco-2 monolayer permeability

To assess the effect of particles on intestinal barrier function in cell culture, we applied silica nanoparticles ranging from 20 to 1200 nm in diameter to the apical side of Caco-2 monolayers, which represent the most common *in vitro* model of the intestinal epithelium[17]. For three hours following particle addition, we measured trans-epithelial electrical resistance (TEER), which correlates inversely with permeability[18]. While all silica nanoparticles reduced TEER values to some degree, 20 nm and 50 nm particles produced the most dramatic effect (**Figure 5.1a**). After three hours, monolayers were returned to fresh media, where they recovered their barrier function within 24 hours. MTT and LDH release assays showed no reductions in cell viability (**Figures 5.1b and**

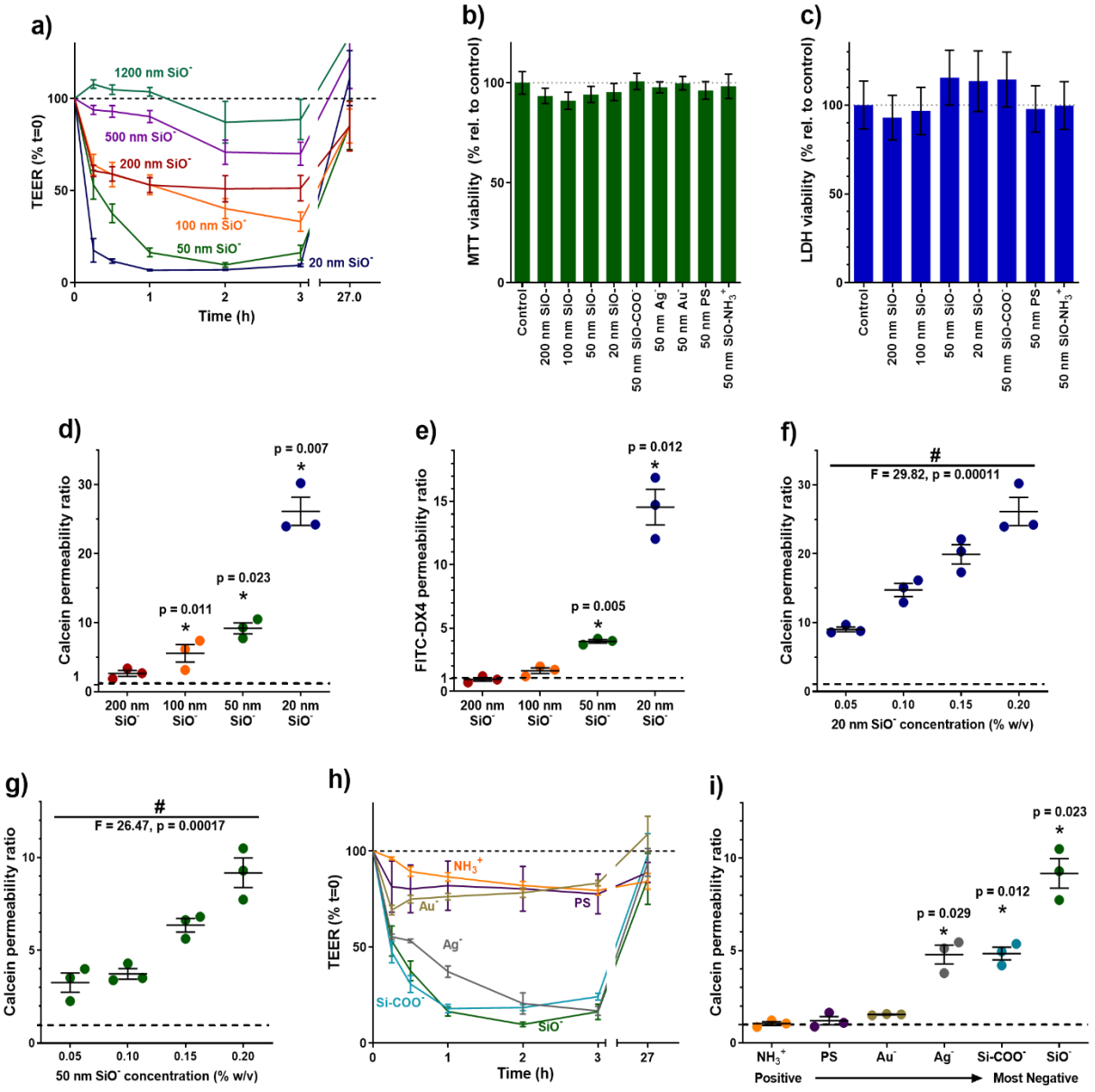

Figure 5.1: Smaller and more negatively charged nanoparticles potently and reversibly increased intestinal monolayer permeability *in vitro*. All measurements are expressed as ratios to values for untreated cells (dotted black lines). **(a)** Smaller silica particles caused greater reductions in the transepithelial electrical resistance (TEER) of Caco-2 monolayers. Particle treatments were removed at three hours, and the monolayers regained their barrier function within 24 hours. (**b)** None of the treatments induced statistically significant reductions ($p < 0.05$) in viability as measured by MTT assay or **(c)** LDH release assay. **(d)** Smaller silica particles induced larger permeability increases for the permeation markers calcein and **(e)** 4 kDa MW FITC-labelled dextran (FITC-DX4). **(f)** Increases in calcein permeability were dose responsive for both 20 nm particles and **(g)** 50 nm particles. **(f**) For a set of 50 nm nanoparticles with varied surface chemistry, those with greater negative surface charge caused greater monolayer permeability by TEER and **(i)** by calcein transport. Neutral and positively charged particles had no significant effect. Error bars display s.e.m. (n = 3), * $p < 0.05$ by one-tailed t-test, with respect to untreated cells. # $p < 0.05$ by one-way ANOVA.

5.1c), further confirming that silica nanoparticles induce reversible increases in permeability without permanently destroying the cell monolayers.

We confirmed that particle size inversely correlated to epithelial permeability for particles ≤ 200 nm by introducing membrane-impermeable diffusion markers to the apical surface of Caco-2 monolayers. Similar to whole proteins, these molecules do not cross the cell membrane, so their accumulation below the epithelial barrier reflects opening of the tight junctions, and has been shown to correlate well with TEER for marker sizes from 180 Da to at least 10 kDa[18,19]. The transport of the markers calcein (**Figure 5.1d**) and 4 kDa FITC-labelled dextran (FITC-DX4) (**Figure 5.1e**) were most effectively improved by 20 nm silica particles. Efficacy diminished with increasing particle diameter. Silica nanoparticles exhibited dose-dependent effects on intestinal cells over a treatment range of 0.05 – 0.2% w/v, with 20 nm (**Figure 5.1f**) and 50 nm (**Figure 5.1g**) particles improving calcein permeability up to 26- and 10-fold, respectively.

In addition to particle size, particle surface chemistry was directly linked to permeation enhancing ability. Only particles with negative surface chemistries – including non-functionalized silica, carboxylated silica, gold, and silver – significantly reduced TEER (**Figure 5.1h**) and increased calcein permeability through the intestinal monolayers (**Figure 5.1i**). Particles with neutral or positive charge had little effect on Caco-2 cells.

5.3.3 – Particles improved absorption of oral macromolecules in mice

We next assessed particle activity *in vivo* by orally dosing mice with silica nanoparticles and the macromolecule dextran (4 kDa, FITC-labelled). Because dextran does not contain any acid- or enzyme-labile bonds, it does not require protection in the GI tract. The 4 kDa molecular weight approximates that of common therapeutic peptides, such as insulin, exenatide, and calcitonin[20]. Particle-induced absorption enhancing effects were monitored by measuring systemic blood serum FITC levels. Unexpectedly, only the 50 and 100 nm particles improved the oral delivery of dextran (**Figure 5.2a**). Despite being the most effective treatment *in vitro*, the 20 nm silica nanoparticles did not substantially affect intestinal absorption in mice.

We hypothesized that the difference between *in vitro* and *in vivo* efficacy of 20 nm particles resulted from the mucus layer that lines the intestines but is not present in the Caco-2 model. To test this, we placed fluorescent silica particles on top of a permeable support that had been coated with a gel of Type II mucin, the predominant component of mucus in the intestines[14]. The particles used were internally doped with FITC or rhodamine B to track their accumulation beneath the mucus layer without affecting surface chemistry and interactions. Interestingly, the 20 nm particles (**Figure 5.2b**) diffused through the mucus at less than one-third the rate of 50 nm particles (**Figure 5.2c**). By applying mathematical models of diffusion through mucus and other, similar hydrated polymer networks[21–23], we can infer some information regarding the interactions between the particle surface and the mucin matrix.

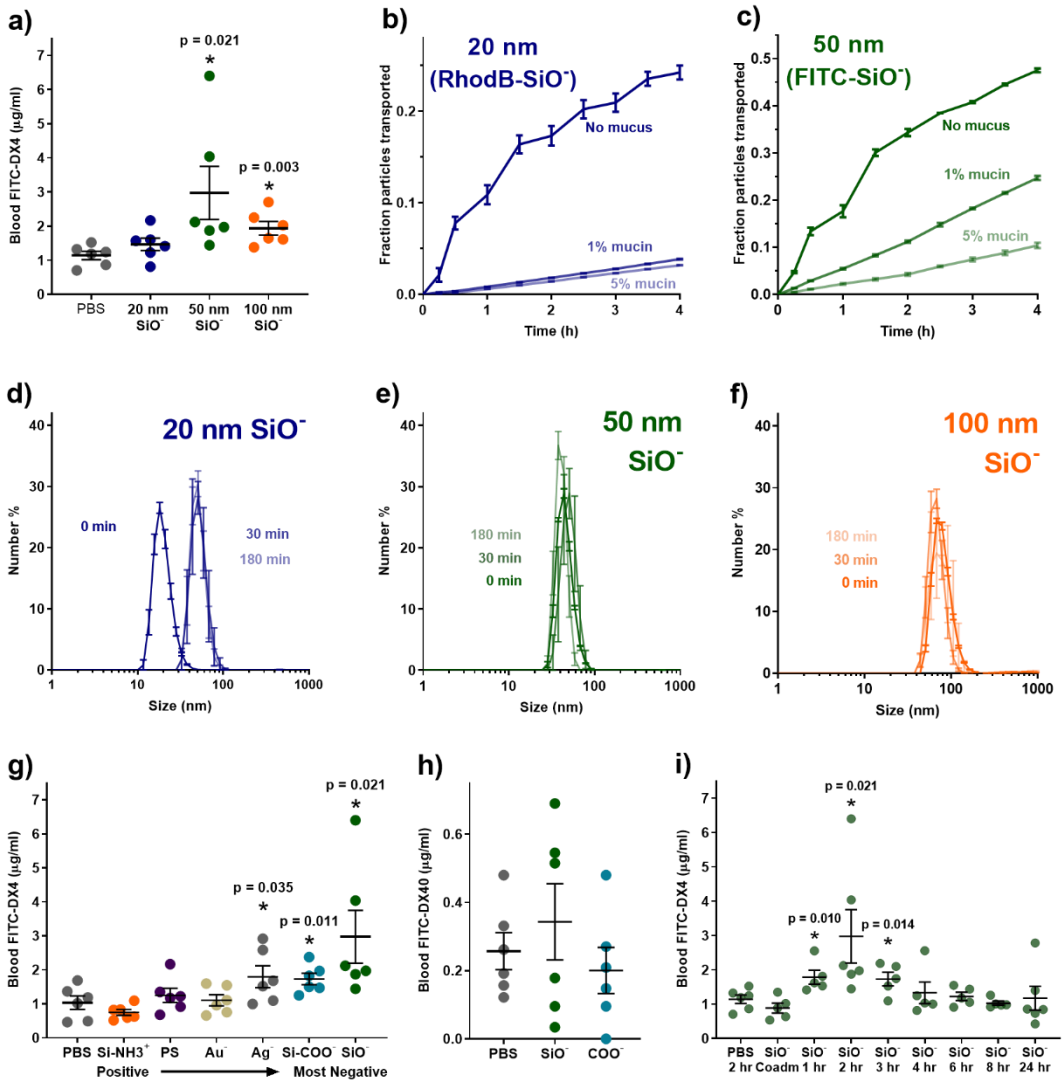

Figure 5.2: 50 nm anionic nanoparticles reversibly permeabilized intestinal epithelia in mice. (a) Oral treatment with silica particles improved absorption of 4 kDa, FITC-labelled dextran (FITC-DX4), with 50 nm particles being most effective. Despite their efficacy *in vitro*, 20 nm silica particles were not effective in mice. **(b)** This discrepancy was likely caused by the mucus present *in vivo*. Diffusion of 20 nm particles through model mucus was hindered compared to **(c)** 50 nm particles. **(d)** Intestinal mucins bound 20 nm particles within 30 minutes of exposure, increasing their apparent size. **(e)** By contrast, 50 nm and **(f)** 100 nm silica particles did not bind to mucin or change size in its presence. **(g)** Negatively charged particles improved absorption of 4 kDa dextran in mice, while positive and neutral particles did not. **(h)** Particles did not improve absorption of larger molecules, such as 40 kDa dextran (FITC-DX40). **(i)** Particle-induced permeability of mouse intestines began to increase within an hour after particle treatment and returned to normal levels within four to six hours of treatment. Error bars display s.e.m. (n = 3 for mucus studies and n =5 - 6 for mouse dextran studies). * $p < 0.05$ by one-tailed t-test, with respect to PBS control mice.

We assume that, in this one-dimensional diffusion problem, there will be a positive, linear correlation between diffusivity and particle translocation through the mucus layer. First, if the reduction in particle passage were due solely to volume occupation by the dilute mucin chains, we would expect the diffusivity to scale only with the volume fraction of the silica-containing, aqueous phase ($D_{eff} = D_0\varepsilon$, where D_{eff} is the effective diffusivity of the particles, D_o is the free diffusivity in water, and ε is the aqueous volume fraction). Since, in either case, particle translocation through a 1% mucin layer falls well below the expected value of 99%, we know that the mucin volume fraction is not the controlling factor. Next, we can consider the possibility that the porous mesh size in the mucin hydrogen hinders the passage of particles. The guiding equation in such a case is $D_{eff} = \frac{D_0}{e^{\left(\frac{r_m+r_p}{r_m}\sqrt{\varphi}\right)}}$, where D_{eff} is the effective diffusivity of the particles through the mucin mesh, D_o is the free diffusivity in water, r_m is the average mesh radius, r_p is the particle radius, and φ is the aqueous volume fraction. Here, given the same mucus mesh, we would expect the diffusivity of a larger particle to be less than that of a smaller particle. However, that is not the trend seen with either the 1% or 5% mucin layers. With neither of these factors explaining the more rapid transport of 50 nm particles than 20 nm particles through the mucus layer, we hypothesized that differential adsorption or binding interactions between the particles and mucin were responsible.

We confirmed that 20 nm particles are likely binding to mucin proteins by mixing 20, 50, and 100 nm silica particles each with a 1% (w/v) solution of type II mucin proteins and tracking their number average size over time via DLS. The 20 nm particles "grew" to three times their original size within thirty minutes (**Figure 5.2d**), indicating that the mucin bound to their surfaces. In contrast, 50 nm (**Figure 5.2e**) and 100 nm

silica particles (**Figure 5.2f**) did not grow in apparent size. While not visible in the figures, all three species exhibit a small peak (0.6 – 1%) at the micron scale, indicating that a limited number of the particles were aggregating or becoming entangled with the mucin chains. Nonetheless, a substantial number of the 50 and 100 nm particles remained unbound, and all further *in vivo* work was conducted with 50 nm particles to balance high permeation-enhancing efficacy and reduced mucus binding.

We also investigated whether particle surface charge has the same dramatic effect *in vivo* as it did in cell culture. Mice were orally gavaged with 50 nm particles of varied surface chemistry, followed by 4 kDa, FITC-labelled dextran. As in cell culture experiments, oral dextran delivery correlated with the strength of the negative charge on particles (**Figure 5.2g**). Neutral and positively-charged particles caused no significant change in dextran uptake.

Next, we assessed two potential safety concerns for any permeation enhancer. One potential concern is that the enhancers might permit the passage of bacteria or digestive byproducts into systemic circulation. The data in **Figure 5.2h** suggest that this would be an unlikely issue for silica nanoparticles, as 40 kDa FITC-labelled dextran did not experience increased transport when delivered with silica nanoparticles. Intestinal bacteria are much larger than 40 kDa dextran, so the permeation enhancing effect of silica is unlikely to allow their transepithelial migration[24]. The second potential concern pertains to the duration of action of the enhancer, as some chemical permeation enhancers have been shown to permanently disrupt the epithelial barrier[18,19,25,26]. Fortunately, the silica particles increased intestinal permeability rapidly, but only for a short duration of time. When 4 kDa dextran was delivered at differing times after particle

treatment, ranging from zero hours (coadministration) to twenty-four hours, permeability increased by one hour after treatment (**Figure 5.2i**), peaking at two hours. However, the measured intestinal permeability returned to baseline levels within four hours after treatment, and remained there through the rest of the trial, indicating that silica nanoparticle-induced permeation enhancement was transient and reversible.

5.3.4 – Silica particles enabled oral protein delivery in mice

Ultimately, we are interested in using silica nanoparticles to enhance the delivery of a functional, therapeutically relevant protein. As a proof-of-concept, we asked whether a protein drug could maintain its activity through silica-assisted intestinal translocation. We chose insulin for these studies, as it is a modestly-sized (5.8 kDa) protein that does not readily undergo transepithelial intestinal transport in healthy animals. Furthermore, its bioactivity is easily assessed by monitoring the depression of blood glucose concentration that results from increased insulin circulation. In a first set of experiments, mice received a 100 mg/kg oral dose of 50 nm silica nanoparticles, followed by an injection of 1 U/kg dose of insulin directly into the small intestine, circumventing digestion in the stomach. Blood glucose levels were monitored each hour and normalized to each mouse's blood sugar before the procedure. Mice that received insulin and silica nanoparticles experienced a substantial reduction in blood glucose compared to mice that received insulin and polystyrene nanoparticles (**Figure 5.3a**). Further, the silica nanoparticle and insulin combination sustained hypoglycemia several hours longer than the same 1 U/kg dose of subcutaneous insulin.

To compare the total insulin bioactivity between these administration methods, we integrated the areas between each mouse's glucose curve and its starting blood sugar value. The areas above the curve (AACs) show that pharmacodynamic activity of intestinal insulin in silica-treated mice is comparable to that of subcutaneous insulin (**Figure 5.3b**), yielding a relative bioactivity value of 100% (**Table 5.2**). Importantly, the more modest but longer-sustained activity of the intestinal insulin indicates that this administration route may be advantageous for drugs that require extended release profiles.

To ensure that the observed hypoglycemia was not a procedural artifact, we examined the dose responsiveness of both elements of the delivery system (i.e. the particles and the drug). While maintaining an insulin dose of 1 U/kg, increases in the nanoparticle dose from 50 to 200 mg/kg induced more pronounced and sustained reductions in blood glucose levels (**Figure 5.3c**). This trend is also reflected in the AAC calculations (**Figure 5.3d**). Because hypoglycemia did not resolve within 5 hours of treatment, the reported AAC values for the higher dose groups are an underestimate. The delivery system was also dose-dependent on insulin. When particles were administered at a constant dose of 100 mg/kg, increasing insulin dose from 0.5 – 2 U/kg correlated with increased magnitude and duration of hypoglycemia (**Figures 5.3e-f**).

Next, we assessed the pharmacokinetics of intestinally administered insulin by quantifying serum insulin concentrations using enzyme-linked immunosorbent assay (ELISA). Mice that received 1 U/kg subcutaneous insulin injections experienced large spikes in blood insulin concentration within fifteen minutes that returned to normal levels

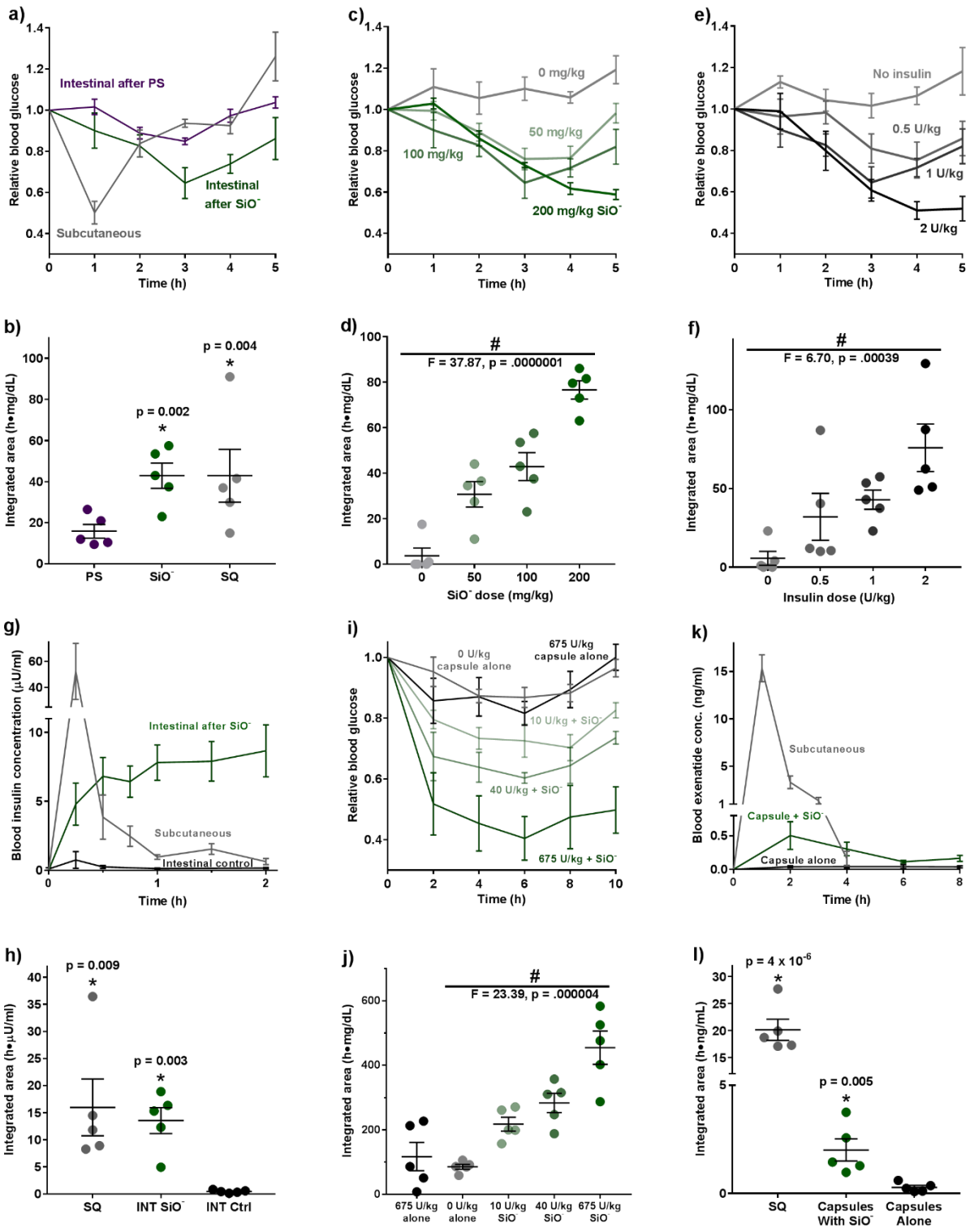
a)
Relative blood glucose
Time (h)
Intestinal after PS
Intestinal after SiO⁻
Subcutaneous
c)
Relative blood glucose
Time (h)
0 mg/kg
50 mg/kg
100 mg/kg
200 mg/kg SiO⁻
e)
Relative blood glucose
Time (h)
No insulin
0.5 U/kg
1 U/kg
2 U/kg
b)
Integrated area (h•mg/dL)
p = 0.004
p = 0.002
PS
SiO⁻
SQ
d)
Integrated area (h•mg/dL)
#
F = 37.87, p = .0000001
SiO⁻ dose (mg/kg)
f)
Integrated area (h•mg/dL)
#
F = 6.70, p = .00039
Insulin dose (U/kg)
g)
Blood insulin concentration (µU/ml)
Intestinal after SiO⁻
Subcutaneous
Intestinal control
Time (h)
i)
Relative blood glucose
0 U/kg capsule alone
675 U/kg capsule alone
10 U/kg + SiO⁻
40 U/kg + SiO⁻
675 U/kg + SiO⁻
Time (h)
k)
Blood exenatide conc. (ng/ml)
Subcutaneous
Capsule + SiO⁻
Capsule alone
Time (h)
h)
Integrated area (h•µU/ml)
p = 0.009
p = 0.003
SQ
INT SiO⁻
INT Ctrl
j)
Integrated area (h•mg/dL)
#
F = 23.39, p = .000004
675 U/kg alone
0 U/kg alone
10 U/kg SiO
40 U/kg SiO
675 U/kg SiO
l)
Integrated area (h•ng/mL)
p = 4 x 10⁻⁶
p = 0.005
SQ
Capsules With SiO⁻
Capsules Alone

Figure 5.3: Silica nanoparticles enabled oral protein delivery in mice. (a) Two hours following oral gavage of silica particles to mice, an intestinal injection of 1 U/kg insulin induced sustained reductions in blood glucose levels. Polystyrene nanoparticles did not enable insulin absorption. A 1 U/kg subcutaneous insulin dose induced a pronounced but brief response. **(b)** Integrated areas above the curves from (a) show that oral delivery with silica nanoparticles and subcutaneous injection resulted in comparable total pharmacodynamic effect. Blood glucose levels and areas above the curves were **(c, d)** particle dose dependent with a constant insulin dose of 1 U/kg and **(e, f)** insulin dose dependent with a constant particle dose of 100 mg/kg. **(g)** Pharmacokinetically, subcutaneous injection caused a spike in blood insulin concentration followed by a rapid decline. By contrast, intestinal administration after silica nanoparticles sustained more modest elevations in serum levels over several hours, leading to **(h)** nearly equal areas under the blood insulin curves for the two administration methods. **(i)** Orally delivered insulin induced pronounced and sustained hypoglycemia at doses as low as 10 U/kg when administered to silica-treated mice. Oral insulin without particles produced no effect compared to the control protein BSA. **(j)** Particle treatments resulted in multiple-fold increases in the area above the blood glucose curve calculated to 10 hours. **(k)** Particle treatments enabled systemic uptake of exenatide administered orally in capsules (1 mg/kg), leading to (**l**) a substantially higher area under the serum concentration curve when compared to capsules administered without silica. Error bars display s.e.m. (n = 5). * $p < 0.05$ w.r.t. control by one-tailed t-test. # $p < 0.05$ by one-way ANOVA.

shortly after two hours (**Figure 5.3g**). By contrast, mice that received the same intestinal insulin along with 200 mg/kg silica nanoparticles demonstrated more moderate elevations in blood insulin that persisted beyond two hours. Intestinal insulin with no particle treatment gave no substantial increase in serum insulin levels. Integrating the areas under the concentration curve for both administration routes yields approximately the same total serum values (**Figure 5.3h**) and nearly 100% relative bioavailability for the intestinal insulin (**Table 5.2**). This compares favorably to another promising oral protein delivery technology - CAGE ionic liquid – which registered 51% relative bioavailability upon intestinal injection[27].

Interestingly, the integrated bioavailability of the insulin appears to much better predict its relative bioactivity than does the peak serum concentration. Such a discrepancy between total insulin activity and maximal systemic insulin concentration is common when comparing subcutaneous to oral insulin systems[28,29], and is likely due to first-pass liver processing of all material absorbed by the intestines. This uptake leads to

Table 5.2: **Summary of relative bioavailability and relative bioactivity values for proteins delivered with or without silica nanoparticle absorption enhancers.** Data is presented as arithmetic average ± standard error. rBG_{min} = minimum average relative blood sugar achieved. AAC = insulin dose adjusted area above the blood glucose curve. rBA = dose-adjusted relative bioactivity. C_{max} = maximum average serum drug concentration achieved. AUC = dose adjusted area beneath the serum concentration curve. F = relative bioavailability.

Bioactivity						
Drug	**Delivery Route**	**Dose**	**Silica NPs**	**rBG_{min}**	**AAC**	**rBA**
		U/kg		%	$\frac{h * mg/dl}{U/kg}$	%
Insulin	SQ	1	No	50.1 ± 5.5	37.3 ± 13.6	100.0 ± 42.3
	INT	1	No	100.0 ± 0.0	0.0 ± 5.6	0.0 ± 0.0
		1	Yes	64.6 ± 7.5	37.3 ± 7.5	100.0 ± 33.1
	Oral	675	No	81.6 ± 3.9	0.0 ± 0.1	0.0 ± 0.0
		10	Yes	70.3 ± 4.3	13.2 ± 2.2	35.4 ± 11.1
		40	Yes	60.3 ± 1.8	4.9 ± 0.7	13.3 ± 4.2
		675	Yes	40.4 ± 7.2	0.5 ± 0.1	1.4 ± 0.4
Bioavailability						
Drug	**Delivery Route**	**Dose**	**Silica NPs**	**C_{max}**	**AUC**	**F**
		U/kg		$\mu U/ml$	$h * \mu U/ml$	%
Insulin	SQ	1	No	52.5 ± 21.6	16.0 ± 5.2	100.0 ± 46.3
	INT	1	Yes	8.7 ± 1.9	13.6 ± 2.4	84.8 ± 31.5
		1	No	0.7 ± 0.6	0.5 ± 0.1	2.9 ± 1.2
		U/kg		ng/ml	$h * ng/ml$	%
Exenatide	SQ	1	No	15.3 ± 1.4	20.2 ± 2.0	100.0 ± 13.7
	Oral	1	Yes	0.5 ± 0.2	2.0 ± 0.5	10.0 ± 2.3
		1	No	0.0 ± 0.0	0.3 ± 0.1	1.4 ± 0.4

a rapid decline in hepatic glucose output and more stable regulation of blood sugar than that achieved by injected insulin[30]. Thus, patients treated with oral insulin should experience superior glycemic control and significantly reduced risk of dangerous hypoglycemic episodes when compared to patients treated with subcutaneous insulin[31].

Given the successful proof-of-concept that silica nanoparticles facilitate intestinal delivery of insulin, we next demonstrated that particles enable fully oral delivery. To protect insulin in the upper GI tract, it was loaded into mouse-specific (Size M) gel capsules along with the protease inhibitor aprotinin, which improves protein survival in digestive fluids[32]. Furthermore, loaded capsules were coated with Eudragit L100-55, a pH-responsive polymer that remains intact at low pH (e.g. in the stomach) and dissolves at pH 5.5 to ensure delivery to the intestines. Mice weighing at least 30 g were used for capsule experiments to ensure that their GI tracts would be large enough for the material to transit, and a subcutaneous injection of 1 mg/kg metoclopramide hydrochloride was given at the time of capsule administration to induce gastric emptying into the small intestine.

We tested insulin at three doses: 675 U/kg to observe maximal effect given the packing limitations of the mouse capsules, 40 U/kg to closely compare with many of the oral insulin systems in literature[3–5,7,29,33], and 10 U/kg to probe how low of an oral insulin dose could produce an observable therapeutic effect. When delivered orally to mice treated with 200 mg/kg silica nanoparticles, these insulin capsules provoked intense, sustained hypoglycemia that lasted at least ten hours past administration (**Figure 5.3i**). In contrast, maximum dose insulin capsules given to mice without nanoparticle treatment did not affect blood glucose or corresponding AACs when compared to control capsules containing only BSA and aprotinin (**Figure 5.3j**).

Using the blood glucose AACs to compare insulin pharmacodynamics between subcutaneous and oral administrations, we calculated per-dose, relative bioactivities of the insulin capsules (**Table 5.2**). Notably, the 10 U/kg capsules were approximately

35% bioactive compared to the 1 U/kg subcutaneous injection. This compares favorably with many of the most promising technologies for oral protein delivery. For example, studies using starch microgels[5] and permeation enhancer loaded mucoadhesive intestinal patches[29] have achieved up to 7% relative insulin bioactivity in rats. Similarly, nanoparticles particles decorated with penetratin[4] or low molecular weight protamine[6] for cellular uptake, reach 10-18 % relative bioavailability. These comparisons suggest that silica nanoparticle system may be a particularly promising option for oral insulin delivery.

To confirm that the silica nanoparticles promote the intestinal absorption of protein drugs beyond insulin, we next sought to deliver the anti-diabetic peptide exenatide. Exenatide mimics native hormones to help stabilize blood sugar and is injected subcutaneously for long-term management of type 2 diabetes[34]. To orally deliver this peptide, exenatide-loaded capsules (1 mg/kg dose) were enterically coated for protection against the stomach environment, and washed down the esophagus with either silica nanoparticle suspension (200 mg/kg), or saline for a negative control. Blood samples, which were analyzed for exenatide concentration via ELISA, showed that the particle treatments greatly improved exenatide uptake compared to the peptide capsules without particle treatment (**Figure 5.3k**). When compared to the same dose of subcutaneously administered exenatide, the silica-assisted, orally delivered peptide achieved 10% bioavailability (**Figure 5.3l** and **Table 5.2**). While this is lower than bioavailability following intestinal injection due to less spatial control and particle-protein co-localization, it does compare closely with oral protein delivery by promising technologies in the literature. For example, nanoparticles that exploit the bile salt

pathway for intestinal cell uptake can reach 15.9% oral bioavailability, and GIPET-enhanced tablets achieve 8-9% oral delivery of 4-6 kDa proteins[35]. Given that GIPET has advanced into Stage II clinical trials[36], and our successful delivery of both insulin and exenatide, we believe that these silica nanoparticle treatments have the potential to translate into the clinic as a platform technology for the oral administration of small protein drugs.

5.3.5 – Particles induce integrin-mediated tight junction remodeling

Having demonstrated that silica improves oral absorption and bioactivity of protein drugs, we asked how the nanoparticles increase epithelial permeability. First, we determined that permeabilizing activity was not a colligative property (**Figure 5.4a**), indicating that activity was not caused by an osmotic pressure gradient. Next, we applied silica particles of different sizes while maintaining the total particle surface area per treatment to determine that the total anionic charge is not a controlling factor (**Figure 5.4b**). We also examined particles for calcium chelation activity, a mechanism by which some chemical permeation enhancers improve epithelial permeability[37,38] (**Figure 5.4c**). While some particles caused slight decreases in free calcium ions, none approached the full calcium depletion necessary to induce tight junction opening.

Next, we examined the integrin family of epithelial cell surface receptors. Integrins have been implicated in the mechanism of action for mechanical permeation enhancement by nanostructured films[39]. When these receptors are bound, the resulting signal cascade activates the enzyme myosin light chain kinase (MLCK). Activated MLCK phosphorylates a portion of the cytoskeleton, which then contracts and exerts

tension on the tight junctions, causing them to open[39,40] **(Figure 5.5a**). This action of MLCK has previously been exploited for oral insulin delivery by using rationally designed PIP (permeant inhibitor of phosphatase) peptides to force the kinase into a perpetually active state, leading to actin contraction and tight junction opening[28]. In the intestinal epithelium, because tight junctions represent the major barrier to passive transepithelial diffusion, their opening facilitates protein transport from the intestinal lumen into the body and systemic circulation. The physiologic purpose for this process in the intestinal epithelium is unknown. However, a purpose for integrin-mediated

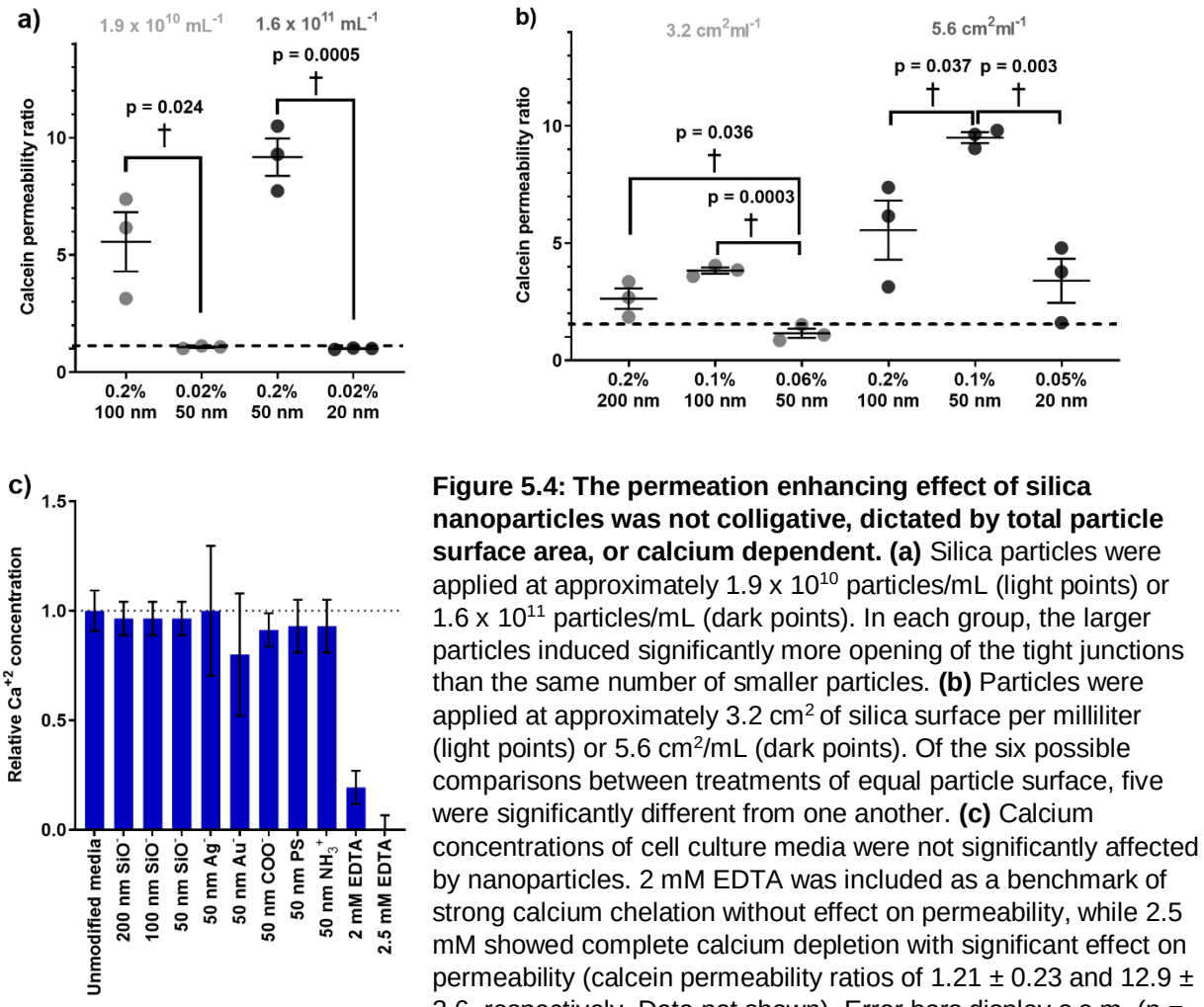

Figure 5.4: The permeation enhancing effect of silica nanoparticles was not colligative, dictated by total particle surface area, or calcium dependent. (a) Silica particles were applied at approximately 1.9 x 10^{10} particles/mL (light points) or 1.6 x 10^{11} particles/mL (dark points). In each group, the larger particles induced significantly more opening of the tight junctions than the same number of smaller particles. **(b)** Particles were applied at approximately 3.2 cm^2 of silica surface per milliliter (light points) or 5.6 cm^2/mL (dark points). Of the six possible comparisons between treatments of equal particle surface, five were significantly different from one another. **(c)** Calcium concentrations of cell culture media were not significantly affected by nanoparticles. 2 mM EDTA was included as a benchmark of strong calcium chelation without effect on permeability, while 2.5 mM showed complete calcium depletion with significant effect on permeability (calcein permeability ratios of 1.21 ± 0.23 and 12.9 ± 3.6, respectively. Data not shown). Error bars display s.e.m. (n = 3), † $p < 0.05$ by two-tailed t-test.

junction-opening has been identified in the endothelium: it aids the migration of immune cells from the blood stream into surrounding tissue. Specifically, the cells undergo integrin binding with the top of the endothelial monolayer, inducing the tight junctions to briefly open before re-forming the barrier[41]. Based on this behavior, we hypothesized that the silica nanoparticles were stimulating a similar pathway, binding to the epithelial cells to briefly and reversibly open the junctions, allowing protein absorption.

To test this hypothesis, we first blocked integrins commonly associated with extracellular matrices[42] on Caco-2 monolayers and re-examined the particles' permeabilizing effects on these cells (**Figure 5.5b**). Even though only two (ITGαV and ITGβ1) of twenty-four known human integrin subunits[42] were prevented from interacting with the nanoparticles, the boost to permeability was reduced by approximately 30%. From this, we can conclude that integrins αV and β1 are partially responsible for particle binding and signal activation, but other integrin subtypes are likely also involved and account for the partial conservation of particle efficacy. By contrast, treatment with an MLCK inhibitor cut off the signal cascade downstream and completely prevented the particles from increasing monolayer permeability. From this, we can conclude that silica nanoparticles increase intestinal permeability by contracting the cytoskeleton through the MLCK-dependent signaling pathway.

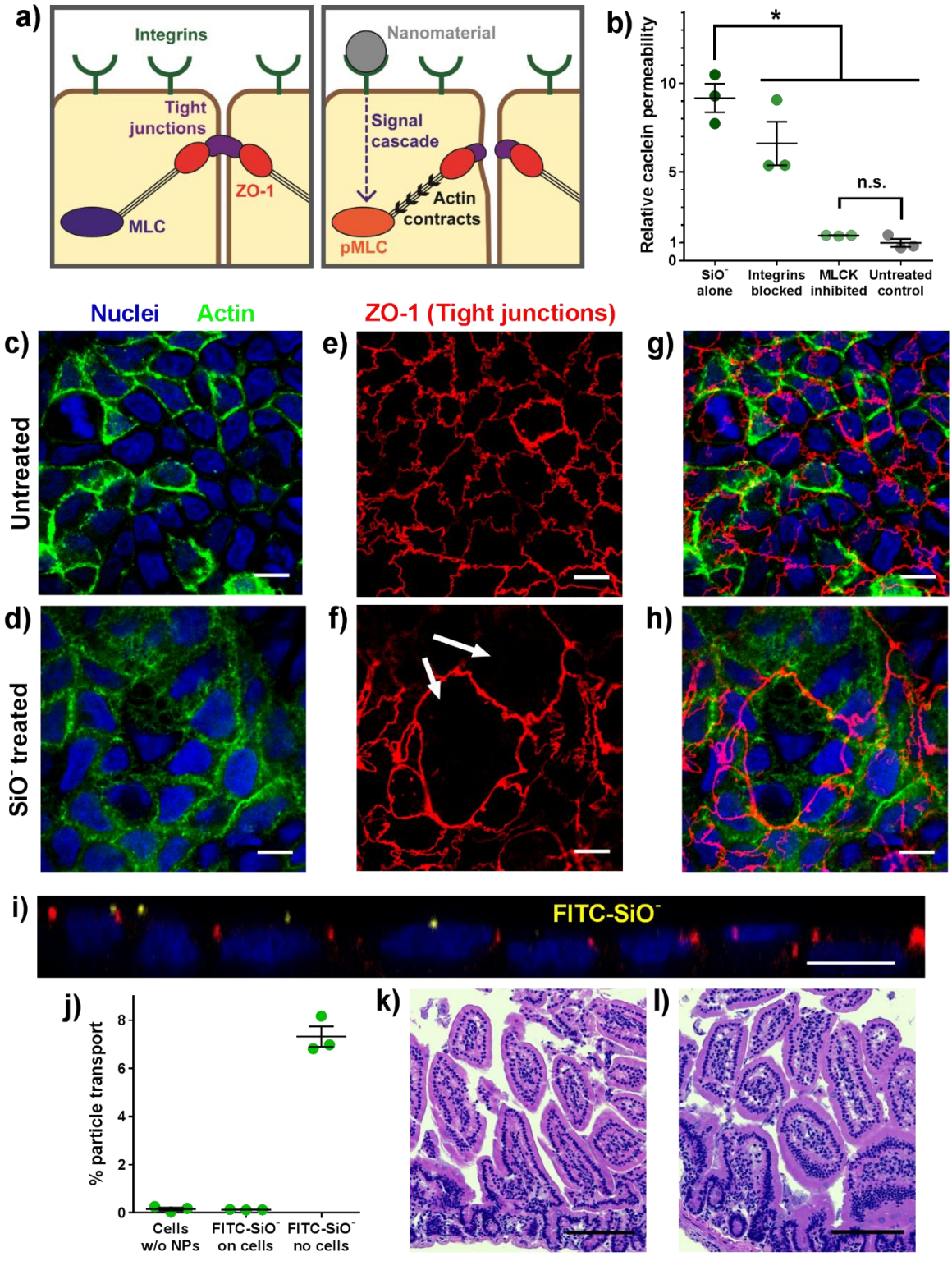
a)
Integrins
Tight junctions
ZO-1
MLC
Nanomaterial
Signal cascade
Actin contracts
pMLC
b)
Relative caclein permeability
*
n.s.
10
5
1
0
SiO⁻ alone
Integrins blocked
MLCK inhibited
Untreated control
Nuclei
Actin
ZO-1 (Tight junctions)
c)
e)
g)
Untreated
d)
f)
h)
SiO⁻ treated
i)
FITC-SiO⁻
j)
% particle transport
8
6
4
2
0
Cells w/o NPs
FITC-SiO⁻ on cells
FITC-SiO⁻ no cells
k)
l)

Figure 5.5: Silica nanoparticles increased permeability by binding cell surface integrins and inducing tight junction rearrangement. (a) An integrin- and myosin light chain (MLC)-dependent cell signaling pathway has been previously linked to intestinal permeability. **(b)** The permeation enhancing effect of silica nanoparticles *in vitro* was reduced when either a subset of integrins was blocked or pMLC activation was inhibited. **(c, d)** In Caco-2 monolayers imaged at 63x magnification, actin (green) and nuclei (blue) did not rearrange in response to particle treatment. **(e)** The tight junction protein ZO-1 (red) localized around the perimeter of each untreated cell while **(f)** silica particle treatment induced ZO-1 rearrangement, creating clusters of cells between which no ZO-1 was present (white arrows). (**g)** Overlaid images show that the general 1:1 ratio of tight junctions to nuclei in the untreated sample was not maintained in (**h**) the nanoparticle treated cells, where a single tight junctional boundary encompassed several nuclei. **(i)** A side view confocal image of a nanoparticle-treated monolayer confirmed that nanoparticles (yellow) localized on top of the cells but did not permeate the tight junctions. **(j)** FITC-labeled silica nanoparticles did not cross *in vitro* intestinal barriers. Particles diffused into the basolateral chamber when no epithelial cells were present. **(k)** Histological analysis of untreated and **(l)** particle treated mice showed no inflammation and no change in epithelial architecture. Error bars display s.e.m. (n = 3). * $p < 0.05$ by one-tailed t-test. White scale bars = 10 μm. Black scale bars = 100 μm.

To visualize how particle-induced cytoskeletal tension affects tight junction arrangement, we stained Caco-2 monolayers for nucleic acids, actin, and the tight junction protein ZO-1. There was no apparent rearrangement of nuclei or the actin skeleton (**Figure 5.5 c-d**), despite actin rearrangement being a common mechanism of action for intestinal permeation enhancers[26,43]. However, when compared to ZO-1 patterns in untreated samples, some particle-treated cells formed clusters that did not contain ZO-1 within their junctions (**Figure 5.5 e-h**). This rearrangement may create an effective permeation pathway for macromolecule drugs to diffuse between the cells. To the best of our knowledge, this phenomenon has not previously been reported in literature. To quantitatively assess these permeation hotspots, we counted the number of nuclei and ZO-1 loops in both untreated and particle-treated monolayers. Cells exposed to silica nanoparticles had a significantly higher ratio of nuclei to ZO-1 enclosures (1.27 +/- 0.07, mean +/- s.e.m.) than untreated cells (1.05 +/- 0.03), indicating that the particle treatments deplete ZO-1 between epithelial cells.

Given that permeation enhancing silica nanoparticles need only to interact with apical cell surface integrins to take effect, we performed a set of studies to determine whether they penetrate or traverse the epithelium. In these experiments, silica nanoparticles containing FITC in their cores were applied to the apical side of Caco-2 monolayers, which were subsequently imaged using confocal microscopy. Composite stacks of monolayer images showed that the particles accumulate at the apical cell surface but do not localize within junctions or inside the cells (**Figure 5.5i**). Additionally, the particles did not traverse the monolayers, with only the cell-free membrane supports allowing FITC passage (**Figure 5.5j**). This is consistent with previous studies that have shown that negatively charged particles do not readily translocate through epithelial models[44,45]. These studies add further evidence that silica nanoparticles are acting solely as permeation enhancers and not as delivery vehicles that transport macromolecules across the intestinal barrier.

To assess the integrity of intestinal tissue following treatment, histology was performed on the intestines of untreated and particle-treated mice. There were no significant differences between the control (**Figure 5.5k**) and experimental mice (**Figure 5.5l**). Further, semi-quantitative analysis by a trained pathologist indicated no difference in immune cell infiltration or inflammatory response between the samples. These results are consistent with several studies that have shown that chronic gastrointestinal exposure to nanosilica does not cause lasting health effects in animal models[46]. Most notably, a study in rats examined particles ranging from 20 to 100 nm, delivering a particle dose ten times the largest used here (2000 mg/kg vs 200 mg/kg) every day for ninety days. Afterwards, there were no signs of particle uptake into the animals' bodies

and no observable changes in clinical signs, blood biochemistry, or histopathological markers.

Given that our experiments showed efficacy at doses at least as low as 50 mg/kg (**Figures 5.3c** and **5.3d**), the particles can be inferred to have a therapeutic window spanning at least 1.5 orders of magnitude. By contrast, many of the most promising chemical permeation enhancers, including piperazines, bile salts, fatty acids, and surfactants, have very narrow therapeutic windows, often less than an order of magnitude concentration *in vitro*[18,19,26,47]. Despite their narrow therapeutic windows, several of these species have nonetheless advanced to early stage clinical trials[25]. We also anticipate that the incorporation of silica nanoparticles into a delivery vehicle, such as a polymer-based intestinal patch[29,48,49], will drastically reduce the dose of particles needed to achieve the same protein uptake when scaling up to larger animal models. Whereas the particles and protein drugs are currently spreading throughout the intestines upon administration, we anticipate the same magnitude of effect at lower doses when nanoparticles are co-localized with drug at the surface of the intestinal epithelium.

5.4 Conclusions and Outlook

The oral delivery of protein drugs has the potential to improve the patient experience and disease outcomes by mitigating the fear and non-compliance associated with injections. Unfortunately, no approved oral protein therapies exist because clinical translation requires high bioavailability of drug without toxicity. We have shown here that small, negatively charged nanoparticles may fill this therapeutic void for

small proteins and macromolecules. Specifically, 50 nm silica nanoparticles potently improved intestinal permeability to macromolecular therapeutics and enabled the oral delivery of two protein drugs: insulin and exenatide. Silica particles enhanced intestinal permeability by binding integrins on the apical epithelial surface, triggering an MLCK-dependent opening of the tight junctions. Intestinal permeation enhancement was reversible and non-toxic in mice. Together, our data demonstrate that silica and other strongly anionic nanoparticles have the potential to make oral protein delivery a reality, and should move to be tested for both efficacy and safety in higher animal models.

5.5 References

(1) Kam, K. R.; Walsh, L. a.; Bock, S. M.; Koval, M.; Fischer, K. E.; Ross, R. F.; Desai, T. a. Nanostructure-Mediated Transport of Biologics across Epithelial Tissue: Enhancing Permeability via Nanotopography. *Nano Lett.* **2013**, *13* (1), 164–171. https://doi.org/10.1021/nl3037799.

(2) Schoellhammer, C. M.; Schroeder, A.; Maa, R.; Lauwers, G. Y.; Swiston, A.; Zervas, M.; Barman, R.; DiCiccio, A. M.; Brugge, W. R.; Anderson, D. G.; et al. Ultrasound-Mediated Gastrointestinal Drug Delivery. *Sci. Transl. Med.* **2015**, *7* (310). https://doi.org/10.1126/scitranslmed.aaa5937.

(3) Fan, W.; Xia, D.; Zhu, Q.; Li, X.; He, S.; Zhu, C.; Guo, S.; Hovgaard, L.; Yang, M.; Gan, Y. Functional Nanoparticles Exploit the Bile Acid Pathway to Overcome Multiple Barriers of the Intestinal Epithelium for Oral Insulin Delivery. *Biomaterials* **2018**, *151*, 13–23. https://doi.org/10.1016/j.biomaterials.2017.10.022.

(4) Zhu, X.; Shan, W.; Zhang, P.; Jin, Y.; Guan, S.; Fan, T.; Yang, Y.; Zhou, Z.; Huang, Y. Penetratin Derivative-Based Nanocomplexes for Enhanced Intestinal Insulin Delivery. *Mol. Pharm.* **2014**, *11* (1), 317–328. https://doi.org/10.1021/mp400493b.

(5) Liu, L.; Zhang, Y.; Yu, S.; Zhang, Z.; He, C.; Chen, X. PH- and Amylase-Responsive Carboxymethyl Starch / Poly (2-Isobutyl-Acrylic Acid) Hybrid Microgels as Effective Enteric Carriers for Oral Insulin Delivery PH- and Amylase-Responsive Carboxymethyl Starch / Poly (2-Isobutyl-Acrylic Acid) Hybrid Microgels. *Biomacromolecules* **2018**, *19*, 2123–2136. https://doi.org/10.1021/acs.biomac.8b00215.

(6) Sheng, J.; He, H.; Han, L.; Qin, J.; Chen, S.; Ru, G.; Li, R.; Yang, P.; Wang, J.; Yang, V. C. Enhancing Insulin Oral Absorption by Using Mucoadhesive Nanoparticles Loaded with LMWP-Linked Insulin Conjugates. *J. Control. Release* **2016**, *233*, 181–190. https://doi.org/10.1016/j.jconrel.2016.05.015.

(7) Shan, W.; Zhu, X.; Tao, W.; Cui, Y.; Liu, M.; Wu, L.; Li, L.; Zheng, Y.; Huang, Y. Enhanced Oral Delivery of Protein Drugs Using Zwitterion-Functionalized Nanoparticles to Overcome Both the Diffusion and Absorption Barriers. *ACS Appl. Mater. Interfaces* **2016**, *8* (38), 25444–25453. https://doi.org/10.1021/acsami.6b08183.

(8) Lee, J. H.; Sahu, A.; Choi, W. Il; Lee, J. Y.; Tae, G. ZOT-Derived Peptide and Chitosan Functionalized Nanocarrier for Oral Delivery of Protein Drug. *Biomaterials* **2016**, *103*, 160–169. https://doi.org/10.1016/j.biomaterials.2016.06.059.

(9) Wong, C. Y.; Al-Salami, H.; Dass, C. R. Potential of Insulin Nanoparticle Formulations for Oral Delivery and Diabetes Treatment. *J. Control. Release* **2017**, *264* (September), 247–275. https://doi.org/10.1016/j.jconrel.2017.09.003.

(10) Young, L.; Sung, J.; Stacey, G.; Masters, J. R. Detection of Mycoplasma in Cell Cultures. *Nat. Protoc.* **2010**, *5* (5), 929–934. https://doi.org/10.1038/nprot.2010.43.

(11) Chong, Saeho; Dando, Sandra A.; Morrison, R. A. Evaluation of Biocoat Intestinal Epithelium Differentiation Environment (3-Day Cultured Caco-2 Cells) as an Absorption Screening Model with Improved Screening Productivity. *Pharmaceutical Research*. 1997, pp 1835–1837.

https://doi.org/10.1023/A:1012160703533.
(12) Yamashita, S.; Konishi, K.; Yamazaki, Y.; Taki, Y.; Sakane, T.; Sezaki, H.; Furuyama, Y. New and Better Protocols for a Short-Term Caco-2 Cell Culture System. *J. Pharm. Sci.* **2002**, *91* (3), 669–679. https://doi.org/10.1002/jps.10050.
(13) Gupta, V.; Doshi, N.; Mitragotri, S. Permeation of Insulin, Calcitonin and Exenatide across Caco-2 Monolayers: Measurement Using a Rapid, 3-Day System. *PLoS One* **2013**, *8* (2). https://doi.org/10.1371/journal.pone.0057136.
(14) Atuma, C.; Strugala, V.; Allen, a; Holm, L. The Adherent Gastrointestinal Mucus Gel Layer: Thickness and Physical State in Vivo. *Am. J. Physiol. Gastrointest. Liver Physiol.* **2001**, *280* (5), G922–G929.
(15) Xu, Q.; Ensign, L. M.; Boylan, N. J.; Schön, A.; Gong, X.; Yang, J.-C.; Lamb, N. W.; Cai, S.; Yu, T.; Freire, E.; et al. Impact of Surface Polyethylene Glycol (PEG) Density on Biodegradable Nanoparticle Transport in Mucus *Ex Vivo* and Distribution *in Vivo*. *ACS Nano* **2015**, No. 9, 150824093910007. https://doi.org/10.1021/acsnano.5b03876.
(16) Pereira De Sousa, I.; Steiner, C.; Schmutzler, M.; Wilcox, M. D.; Veldhuis, G. J.; Pearson, J. P.; Huck, C. W.; Salvenmoser, W.; Bernkop-Schnürch, A. Mucus Permeating Carriers: Formulation and Characterization of Highly Densely Charged Nanoparticles. *Eur. J. Pharm. Biopharm.* **2015**, *97*, 273–279. https://doi.org/10.1016/j.ejpb.2014.12.024.
(17) Larregieu, C. a; Benet, L. Z. Drug Discovery and Regulatory Considerations for Improving in Silico and in Vitro Predictions That Use Caco-2 as a Surrogate for Human Intestinal Permeability Measurements. *AAPS J.* **2013**, *15* (2), 483–497. https://doi.org/10.1208/s12248-013-9456-8.
(18) Whitehead, K.; Karr, N.; Mitragotri, S. Safe and Effective Permeation Enhancers for Oral Drug Delivery. *Pharm. Res.* **2008**, *25* (8), 1782–1788. https://doi.org/10.1007/s11095-007-9488-9.
(19) Lamson, N. G.; Cusimano, G.; Suri, K.; Zhang, A.; Whitehead, K. A. The PH of Piperazine Derivative Solutions Predicts Their Utility as Transepithelial Permeation Enhancers. *Mol. Pharm.* **2016**, *13* (2), 578–585. https://doi.org/10.1021/acs.molpharmaceut.5b00803.
(20) Aguirre, T. A. S.; Teijeiro-Osorio, D.; Rosa, M.; Coulter, I. S.; Alonso, M. J.; Brayden, D. J. Current Status of Selected Oral Peptide Technologies in Advanced Preclinical Development and in Clinical Trials. *Adv. Drug Deliv. Rev.* **2016**, *106*, 223–241. https://doi.org/10.1016/j.addr.2016.02.004.
(21) Grießinger, J.; Dünnhaupt, S.; Cattoz, B.; Griffiths, P.; Oh, S.; Borrós, S.; Wilcox, M.; Pearson, J.; Gumbleton, M.; Bernkop-schnürch, A. Methods to Determine the Interactions of Micro- and Nanoparticles with Mucus. *Eur. J. Pharm. Biopharm.* **2015**, *96* (February), 464–476. https://doi.org/10.1016/j.ejpb.2015.01.005.
(22) Cu, Y.; Saltzman, W. M. Mathematical Modeling of Molecular Diffusion through Mucus. *Adv. Drug Deliv. Rev.* **2009**, *61* (2), 101–114. https://doi.org/10.1016/j.addr.2008.09.006.
(23) Satterfield, C. N.; Colton, C. K.; Pitcher, W. H. Restricted Diffusion in Liquids within Fine Pores. *AIChE J.* **1973**, *19* (3), 628–635. https://doi.org/10.1002/aic.690190332.
(24) Bischoff, S. C.; Barbara, G.; Buurman, W.; Ockhuizen, T.; Schulzke, J.-D.; Serino,

M.; Tilg, H.; Watson, A.; Wells, J. M. Intestinal Permeability – a New Target for Disease Prevention and Therapy. *BMC Gastroenterol.* **2014**, *14* (1), 189. https://doi.org/10.1186/s12876-014-0189-7.

(25) McCartney, F.; Gleeson, J. P.; Brayden, D. J. Safety Concerns over the Use of Intestinal Permeation Enhancers: A Mini-Review. *Tissue Barriers* **2016**, *4* (April), 00–00. https://doi.org/10.1080/21688370.2016.1176822.

(26) Fein, K. C.; Lamson, N. G.; Whitehead, K. A. Structure-Function Analysis of Phenylpiperazine Derivatives as Intestinal Permeation Enhancers. *Pharm. Res.* **2017**, *34* (6), 1320–1329. https://doi.org/10.1007/s11095-017-2149-8.

(27) Banerjee, A.; Ibsen, K.; Brown, T.; Chen, R.; Agatemor, C.; Mitragotri, S. Ionic Liquids for Oral Insulin Delivery. *Proc. Natl. Acad. Sci.* **2018**, *115* (28), 7296–7301. https://doi.org/10.1073/pnas.1722338115.

(28) Taverner, A.; Dondi, R.; Almansour, K.; Laurent, F.; Owens, S. E.; Eggleston, I. M.; Fotaki, N.; Mrsny, R. J. Enhanced Paracellular Transport of Insulin Can Be Achieved via Transient Induction of Myosin Light Chain Phosphorylation. *J. Control. Release* **2015**, *210*, 189–197. https://doi.org/10.1016/j.jconrel.2015.05.270.

(29) Gupta, V.; Hwang, B. H.; Doshi, N.; Banerjee, A.; Anselmo, A. C.; Mitragotri, S. Delivery of Exenatide and Insulin Using Mucoadhesive Intestinal Devices. *Ann. Biomed. Eng.* **2016**, *44* (6), 1993–2007. https://doi.org/10.1007/s10439-016-1558-x.

(30) Edgerton, D. S.; Lautz, M.; Scott, M.; Everett, C. a; Stettler, K. M.; Neal, D. W.; Chu, C. a; Cherrington, A. D. Insulin' s Direct Effects on the Liver Dominate the Control of Hepatic Glucose Production. *J Clin Invest* **2006**, *116* (2), 521–527. https://doi.org/10.1172/JCI27073.rectly.

(31) Arbit, E.; Kidron, M. Oral Insulin Delivery in a Physiologic Context: Review. *J. Diabetes Sci. Technol.* **2017**, *11* (4), 825–832. https://doi.org/10.1177/1932296817691303.

(32) Morishita, I.; Morishita, M.; Takayama, K.; Machida, Y.; Nagai, T. Hypoglycemic Effect of Novel Oral Microspheres of Insulin with Protease Inhibitor in Normal and Diabetic Rats. *Int. J. Pharm.* **1992**, *78* (1992), 9–16.

(33) Lowman, A. M.; Morishita, M.; Kajita, M.; Nagai, T.; Peppas, N. A. Oral Delivery of Insulin Using PH Responsive Complexation Gels. *J. Pharm. Sci.* **1999**, *88* (Sep), 933–937. https://doi.org/10.1021/js980337n.

(34) Genovese, S.; Mannucci, E.; Ceriello, A. A Review of the Long-Term Efficacy, Tolerability, and Safety of Exenatide Once Weekly for Type 2 Diabetes. *Adv. Ther.* **2017**, *34* (8), 1791–1814. https://doi.org/10.1007/s12325-017-0499-6.

(35) Walsh, E. G.; Adamczyk, B. E.; Chalasani, K. B.; Maher, S.; O'Toole, E. B.; Fox, J. S.; Leonard, T. W.; Brayden, D. J. Oral Delivery of Macromolecules: Rationale Underpinning Gastrointestinal Permeation Enhancement Technology (GIPET). *Ther. Deliv.* **2011**, *2* (12), 1595–1610. https://doi.org/10.4155/tde.11.132.

(36) Moroz, E.; Matoori, S.; Leroux, J. C. Oral Delivery of Macromolecular Drugs: Where We Are after Almost 100years of Attempts. *Adv. Drug Deliv. Rev.* **2015**, *101*, 108–121. https://doi.org/10.1016/j.addr.2016.01.010.

(37) Sun, H.; Chow, E. C.; Liu, S.; Du, Y.; Pang, K. S. The Caco-2 Cell Monolayer: Usefulness and Limitations. *Expert Opin. Drug Metab. Toxicol.* **2008**, *4* (4), 395–

411. https://doi.org/10.1517/17425255.4.4.395.
(38) Lopes, M. A.; Abrahim, B. A.; Cabral, L. M.; Rodrigues, C. R.; Seiça, R. M. F.; de Baptista Veiga, F. J.; Ribeiro, A. J. Intestinal Absorption of Insulin Nanoparticles: Contribution of M Cells. *Nanomedicine Nanotechnology, Biol. Med.* **2014**, *10* (6), 1139–1151. https://doi.org/10.1016/j.nano.2014.02.014.
(39) Walsh, L.; Ryu, J.; Bock, S.; Koval, M.; Mauro, T.; Ross, R.; Desai, T. Nanotopography Facilitates *in Vivo* Transdermal Delivery of High Molecular Weight Therapeutics through an Integrin-Dependent Mechanism. *Nano Lett.* **2015**, *15* (4), 2434–2441. https://doi.org/10.1021/nl504829f.
(40) Gilcrease, M. Z. Integrin Signaling in Epithelial Cells. *Cancer Lett.* **2007**, *247* (1–2), 1–25. https://doi.org/10.1016/j.canlet.2006.03.031.
(41) Muller, W. A. Mechanisms of Leukocyte Transendothelial Migration. *Annu Rev Pathol* **2011**, *6*, 323–344. https://doi.org/10.1146/annurev-pathol-011110-130224.Mechanisms.
(42) Takada, Y.; Ye, X.; Simon, S. The Integrins. *Genome Biol.* **2007**, *8* (5). https://doi.org/10.1186/gb-2007-8-5-215.
(43) Salama, N. N.; Eddington, N. D.; Fasano, A. Tight Junction Modulation and Its Relationship to Drug Delivery. *Adv. Drug Deliv. Rev.* **2006**, *58* (1), 15–28. https://doi.org/10.1016/j.addr.2006.01.003.
(44) Walczak, A. P.; Kramer, E.; Hendriksen, P. J. M.; Tromp, P.; Helsper, J. P. F. G.; van der Zande, M.; Rietjens, I. M. C. M.; Bouwmeester, H. Translocation of Differently Sized and Charged Polystyrene Nanoparticles in *in Vitro* Intestinal Cell Models of Increasing Complexity. *Nanotoxicology* **2014**, *5390*, 1–9. https://doi.org/10.3109/17435390.2014.944599.
(45) Yu, S. H.; Tang, D. W.; Hsieh, H. Y.; Wu, W. S.; Lin, B. X.; Chuang, E. Y.; Sung, H. W.; Mi, F. L. Nanoparticle-Induced Tight-Junction Opening for the Transport of an Anti-Angiogenic Sulfated Polysaccharide across Caco-2 Cell Monolayers. *Acta Biomater.* **2013**, *9* (7), 7449–7459. https://doi.org/10.1016/j.actbio.2013.04.009.
(46) Murugadoss, S.; Lison, D.; Godderis, L.; Van Den Brule, S.; Mast, J.; Brassinne, F.; Sebaihi, N.; Hoet, P. H. Toxicology of Silica Nanoparticles: An Update. *Arch. Toxicol.* **2017**, *91* (9), 2967–3010. https://doi.org/10.1007/s00204-017-1993-y.
(47) Bzik, V. A.; Brayden, D. J. An Assessment of the Permeation Enhancer, 1-Phenyl-Piperazine (PPZ), on Paracellular Flux Across Rat Intestinal Mucosae in Ussing Chambers. *Pharm. Res.* **2016**, *33* (10), 2506–2516. https://doi.org/10.1007/s11095-016-1975-4.
(48) Whitehead, K.; Shen, Z.; Mitragotri, S. Oral Delivery of Macromolecules Using Intestinal Patches: Applications for Insulin Delivery. *J. Control. Release* **2004**, *98* (1), 37–45. https://doi.org/10.1016/j.jconrel.2004.04.013.
(49) Banerjee, A.; Lee, J.; Mitragotri, S. Intestinal Mucoadhesive Devices for Oral Delivery of Insulin. *Bioeng. Transl. Med.* **2016**, No. March, 1–9. https://doi.org/10.1002/btm2.10015.

Chapter 6:
Reflections and Future Directions

It is said so often that it has become a cliché in the field: oral protein administration is the holy grail of modern drug delivery. However, trite is not the equivalent of incorrect. There remain both massive opportunities and tremendous hurdles to current researchers seeking platform technologies for oral protein formulations. However, we are closer than ever before to the day when diabetic patients can start their day with a long-acting insulin pill instead of an injection, or children with endocrine disorders can replace constant doctor's office trips for hormone therapy shots with oral tablets in the comfort of their own homes. The key to this success will be to maintain the steady pace of innovation that the field has built up over the past century of efforts, and to keep open minds as new and seemingly crazy approaches come along, as we seek out as much fundamental, mechanistic understanding of oral drug delivery systems as we can find.

In the context of this work, we first sincerely hope that the newly-designed TRIM system will be of use to other labs that are performing research on Caco-2 monolayers. By employing them, we were able to make much more progress in permeation enhancer identification and characterization than either the long-term, 21-day system or the expensive, proprietary kits would allow. With so much left to be understood about the mechanisms and tolerability of even the most promising permeation enhancers, we expect that any technology enabling more, faster and larger volumes of screening will

aid in forward progress toward a clinically viable oral protein delivery formulation. Optimistically, TRIM will provide this necessary improvement to Caco-2 models for researchers around the globe.

When considering the piperazines family, it was, to say the least, disappointing to discover the systematic toxicity of most members of the family, especially since they are otherwise outstanding permeation enhancers. Luckily, there are some determined researchers that have taken up the mantle on applying piperazines in new ways, harnessing their permeabilizing behavior while sidestepping the issues of toxicity. In particular, I would like to give a nod to fellow Whitehead Lab PhD student Kathy Fein, who has worked wonders by combining the piperazines with polymer based protein engineering approaches. Her strategy to co-localize the protein and enhancer, opening tight junctions only in the precise place where a protein molecule is poised to enter, could offer a paradigm shift to the entire field of permeation enhancer research.

An active effort through the entire duration of my PhD tenure, the strawberry research has always been my favorite project, both to work on and to discuss. In a field dominated by synthetic permeation enhancers, and a department that never had “fruit” in its vocabulary, it has been a constant source of joy to watch looks of bewilderment melt into intrigue and delight as we describe why, for example, there are three kilograms of strawberry on the lyophilizer. Fortunately, the identification of pelargonidin opens a long list of exciting, potential forward directions for the project. First, pelargonidin itself will need to successfully orally deliver proteins in mice before graduating to higher order animal models. Along this path, it will also need to acquire a delivery vehicle to help co-localize the pelargonidin and protein drug to the same locations on the epithelium,

decreasing the total amount of material required for oral delivery. Finally, there exists an exciting opportunity to tease more mechanistic and structure-function information out of the pelargonidin. First, to understand why glycosylation inhibits its activity as a permeation enhancer. Next, to compare the activities of the other food-derived members of the anthocyanidin family, which each differ from pelargonidin by only one or two hydroxy or methoxy functional groups. Finally, the cationic oxygen in pelargonidin is a rare chemical entity, and begs the question: would other oxycations be similarly effective permeation enhancers? Once again, an answer to this question could prove invaluable to mechanistic understanding of our most promising permeation enhancers.

A close second to the strawberry project, I never could have guessed that we would discover a novel use for something as mundane and commonplace as a silica nanoparticle. Especially with silica particles having long been employed for other drug delivery purposes, it startled us (and has elicited similar reactions from audience members at conference talks) that their activity went unnoticed for so long. It is worth noting that, like those before us, it was never our intention to study nanoparticles as permeation enhancers. Rather, the entire project sprung out of some frustration with poorly soluble fruit extracts that turned out to be forming nano-precipitates. For me, this very much underscores the need for open-mindedness in oral drug delivery research and beyond. I will offer a piece of advice to those who follow me: do not be afraid to try something because it seems crazy or like it should be an obvious answer. Every researcher has their own unique perspective and potential discoveries to bring to the table, and you never know what strange fact you may discover.

As the development of the silica nanoparticle permeation enhancers continue, I am thrilled to see what could become of this new fusion between physical and chemical tight junction disruption. Having successfully delivered oral proteins in mice, our next steps will be to move into higher animal models; we hope to begin those experiments around the time that this thesis is submitted (April 2019). Additionally, as with the piperazines and the pelargonidin, the particles will likely require a method of co-localizing with the protein drugs at the epithelial surface. A very talented colleague, Sijie Xian, rigorously investigated the use of protein-loaded, mesoporous silica particles for this purpose. Unfortunately, she discovered that the porous surface of the particles precluded their interaction with the cells to function as permeation enhancers. Moving forward, other strategies (such as loading into polymer microspheres or mucoadhesive intestinal patches) should be investigated for better particle-protein co-localization.

To conclude, I would like to offer another piece of advice to the lab mates and other CMU researchers who follow me: explore the university around you. Poke your nose into other labs, other departments, even across Oakland into Pitt and UPMC. There is so much knowledge to gain from one another, and from seemingly unrelated researchers. Especially in the context of the strawberry and silica nanoparticle projects, I was offered advice or experimental assistance from more researchers in more labs than I can count, and did my best to offer whatever know-how I could in return. As we work to innovate our ways forward, it will never be a disadvantage to add another skill set and a new, fresh frame of reference onto our quest into the scientific unknown.